Copyright Warning & Restrictions

The copyright law of the United States (Title 17, United States Code) governs the making of photocopies or other reproductions of copyrighted material.

Under certain conditions specified in the law, libraries and archives are authorized to furnish a photocopy or other reproduction. One of these specified conditions is that the photocopy or reproduction is not to be "used for any purpose other than private study, scholarship, or research." If a, user makes a request for, or later uses, a photocopy or reproduction for purposes in excess of "fair use" that user may be liable for copyright infringement,

This institution reserves the right to refuse to accept a copying order if, in its judgment, fulfillment of the order would involve violation of copyright law.

Please Note: The author retains the copyright while the New Jersey Institute of Technology reserves the right to distribute this thesis or dissertation

Printing note: If you do not wish to print this page, then select "Pages from: first page # to: last page #" on the print dialog screen

ABSTRACT

USING FEED-FORWARD NETWORKS TO INFER THE ACTIVITY OF FEEDBACK NEURONAL NETWORKS

by
Xinxian Huang

The nervous system is one of the most important organ systems in a multicellular body. Animals, including human beings perceive, learn, think and deliver motion instructions through their nervous system. The basic structural units of the nervous system are individual neurons which constitute different neuronal networks with distinct functions. In each network, constituent neurons are coupled with different connection patterns, for example, some neurons send feed-forward information to the coupling neurons while others are mutually coupled. Because it is often difficult to analyze large interconnected feedback neuronal networks, it is important to derive techniques to reduce the complexity of the analysis. My research focuses on using the information of different feed-forward neuronal networks to infer the activity of feedback networks. To accomplish this objective, I use geometric analysis combined with numerical simulations for some typical neuronal systems to determine the activity of the feedback neuronal network in the context of central pattern generating networks.

In my study, I am interested in deriving reduced methods to understand the combined effect of short-term plasticity on the phase-locked activity of networks. I consider a network of two reciprocally coupled heterogenous neurons, A and B, with synaptic depression from neuron A to neuron B. Suppose we are given two pieces of feed-forward information, the effect of neuron A on the activity of neuron B in the feed-forward network of A entraining B and vice versa. Moreover, suppose these effects are not limited to the weak coupling regime. We have developed a method to combine these pieces of feed-forward information into a 2D map that predicts the activity phase of these two neurons when they are mutually coupled. The analysis

of the map is based on certain geometric constructs that arise from each of the feed-forward processes. Our analysis has two parts corresponding to different intrinsic firing patterns of these two neurons. In the first part, we assume that neuron A is oscillatory, while neuron B is not. In the second part, both neurons A and B are assumed to be oscillatory. Both sets of assumptions lead to different feedback maps.

USING FEED-FORWARD NETWORKS TO INFER THE ACTIVITY OF FEEDBACK NEURONAL NETWORKS

by
Xinxian Huang

A Dissertation
Submitted to the Faculty of
New Jersey Institute of Technology and
Rutgers, The State University of New Jersey – Newark
in Partial Fulfillment of the Requirements for the Degree of
Doctor of Philosophy in Mathematical Sciences

Department of Mathematical Sciences, NJIT
Department of Mathematics and Computer Science, Rutgers-Newark

May 2011

APPROVAL PAGE

USING FEED-FORWARD NETWORKS TO INFER THE ACTIVITY OF FEEDBACK NEURONAL NETWORKS

Xinxian Huang

Dr. Amitabha Bose, Dissertation Advisor — Date
Professor, Department of Mathematical Sciences, NJIT

Dr. Denis Blackmore, Committee Member — Date
Professor, Department of Mathematical Sciences, NJIT

Dr. Jorge Golowasch, Committee Member — Date
Associate Professor, Federated Department of Biological Sciences, NJIT

Dr. Farzan Nadim, Committee Member — Date
Professor, Department of Mathematical Sciences, NJIT, Federated Department of Biological Sciences, NJIT

Dr. Horacio Rotstein, Committee Member — Date
Assistant Professor, Department of Mathematical Sciences, NJIT

BIOGRAPHICAL SKETCH

Author: Xinxian Huang

Degree: Doctor of Philosophy

Date: May 2011

Undergraduate and Graduate Education:

- Doctor of Philosophy in Mathematical Sciences,
  New Jersey Institute of Technology, Newark, NJ, 2011
- Master of Science in Computational Mathematics,
  Zhejiang University, Hangzhou, Zhejiang, 2004
- Bachelor of Science in Information and Computational Science,
  Zhejiang University, Hangzhou, Zhejiang, 2001

Major: Mathematical Sciences

Presentations and Publications:

X. Huang, "Using phase response curves to infer the activity of feedback neuronal networks with synaptic depression," poster, *BNS Minisymposium*, Rutgers University, Newark, NJ, November 2010.

X. Huang, "Using phase response curves to infer the activity of feedback neuronal networks with synaptic depression," *Mathematical Biology Seminar*, Department of Mathematical Sciences, New Jersey Institute of Technology, Newark, NJ, October 2010.

X. Huang, "Using feed-forward networks to infer the activity of feedback neuronal networks," poster, *19th Annual Computational Neuroscience Meeting*, San Antonio, TX, July 2010.

X. Huang, "Using feed-forward networks to infer the activity of feedback neuronal networks," poster, *SIAM Conference on Life Sciences*, Pittsburgh, PA, July 2010.

X. Huang, "Using feed-forward networks to infer the activity of feedback neuronal networks," *Student Seminar*, Department of Mathematical Sciences, New Jersey Institute of Technology, Newark, NJ, June 2010.

X. Huang, "Using feed-forward networks to infer the activity of feedback neuronal networks," *Mathematical Biology Seminar*, Department of Mathematical Sciences, New Jersey Institute of Technology, Newark, NJ, December 2009.

X. Huang, "Using feed-forward networks to infer the activity of feedback neuronal networks," *Student Seminar*, Department of Mathematical Sciences, New Jersey Institute of Technology, Newark, NJ, July 2009.

X. Huang, "The activity phase of neurons in a reciprocally inhibitory network," poster, *Frontiers in Applied and Computational Mathematics*, New Jersey Institute of Technology, Newark, NJ, May 2009.

X. Huang, "The activity phase of neurons in a reciprocally inhibitory network," poster, *20th Annual Sigma Xi Student Research Symposium*, Saint Joseph's University, Philadelphia, PA, April 2009.

X. Huang, "The activity phase of neurons in a reciprocally inhibitory network," *Mathematical Biology Seminar*, Department of Mathematical Sciences, New Jersey Institute of Technology, Newark, NJ, February 2009.

Q. Wu, X. Huang and Y. Han, "A clipping algorithm for parabola segments against circular windows," *Computers and Graphics*, 30(4), 2006 .

X. Huang and Q. Wu, "A Fast Line Clipping Algorithm for Ellipse Windows," *Computer Applications and Software*, 22(2), 2005 .

Q. Wu, X. Huang and Y. Han, "Computer Simulation on Queuing System Model of the Priority Level Service," *Application Research of Computers*, 21(4), 2004 .

For my parents, Delin Wang and Yubao Huang and all my family members.

ACKNOWLEDGMENT

First of all, I wish to express my gratitude to my advisor, Professor Amitabha Bose for his tremendous assistance with this dissertation. From beginning to end, he has been a steadfast source of information, ideas, support, and energy. I am deeply grateful for his guidance, patience, and encouragement at NJIT through the last few years and I will be forever grateful for his trust and support that this dissertation could be completed.

I would like to thank my committee member, Professor Farzan Nadim who has been giving me abundant guidance and suggestions for my dissertation. I am really grateful for his help and support during my PhD research. I also would like to extend my gratitude to the other members of my committee for their encouragement and support throughout my years in graduate school as well as through the process of researching and writing this dissertation: Professor Horacio Rotstein, Professor Denis Blackmore and Professor Jorge Golowasch.

I would also like to thank all of the graduate students in the Department of Mathematical Sciences whom I have got to know in the last five years.

Finally, I would like to thank my parents for their support and encouragement. All have been encouraging, I would quite simply not have completed this project without their support and encouragement.

TABLE OF CONTENTS

TABLE OF CONTENTS
(Continued)

Chapter **Page**

LIST OF FIGURES

Figure **Page**

LIST OF FIGURES
(Continued)

Figure **Page**

LIST OF FIGURES
(Continued)

Figure **Page**

LIST OF FIGURES
(Continued)

Figure **Page**

LIST OF FIGURES
(Continued)

Figure **Page**

LIST OF FIGURES
(Continued)

Figure **Page**

LIST OF FIGURES
(Continued)

Figure **Page**

LIST OF FIGURES
(Continued)

Figure **Page**

CHAPTER 1

INTRODUCTION

1.1 General Overview

Most rhythmic movements are produced by central pattern generating circuits [8, 39, 54, 52, 62]. Central pattern generators (CPGs) can be defined as neural networks that can produce rhythmic patterned outputs without rhythmic sensory or central input [37, 38, 54]. It was first shown by Wilson in 1961 that the rhythmic motor pattern could be generated without sensory input. He showed that the locust nervous system could still produce rhythmic output resembling that during flight when it is isolated from the animal [54]. In addition to flying, many other rhythmic motor patterns are generated by CPGs, e.g., chewing, swallowing, walking, breathing [39, 54]. Some motor rhythms are generated by an endogeneous pacemaker neuron. For example, the pyloric network of the stomatogastric ganglion of crabs is driven by a pacemaker pair, AB and PD, which are electrically coupled. Some others are driven by the coordinated activity of several neurons. The leech heartbeat rhythm generator is driven by two arrays of inter neurons, one of which produces the basic rhythm of the network and the other generates the actual rhythm of network in response to the input from the first group [8, 39]. The rhythm of a CPG is associated with the activity of an animal or human being and it can be isolated from the entire complex neural network to some extent, so it is approachable and important to study the intrinsic properties of its component neurons and the synaptic connections between them.

Phase-locked activity is essential for producing a coordinated activity and can be widely found in the central nervous system [8, 18, 28, 54, 52, 62]. The phase-locked activities of different neurons or neuronal groups are related to rhythmic behaviors. For instance, in the mollusk *clione limacina*, the two rhythmically active

feeding structures, grabbing and pulling are highly coordinated to the phase-locked activities of hook protractor motor neurons, hook retractor motor neurons, radula protractor motor neurons and radula retractor motor neurons. Hook protractor are always co-active with radula retractor and hook retractor always coincide with radula protractor [50]. In the crustacean stomatogastric ganglion, neuronal activity of the pyloric network is correlated with the movement of the pylorus region in the animal's stomach. The tri-phasic pattern of the pyloric network is used to constrict and dilate the muscles in the pylorus of the stomach [23, 40]. The phase-locked activity of neurons depends on the intrinsic properties of the component neurons as well as the properties of the synaptic connections between them.

Phase-locked activity of neurons could be in the form of synchronization, anti-phase or with a fixed delay time. Each of these three forms is ubiquitous in the neuronal networks in which neurons are connected by excitatory synapses or inhibitory synapses [9, 43, 59, 62]. It is believed that the theta rhythm in the brain is related to the synchronized activity of a large amount of neurons in the hippocampal region [10]. The neurons in the pyloric network of the stomatogastric ganglion of crabs are not exactly synchronized, but lock at some phase delay [62].

Synchronous activity can be observed in many regions of the brain and is correlated to some behavior and cognition [9, 33, 46]. There is much research focusing on the conditions for the synchronization of coupled neurons as well as the factors for the loss of synchrony in a network. Intuitively, neurons coupled with excitatory synapses lead to synchronization, but many studies have shown that inhibitory synapses could also produce synchronous firing of neurons. Van Vreeswijk et al. showed that when the duration of an action potential is shorter than the rising time of the synapse, inhibition instead of excitation leads to the synchronous firing of neurons [76]. In [72], Terman et al. presented that the appropriate interaction of the intrinsic timescales of neurons and the rates of onset and decay of inhibition yields stable synchronous

coupling of neurons, for which, they proposed two parameter regimes of different combinations of time constants for the intrinsic properties and those for the inhibitory synapses. Besides the fact that properties of neurons and the synapses between them affect the synchrony of neurons, it was found that the stability of synchrony also depends on the number of cells in the network [2, 20, 31]. Chandrasekaran et al. proved that the reciprocal coupling between two neuronal groups helps to stabilize the synchronization of the pulse coupled neurons within each group [14]. Strong inhibitory coupling between neurons destabilize the synchronization of neurons and even breaks the phase locking between them. In [63], it was examined how increasing synaptic strength causes the loss of synchrony. From the view of intrinsic properties, it is relatively harder for heterogeneous neurons to be synchronized than for homogeneous neurons. With mild heterogeneity, synchrony is never perfect and is fragile [78]. Moreover, the pattern in which two neurons are coupled depends on the ratio of the synaptic decay time of inhibition and the network period. In [68], it was showed that heterogeneity has a strong influence on the synchronization of neurons and the ability to synchronize with heterogeneity non-monotonically depends on the synaptic time constants, synaptic conductances and some other parameters in the network.

Beside exact synchrony, neurons can be anti-phase locked or locked with some time delay. The phase-locked activity of neurons often determines the output of the network and the behavior of the animal [23, 40, 50]. Both excitation and inhibition can yield synchronization of two coupled neurons, depending on the rising time of the synapse and the duration of the action potential [76]. Dror et al. examined the criteria for 1:1 phase locking of a two cell network and the conditions for the network with N oscillators pulse-coupled in a ring. The conditions for 2:2 phase locking with preserved firing order or with alternating order were investigated in [53, 63]. It was showed that the synaptic properties between neurons play an important role in generating the firing pattern of the network. Ermentrout studied a more general coupled firing

pattern, $n : m$ phase locking in a two oscillator network with weak coupling and found the conditions based on the natural frequencies of the oscillators for the $n : m$ phase locking pattern [24]. In this work, we examine the conditions for 1:1 phase-locked pattern of two mutually coupled neurons. But we incorporate the short-term synaptic plasticity in our feedback network, which was not included in the previous works.

Except the neurons with spiking firing pattern, bursting oscillations are widely observed in many neurons [4, 47, 59]. For this type of firing pattern of neurons, Matveev et al. proposed a method to investigate the existence and stability for the anti-phase locking of two mutually inhibiting neurons [57]. The Morris-Lecar model is widely used to model the envelope of the burst without describing the intraburst activity. It is a reduced two dimensional biological model producing the neuronal activity related to the Ca^{2+} and K^{+} ionic currents [41, 43, 69]. Zhang et al. investigated the dependence of the activity phase of a follower neuron on the period and duty cycle of the pacemaker neuron in a feed-forward network with A-current [80]. In [62], Mouser et al. studied the phase-locked activity of the tri-phasic pyloric network of the crustacean stomatogastric ganglion and derived analytic expressions for the locked phase of two follower neurons.

1.2 Short-term Synaptic Plasticity

Information is transmitted through synapses between neurons in neural networks. The information transmission is not necessarily uniform, but may depend on the pattern of the presynaptic potentials. This is known as short-term synaptic plasticity [1, 5, 48]. With short-term plasticity, the synaptic strength from the presynaptic neuron to the postsynaptic cell depends on the firing rate of the presynaptic input. On the other hand, for the same presynaptic input, the postsynaptic neurons code the information in different ways according to their distinct properties of the synapses

between them. It has been established experimentally [22, 73] and theoretically [29] that short-term synaptic plasticity contributes to temporal filtering of synaptic transmission.

Short-term plasticity is a universal property of synapses in all animals [16, 55, 81]. For example, in the weakly electric fish, cerebellar granule cells provide parallel fiber inputs to the electrosensory lateral line lobe and the parallel fibers provide feedback input onto apical dendritic spines of the electrosensory lateral line lobe pyramidal neurons [44, 45]. Synapses between them exhibit multiple forms of synaptic plasticity on multiple time scales. Three synapses in the rat brain were examined in [19], the climbing fiber to Purkinje cell synapse, the parallel fiber to Purkinje cell synapse and the Schaffer collateral to CA1 pyramidal cell synapse. These three synapses exhibit different responses to the same periodic stimulation. The first synapse depresses during the stimulation train, the second synapse exhibits enhancement during the stimulation, and the strength of the last one first increases and then decreases during the stimulus train. Thus, the types of short-term plasticity may be very diverse even within an animal.

Short-term synaptic plasticity results from the variation in presynaptic neurotransmitter release [19, 77] and from the different postsynaptic responses to a given stimulus [19, 49]. The mechanism underlying the short-term synaptic plasticity could be very complicated [73]. Some simplified phenomenological models were proposed for its kinetics [55, 56, 75]. Suppose the pre- and postsynaptic neurons are connected by synaptic resources which are divided into three states, effective, inactive and recovered. If all resources can be activated by an action potential, the postsynaptic neuron receives maximal input, which is defined as absolute synaptic efficacy. There is no synaptic plasticity in this case. Otherwise, the action potential activates and makes effective certain fraction of resources. This portion instantly becomes inactive and recovers with some time constant in the recovery state[75]. Many mathema-tical

models have been proposed to describe this dynamical process [30, 42, 55, 56, 67, 75] in the form of differential equations, discrete maps or the combination of them. One of the ordinary differential equation models derived in [42] is

$$\begin{aligned} R' &= (1-R)/D - Ru\delta(t-t_n) \\ u' &= (U-u)/F + U(1-u)\delta(t-t_n) \end{aligned}$$

where R represents the recovered resources, called the depression variable and u represents the fraction activated by the action potential, called the facilitation variable. D and F are the recovery time constants for the depression R and facilitation u. When an action potential is elicited at $t = t_n$, it activates a fraction u of the available synaptic resources, i.e., uR, by which amount the resources in the recovery state reduce. At the same time, the action potential increases the facilitation variable by $U(1-u)$. For a burst with five spikes, the traces for R, u, synaptic efficacy and synaptic conductance are shown in Figure 1.1(a). At the moment the action potential appears, the synaptic conductance adjusts its value according to the synaptic efficacy at that time. If the facilitation variable u is fixed, the synapse is called a depressing synapse, behaving as a low-pass filter (red curve in Figure 1.1(b)). If the depression variable R is a constant, the synapse acts as a high-pass filter (blue curve in Figure 1.1(b)). Otherwise, the synaptic conductance reaches its maximum at a preferred burst frequency, called the resonant frequency. [21, 42]

Synaptic depression is ubiquitous in the central and peripheral nervous system [32]. Synapses between neocortical pyramidal cells often exhibit depression property in response to the presynaptic input [74]. Short-term synaptic depression is also observed in the pyloric network of the stomatogastric ganglion [6, 37, 38, 62]. Depression has been suggested to play a role in both the coordination and timing of oscillatory events [32]. In the responses of neurons in the primary visual cortex, short-term synaptic depression is an important element for enhancement of transient responses,

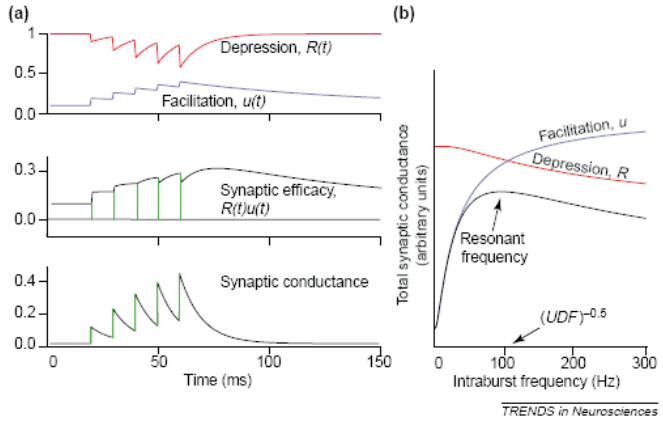

Figure 1.1 Kinetics of short-term synaptic plasticity. (a) The upper left panel are the dynamics of depression and facilitation variables in response to a burst of five spikes. The middle left panel is the response of synaptic efficacy to the burst. The lower left panel is the response of synaptic conductance to the burst. (b) Integral of synaptic conductance for bursts of five spikes with various intra-burst frequencies. Reprinted from [42].

temporal phase shifts and direction selectivity [13]. Slow synaptic depression contributes to the regulation of spontaneous episode activity in the embryonic chick spinal cord [71]. Short-term synaptic depression plays an important role in determining the frequency of a globally inhibitory network and bistability of its solutions [15]. It was showed in [6] that a single depressing synapse can produce oscillation bistability in a network consisting of an excitatory neuron and an inhibitory neuron.

Phase-locked activity is important for producing a coordinated activity. For instance, phase-locked activity is necessary to produce a smooth and coordinated movement of the ventilatory system in crabs [18]. Hooper investigated the extent to which neuronal networks of the stomatogastric ganglion can produce phase-constant motor patterns as cycle frequency is altered [37, 38]. The maintenance of phase in a computational model in which an oscillator neuron inhibits a follower neuron was studied by examining the dependency of phase on cycle period in two cases [51]. The locked phase is generally a monotonically decreasing function of the period

with a non-depressing synapse and there is always a parameter regime in which the phase is a non-monotonic function of the cycle period with a depressing synapse. In [7], it is showed how the interaction between synaptic depression and a transient potassium current in the follower neuron determines the activity phase of this neuron in a simplified network of an oscillator neuron inhibiting a follower neuron. The presence of synaptic depression increases the range of oscillator periods over which phase maintenance of the neurons in a feed-forward network occurs [6, 62].

1.3 Phase Response Curve

Consider a periodically spiking neuron and give a small brief perturbation at a precise time during its oscillation. The next spike of the neuron may be advanced or delayed by the perturbation. Moreover, the extent to which the perturbation affects the oscillation period depends on the timing of the perturbation or the phase of the neuron when it receives the perturbation [11, 41]. A phase response curve (PRC) measures the transient change in the period of an oscillator induced by a weak perturbation [11]. Using mathematical convention, it is defined as

$$F(\phi) = \frac{T_0 - T_1}{T_0}$$

where T_0 is the period of the oscillator without a perturbation and T_1 is the cycle period of the oscillation with the perturbation which is a function of the time when oscillator receives the perturbation, or the phase. Usually, the phase concept is used to denote the perturbation time, defined as $\phi = t_s/T_0$, where t_s represents the elapsed time after the previous spiking of the oscillator to the moment the perturbation comes (Figure 1.2).

The shape of PRCs could be very different according to various models [41]. For neurons, Hansel et al. [35] identified two neural PRCs, Type I and Type II

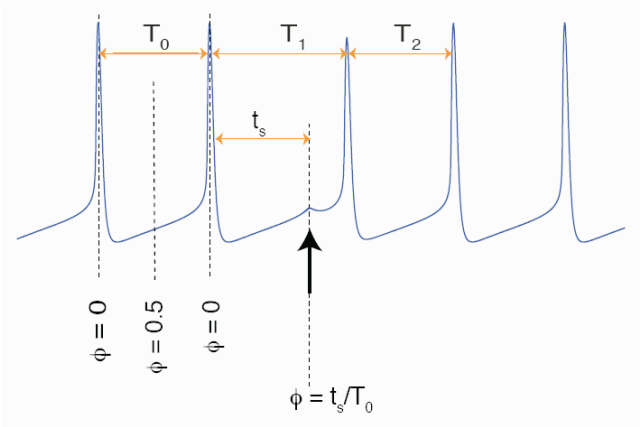

Figure 1.2 Voltage trace of a spiking neuron with a perturbation given at t_s/T_0. Reprinted from [11].

(Figure 1.3). For the neurons with Type I PRC, the phase is only advanced by a small depolarization (Figure 1.3(a)), while for Type II, the phase either can be advanced or can be delayed by a small depolarization, depending on the arriving time of the perturbation (Figure 1.3(b)). If a perturbation comes early, the phase is delayed and if it comes late, the phase is advanced. Ermentrout showed that this classification of PRCs for neurons is closely related to the classification for membrane properties of neurons [26]. When a neuron is depolarized by an applied current, it will repetitively fire with some frequency if the current is big enough. For gradually increasing currents, if the firing frequency can be arbitrarily small near the onset of firing (Figure 1.4(a)), it is called Type I excitable membrane. If the frequency starts with some non-zero number, i.e., there is a threshold firing frequency below which the neuron can not fire (Figure 1.4(b)), it is called Type II excitable membrane [36]. Visually, the $f - I$ curve is continuous for Type I and discontinuous for Type II. Ermentrout showed that neurons with Type I PRCs exhibit Type I excitability and neurons with Type II PRCs exhibit Type II excitability.

The strength of the perturbation is ignored in the phase response curve. It is assumed to be small and can be applied to the weak coupling oscillatory neurons

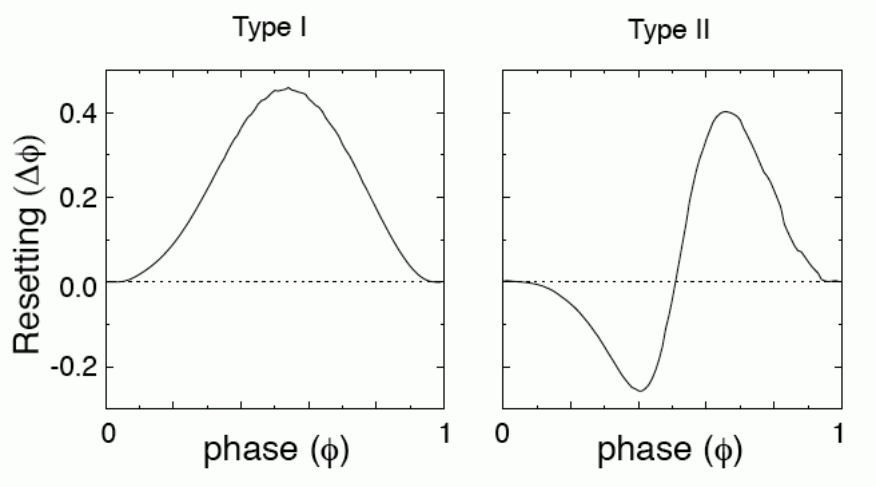

Figure 1.3 (a) Type I phase response curve of a neuron. (b) Type II phase response curve of a neuron. Reprinted from [11].

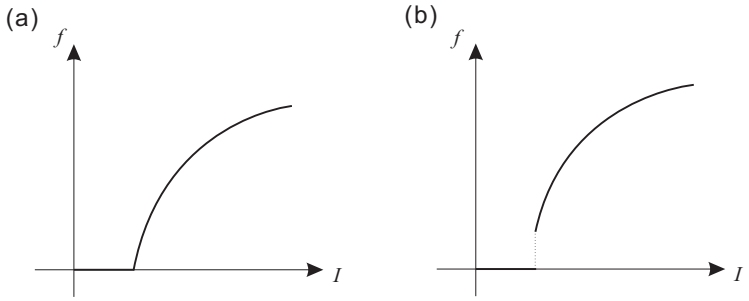

Figure 1.4 The relation between the firing frequency of a neuron and the applied current. (a) Type I excitability. (b) Type II excitability.

[27]. When one considers the synaptically coupled neurons, the postsynaptic neuron is affected by the action potential from the presynaptic one. This influence may not be as small as the assumption needed to define the PRC. But the idea can still be used to measure the change in the period of the postsynaptic neuron induced by the action potential. The PRC generated using an action potential or without the weak coupling assumption is often called spike time response curve (STRC). In our work, we consider the neurons coupled by chemical synapses, the strength of which are not necessarily weak. Thus we use the name 'STRC' without the weak coupling condition,

but many definitions and theories not related to the weak coupling on the PRCs can be applied on the STRCs.

There are many different ways to obtain the PRCs for model oscillators. If the perturbation is weak, some typical mathematical approaches are proposed to calculate the PRCs, e.g., Winfree's approach [41] and Kuramoto's approach [41]. Without the weak coupling condition, PRCs for some simple model oscillators can be analytically calculated, e.g., integrate-and-fire model and the radial isochron clock, etc [31]. But for most biological models, the PRCs can not be exactly calculated, but can be generated numerically or experimentally [31, 41].

PRCs and STRCs are often used to predict the phase-locked activity of neuronal networks [2, 3, 12, 14, 20, 53]. For a network in which all homogeneous neurons are identically coupled, exact synchrony can be obtained only when the PRC has positive slope at phase zero [2]. Furthermore, the stability of synchrony can be lost by increasing the slope of the PRC [2]. Maran and Canavier derived the conditions based on the PRCs of two neurons for the existence and stability of four different phase-locked modes when the neurons are mutually coupled [53]. Oprisan and Canavier [64] considered the effect of synaptic perturbation on the burst duration of an oscillator and proposed the definition of burst resetting curve which was used to analyze the phase locking of two reciprocally coupled neurons. In the above work, the PRCs are all generated using a perturbation approximating the input from the presynaptic neuron, so they are equivalent to STRCs. For neurons coupled in a network, given the information how a single presynaptic action potential affects the status of the postsynaptic, the network activity can be predicted.

1.4 Overview of Thesis

It is often difficult to analyze a large network directly. Analyzing reduced small networks is a useful way to understand the dynamics of the larger network. In our work, given a large feedback network, we want to study smaller feed-forward networks and then combine any obtained information to understand the feedback network. Feed-forward networks may produce different kinds of information, for example, the cycle period of the activity, the firing time, the activity phase the PRC, or the STRC, etc. We use the information from the feed-forward network to predict the phase-locked activity of the feedback network. We are also interested in the effects of short-term plasticity, in particular of synaptic depression of the synapse.

There is much research on predicting the phase-locked activities of feedback networks using the feed-forward information, e.g. phase response curves or spike time response curves [2, 3, 11, 12, 20]. There are also many studies focusing on the effect of the synaptic plasticity on the activity of the postsynaptic neuron as well as their contributions on the associated networks [6, 7, 19, 22, 30, 37, 38]. But so far, few work has connected these two subjects together to investigate the dynamics of a network. In this study, we will consider these two topics together. We are combining pieces of feed-forward information to predict the phase-locked activity of the feedback network in which synapses show the properties of short-term synaptic plasticity.

In the network we consider, there are two neurons, A and B, reciprocally coupled by inhibitory synapses. The activity phase of one neuron has an effect on the activity of the other one, and vice versa. We determine the phase of activity of the mutually inhibitory network from information obtained from two different feed-forward inhibitory networks. The locked phase in the inhibitory network can be determined by approximately combining the two functions of the feed-forward systems. Our analysis has two parts corresponding to different intrinsic firing patterns of these two neurons. In the first part (Chapters 2, 3 and 4), we assume that neuron

A is oscillatory, while neuron B is not in Chapters 2 and 3. In Chapter 4, we apply the method derived in the previous chapters to the pyloric network of the stomatogastric ganglion, which consists of three neurons in our simplified model. The pacemaker AB is an oscillator and the two followers, LP and PY, both have high-voltage resting potentials. In the second part (Chapter 5), both neurons A and B are assumed to be oscillatory.

The outline of this work is as follows. In Chapter 2, we study the phase of activity in a reciprocally inhibitory network. We examine the conditions for the existence and stability of phase-locked activity in a feed-forward inhibitory network in which neuron A receives inhibition from neuron B by analyzing the dependence of the period of A on the relative firing time of B. We obtain this dependency in the feed-forward inhibitory network of B inhibiting A using the software XPPAUT [25]. On the other hand, the relationship between the phase of B and the period of A in A to B feed-forward network was previously given in [51]. Given this information, in Chapter 3, we determine the period of A and the activity phase of B in the mutually coupled network using a simplified Morris-Lecar model [51, 61, 69]. By analyzing this model, we adjust the relation function obtained from the feed-forward network to be applicable to the feedback network. In chapter 4, we extend the work to the pyloric network and construct a 4-dimensional map for the phase-locked activity of a pacemaker driven feed-forward network. We then derive a 6-dimensional map for the phase-locked activity of the network in the presence of a feedback synapse to the pacemaker. We show how feedback can stabilize the ensuing periodic solution. In Chapter 5, the two neurons we consider are both oscillators with tonic spiking patterns but having slightly different intrinsic periods. We use STRCs of these two neurons to infer the activity of the feedback neuronal networks with inhibitory synapses. We compare the phase-locked activity of the feedback network with and without the synaptic depression and investigate the role of this synaptic plasticity in regulating

the activity of the network. Chapter 6 is the discussion of this study and our future work.

CHAPTER 2

PHASE-LOCKED ACTIVITY OF NEURONS IN A FEED-FORWARD NETWORK

In order to understand the phase of activity in a reciprocally inhibitory network, first we want to examine the conditions for the existence and stability of phase-locked activity in a feed-forward inhibitory network in which neuron B inhibits neuron A. We denote $\tilde{P}$ as the intrinsic period of neuron A (in the absence of input from B) and $\tilde{T}$ as the intrinsic period of neuron B (in the absence of input from A). A schematic plot of the voltage versus time is shown in Figure 2.1 for these two neurons.

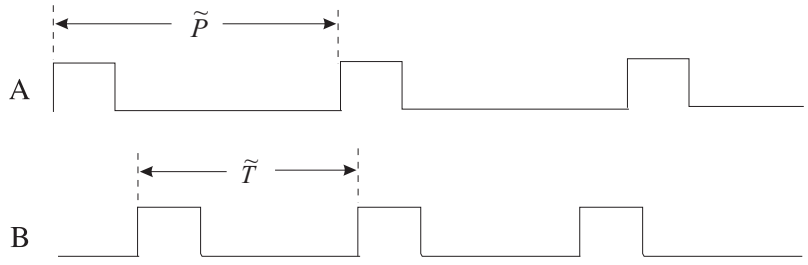

Figure 2.1 Voltage traces for the two uncoupled neurons A and B.

2.1 Phase-locked Activity of a Feed-forward Network if the Period of the Postsynaptic Neuron Linearly Changes with the Relative Firing Time of the Presynaptic Neuron

Suppose that when $t = 0$ neuron A fires. Let t_0 denote the time of B firing. P_1 is the time between subsequent A firings when the inhibition from B exists. t_1 is the time of B firing after the second A firing as shown in Figure 2.2. P_1 depends on t_0, the relative firing time of B, so we can express P_1 as a function of t_0, $f(t_0)$.

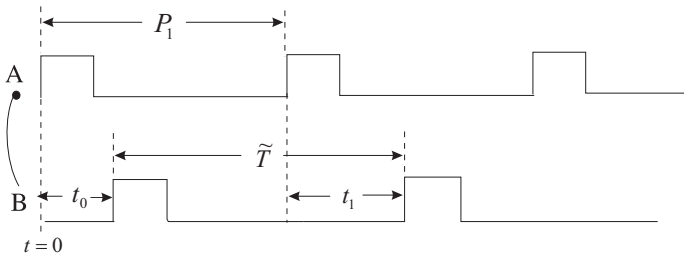

Figure 2.2 Voltage traces of neurons A and B, where B is the presynaptic cell and A is the postsynaptic one with oscillatory trajectory.

For simplicity, first we suppose that $f(t_0)$ is a linear function, $f(t_0) = kt_0 + b$ ($b > 0$) shown in Figure 2.3. We let π be the mapping which maps t_0 to t_1. The fixed point of this map satisfies $t^* = \pi(t^*)$. From Figure 2.2, $t_1 = \pi(t_0) = (1-k)t_0 + \tilde{T} - b$ and $t^* = \frac{\tilde{T}-b}{k}$.

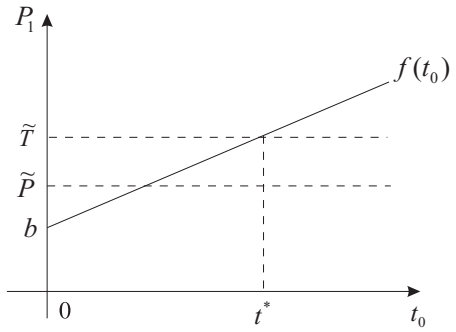

Figure 2.3 $P_1 = f(t_0)$, where f is a linear function of t_0. The fixed point is the intersection of $f(t_0)$ and $\tilde{T}$.

Results

We analyze the mapping π using some mathematical tools and obtain the following conditions for 1:1 firing phase-locked activity of the feed-forward network. For different k values, the specific phase-locked conditions are different.

When $0 < k < 1$, the necessary conditions for the phase-locked activity are as follows: If $\tilde{T} \leq \tilde{P}$, then $(1-k)\tilde{T} \leq b \leq \tilde{T}$. If $\tilde{T} > \tilde{P}$ and $k \geq \tilde{P}/\tilde{T}$, then $\tilde{T} - \tilde{P} < b \leq \tilde{T}$.

If $\tilde{T} > \tilde{P}$ and $k < \tilde{P}/\tilde{T}$, then $(1-k)\tilde{T} < b \leq \tilde{T}$. The sufficient conditions are as follows: If $\tilde{T} \leq \tilde{P}$, then $(1-k)\tilde{T} \leq b < \tilde{T}$. If $\tilde{T} > \tilde{P}$ and $(1-k)\tilde{T} < \tilde{P}$, then $(2-k)\tilde{T} - \tilde{P} < b < \tilde{T}$. If $\tilde{T} > \tilde{P}$ and $(1-k)\tilde{T} \geq \tilde{P}$, no sufficient condition exists for this case.

When $1 < k < 2$, the necessary condition for the phase-locked activity is $(2-k)\tilde{T} - \tilde{P} < b < \tilde{T}$. The sufficient condition is $\tilde{T} - \tilde{P} < b < (2-k)\tilde{T}$.

For the special case when $k = 0, 1, 2$, we have the following analysis.

When $k = 0$, if $b = \tilde{T}$, for any value of t_0, $(0 \leq t_0 \leq \tilde{T})$, t_0 is a fixed point which is neutrally stable. If $b \neq \tilde{T}$, no fixed point exists.

When $k = 1$, the necessary condition and the sufficient condition are the same, $\tilde{T} - \tilde{P} < b < \tilde{T}$ and the fixed point is $t^* = \tilde{T} - b$ which is stable.

When $k = 2$, $t_1 = -t_0 + \tilde{T} - b$. The necessary condition is $b < \tilde{T}$ and no sufficient condition was found. If we pick appropriate initial value t_0 guaranteeing 1:1 firing, there exists another type of periodic solution $t_1 = \pi(t_0)$ and $t_0 = \pi(t_1)$. In this case, the period is $2\tilde{T}$, as shown in Figure 2.4, and $2\tilde{T} = f(t_0) + f(t_1)$. The conditions for guaranteeing 1:1 firing are $\tilde{T} - \tilde{P} - b < t_0 < \tilde{T} - b$ and $\tilde{T} - \tilde{P} - b < t_1 < \tilde{T} - b$. Combining these two inequalities, we obtain t_0 should satisfy $Max(\tilde{T} - \tilde{P} - b, 0) < t_0 < Min(\tilde{T} - b, \tilde{P})$.

Example

Suppose in the feed-forward network of B inhibiting A, B is a square wave with the period 300 (time units) and the duration 100 and A is an oscillating neuron governed by the Morris-Lecar model:

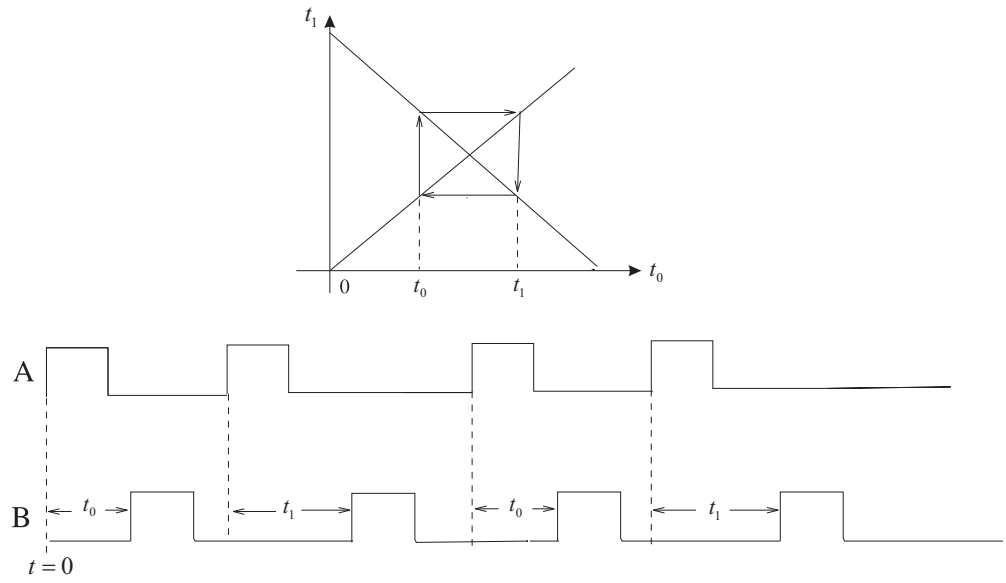

Figure 2.4 When $k = 2$, there exists a period-2 solution, i.e., $t_1 = \pi(t_0)$ and $t_0 = \pi(t_1)$ and the period of the network is $2\tilde{T}$.

$$
\begin{aligned}
\frac{dV_A}{dt} &= -\bar{g}_{Ca} m_\infty(V_A)(V_A - E_{Ca}) - \bar{g}_K w_A(V_A - E_K) - g_L w_A(V_A - E_L) - I_{syn} + I_{ext} \\
\frac{dW_A}{dt} &= \frac{W_\infty(V_A) - W_A}{\tau_A} \\
m_\infty(V_A) &= 0.5(1 + \tanh \frac{V_A - 1}{14.5}) \\
W_\infty(V_A) &= 0.5(1 + \tanh \frac{V_A - 20}{15}) \\
I_{syn} &= \bar{g}_{syn} s(V_A - E_{syn}) \\
\frac{ds}{dt} &= \begin{cases} -\frac{s}{\tau_\kappa} & \texttt{Neuron B is non-active} \\ \frac{1-s}{\tau_\eta} & \texttt{Neuron B is active} \end{cases}
\end{aligned}
$$

where the maximal conductances are $\bar{g}_{Ca} = 0.3, \bar{g}_K = 0.6, g_L = 0.15, \bar{g}_{syn} = 0.185$; the reversal potentials are $E_{Ca} = 100, E_K = -70, E_L = -50, E_{syn} = -70$, and $I_{ext} = 7.5, \tau_A = 150, \tau_\kappa = 1$ and $\tau_\eta = 1$.

We obtained the f function as shown in Figure 2.5, and $k = 1$, $b = 160$, i.e. $f(t_0) = 160 + t_0$. We calculated $t^* = \frac{\tilde{T}-b}{k} \approx 240$ using the mapping π described above. On the other hand, the relative firing time at the steady state obtained directly from the simulation by XPPAUT is 240 (Figure 2.6). These two results are consistent.

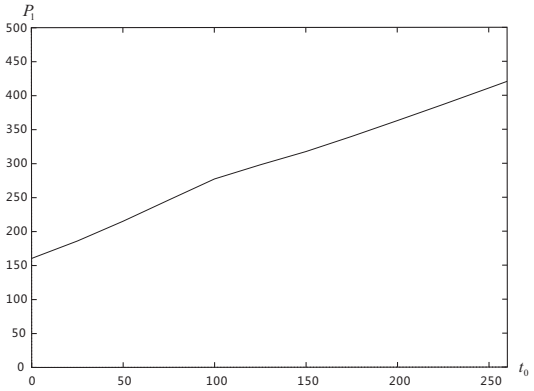

Figure 2.5 Function $f(t_0)$ obtained from simulation by XPPAUT, which is a linear function.

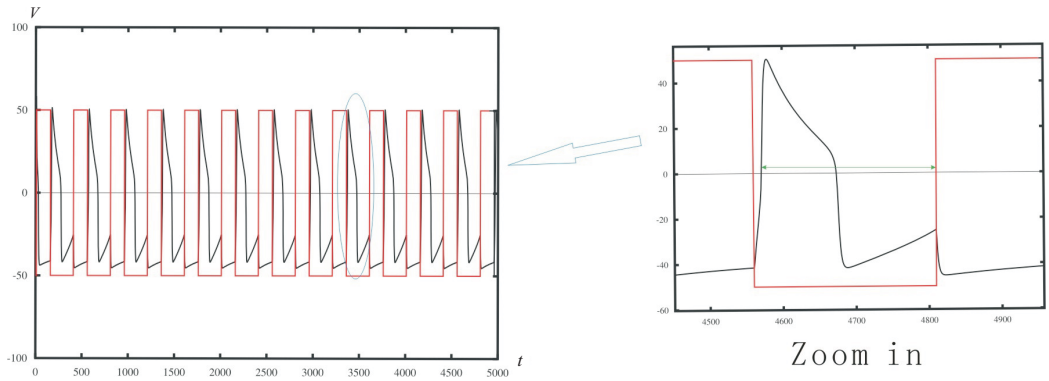

Figure 2.6 Simulation by XPPAUT. The black trace is the voltage of neuron A and the red trace is the square wave for the voltage of neuron B. The right panel is the zoom-in of the circled part in the left panel.

2.2 Phase-locked Activity of a Feed-forward Network if the Relation between the Period of the Postsynaptic Neuron and the Relative Firing Time of the Presynaptic Neuron Is Nonlinear

Generally, the relationship between t_0 and P_1 is nonlinear. Let $P_1 = f(t_0)$, then $t_1 = \pi(t_0) = t_0 + \tilde{T} - f(t_0)$.

Necessary and sufficient conditions

To guarantee 1:1 firing, $\tilde{T}$ can not be too large, otherwise, A may fire twice for every B firing. Therefore, $\tilde{T}$ must satisfy $f(t_0) > t_0 + \tilde{T} - \tilde{P}$. Since $0 \leq t_0 \leq \tilde{T}$, $\tilde{T} - \tilde{P} \leq t_0 + \tilde{T} - \tilde{P} \leq 2\tilde{T} - \tilde{P}$. Let the maximum of $f(t_0)$ in the domain $0 \leq t_0 \leq \tilde{T}$ be M and the minimum be m, i.e. $m \leq f(t_0) \leq M$. The necessary condition for 1:1 firing is $M > \tilde{T} - \tilde{P}$ and the sufficient condition is $m > 2\tilde{T} - \tilde{P}$. Also, $\tilde{T}$ can not be too small. The condition $t_0 + \tilde{T} > f(t_0)$ must be satisfied. Since $0 \leq t_0 \leq \tilde{T} \Rightarrow \tilde{T} \leq t_0 + \tilde{T} \leq 2\tilde{T}$ and $m \leq f(t_0) \leq M$, the necessary condition for 1:1 firing is $m < 2\tilde{T}$ and the sufficient condition is $M < \tilde{T}$.

Existence and stability of the fixed point corresponding to a 1:1 phase-locked firing solution

The fixed point t^* satisfies $t^* = \pi(t^*)$ which implies $f(t^*) - \tilde{T} = 0$. Let $g(t_0) = f(t_0) - \tilde{T}$, then t^* is the root of $g(t_0)$. So the condition for the existence of the fixed point is the same as the condition for the existence of the root of the new function $g(t_0)$ in the domain $0 \leq t_0 \leq \tilde{T}$. The number of the fixed points is the number of the roots of $g(t_0)$ in $0 \leq t_0 \leq \tilde{T}$. The necessary condition for the existence of the fixed point is $M > \tilde{T}$ and $m < \tilde{T}$.

From above, one of the sufficient conditions for 1:1 firing is $M < \tilde{T}$, which conflicts with the existence condition. Therefore, there does not exist sufficient condition for 1:1 firing periodic solution.

For the stability of the fixed point, if $|\pi'(t^*)| < 1$, i.e., $0 < f'(t^*) < 2$, the fixed point t^* is stable.

The curve of the function $f(t_0)$ has various shapes associated with different models. The conditions we derived above can be applied to any relation function. If the function is explicitly formulated, the fixed point can be calculated and the stability conditions can be analytically checked. For the models in Chapter 3, we find the function $f(t_0)$ is a piecewise linear function (Figure 2.7(a)), so existence and stability of the fixed point can be analytically calculated. But for most models, the relation between the new period of the postsynaptic neuron and the relative firing time of the presynaptic neuron is non-linear and it is hard to analytically express their relation. Figure 2.7(b) shows the dependence of the new period of a R15 neuron on the relative firing time of a stimulus [17, 20]. It is impossible to find a mathematical function to describe this curve, but the existence and stability of the fixed point can still be examined by geometric methods. The intersection of the curve and the line for the period of the presynaptic cell yields the fixed point and the stability can be checked by observing the slope of the curve at the fixed point.

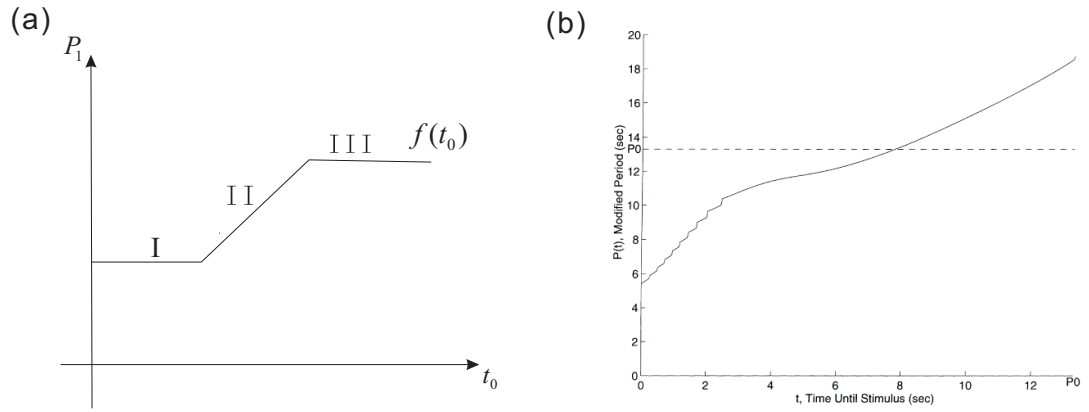

Figure 2.7 (a) $f(t_0)$ is a piecewise linear function. (b) The relation of the new period of a R15 neuron with the relative firing time of a stimulus. Reprinted from [20].

CHAPTER 3

PHASE-LOCKED ACTIVITY OF NEURONS IN A FEEDBACK NETWORK

We consider two reciprocally inhibitory neuronal networks and try to find the phase-locked activity of the feedback system from the two feed-forward systems. Here, we suppose neuron A oscillates through its intrinsic properties and B has a high-voltage resting potential. We examine the phase-locked activities of A and B when they are reciprocally coupled by two different synapses. In section 3.1, we consider non-depressing synapses both from neuron A to B and from B to A. In section 3.2, the synapse from neuron B to A is kept non-depressing, while the synapse from A to B is allowed to be depressing.

3.1 Phase-locked Activity of Two Neurons in a Feedback Network with No Synaptic Depression

Model

Each neuron is modeled with equations of the form:

$$\begin{aligned} \epsilon \frac{dV}{dt} &= f(V,W) \\ \frac{dW}{dt} &= g(V,W) \end{aligned} \tag{3.1}$$

where V denotes the voltage and W is the recovery variable. $f(V,W) = 0$ is the V-nullcline and assumed to be of cubic shape and $g(V,W) = 0$ is the W-nullcline and assumed to be sigmoidal [69]. We study the network dynamics in the phase plane by setting ϵ small enough. Thus, the above equation has two time scales, i.e. the system is singularly perturbed [34, 65, 79]. It is known that for ϵ small and positive,

there is a periodic solution near the solution of the degenerate system, i.e. the system obtained from Equations (3.1) by setting $\epsilon = 0$ [60]. We can use reduced equations to analyze the original dynamics of Equation (3.1). The slow reduced equations are obtained by setting $\epsilon = 0$ in Equation (3.1) to obtain

$$\begin{aligned} f(V, W) &= 0 \\ \frac{dW}{dt} &= g(V, W) \end{aligned} \tag{3.2}$$

The fast reduced equations are obtained by rescaling time in Equation (3.1) by $\xi = t/\epsilon$, and then setting $\epsilon = 0$,

$$\begin{aligned} \frac{dV}{d\xi} &= f(V, W) \\ \frac{dW}{d\xi} &= 0 \end{aligned} \tag{3.3}$$

Equation (3.1) can have a stable fixed point on the left branch of the V-nullcline (Figure 3.1(a)) or on the right branch (Figure 3.1(b)), or on the middle branch leading to a stable oscillation (Figure 3.1(c)) [60, 69]. We suppose A is an oscillating neuron and B has a stable fixed point on the right branch of the V-nullcline. If there exists

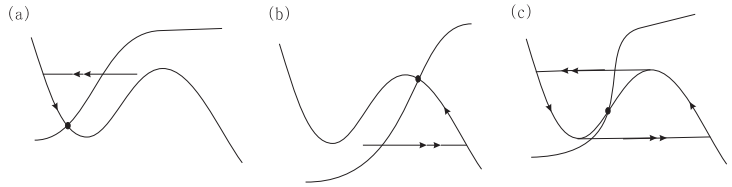

Figure 3.1 Three different stable steady states of free system. The trajectories with one arrow correspond to the solutions for the slow reduced Equations (3.2). The trajectories with two arrows correspond to the solutions for the fast reduced Equations (3.3). (a) A stable fixed point on the left branch of the V-nullcline corresponds to a low-voltage resting potential. (b) A stable fixed point on the right branch of the V-nullcline corresponds to a high-voltage resting potential. (c) The fixed point on the middle branch corresponds to a stable oscillation.

inhibitory influence from one neuron to the other, the V equation of the postsynaptic neuron includes an additional term which represents the synaptic current from the

presynaptic neuron to it [69, 70].

$$\epsilon\frac{dV}{dt} = f(V,W) - I_{syn}$$
$$\frac{dW}{dt} = g(V,W)$$
$$I_{syn} = \bar{g}_{syn}s(V - E_{syn})$$
$$\frac{ds}{dt} = \begin{cases} -s/\tau_\eta & \text{the presynaptic neuron is active} \\ -s/\tau_\kappa & \text{the presynaptic neuron is inactive} \end{cases}$$

where $\bar{g}_{syn}$ denotes the maximal synaptic conductance and E_{syn} denotes the synaptic reversal potential. s is the gating variable representing the fraction of open synaptic channels. When the presynaptic neuron fires, s is set to 1. Assume $\tau_\kappa \ll 1$ and $\tau_\eta \gg 1$, then s decays with fast time constant when the neuron is inactive and remains 1 when the neuron is active. The effect of inhibition is to lower the V-nullcline in the $V - W$ phase plane.

First suppose A is the presynaptic neuron and B is postsynaptic. When the inhibitory synapse is non-depressing, the relative firing time of B, t_0, remains constant as the period of A, $\tilde{P}$ changes. Thus, the phase of B, ϕ, which is defined as the ratio of the relative firing time of B to the period of A, i.e., $\phi = \frac{t_0}{\tilde{P}}$, is a monotonically decreasing function of $\tilde{P}$, as shown in Figure 3.2(a) [51].

On the other hand, assume B is the presynaptic neuron and A is postsynaptic. Suppose that the speed of the neuron traveling along the cubic nullcline only depends on the value of W on the left or right branch of the nullcline, and not on the value of the synaptic variable. From Chapter 2, the period of A, P_1, is a function of the relative firing time of B, t_0, thus, $P_1 = f(t_0)$ as shown in Figure 3.2(b), which is obtained from simulation of the Morris-Lecar model using XPPAUT [25]. In Figure 3.3, W_{L_0} is the local minimum of the intrinsic V-nullcline of neuron A, i.e., the V-nullcline without any synaptic input (the upper cubic curves in Figure 3.3). W_{R_0}

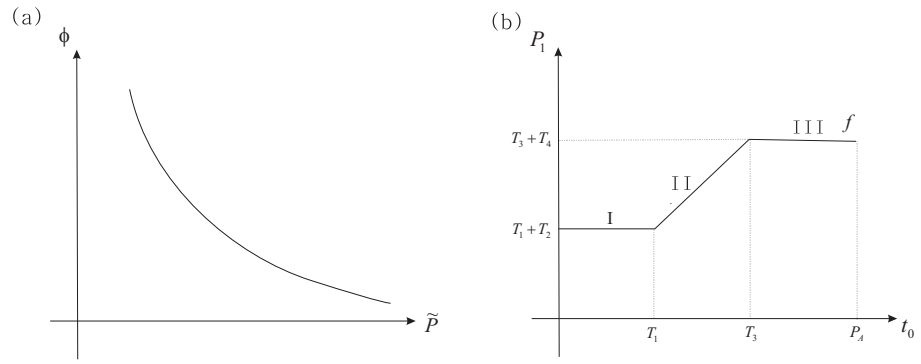

Figure 3.2 (a) Phase of B as a function of period of A when the synapse from A to B is non-depressing (b)Period of A as a function of relative firing time of B in feed-forward network.

is the local maximum of the intrinsic V-nullcline of neuron A. W_{L_1} represents the local minimum of the V-nullcline of neuron A when A receives maximum synaptic inhibition from neuron B (the lower cubic curves in Figure 3.3). W_{R_1} is the local maximum of the V-nullcline of A when it is maximally inhibited. T_1 is the time when neuron A reaches W_{R_1} starting from W_{L_0} on the right branch, T_2 is the time for neuron A to travel from W_{R_1} to W_{L_1} on the left branch. See Figure 3.3. T_3 is the time when neuron A reaches W_{R_0} from W_{L_0} on the right branch. T_4 is the time for neuron A to travel from W_{R_0} to W_{L_1} on the left branch. On Part I in Figure 3.2(b), neuron B fires when A is between W_{L_0} and W_{R_1} on the right branch of the upper nullcline corresponding to $s = 0$. The schematic trajectory of A is shown in Figure 3.3(a). Since the speed on the upper branch is the same as on the lower branch corresponding to $s = 1$, the times A spends on the right branches are the same for different t_0 values. The trajectories of A on the left branch are the same, from W_{R_1} to W_{L_1}. So when $t_0 < T_1$, the cycle period is a constant, independent of the relative firing time of B. On Part II, B fires when A is between W_{R_1} and W_{R_0} on the right branch. At $t = t_0$, A jumps down to the left branch of $s = 1$ nullcline, as shown in Figure 3.3(b). The larger t_0, the longer the trajectory is and the longer the time is. That's why on Part II in Figure 3.2(b), P_1 increases with t_0. On Part III in Figure

3.2(b), B fires when A is inactive. The trajectory of A is shown in Figure 3.3(c). For the same reason as on Part I, the speed on the $s = 0$ nullcline and the speed on the $s = 1$ nullcline are the same on the left part. The time is determined only by W_{R_0}, W_{L_0} and W_{L_1}. So the total time is a constant, $T_3 + T_4$.

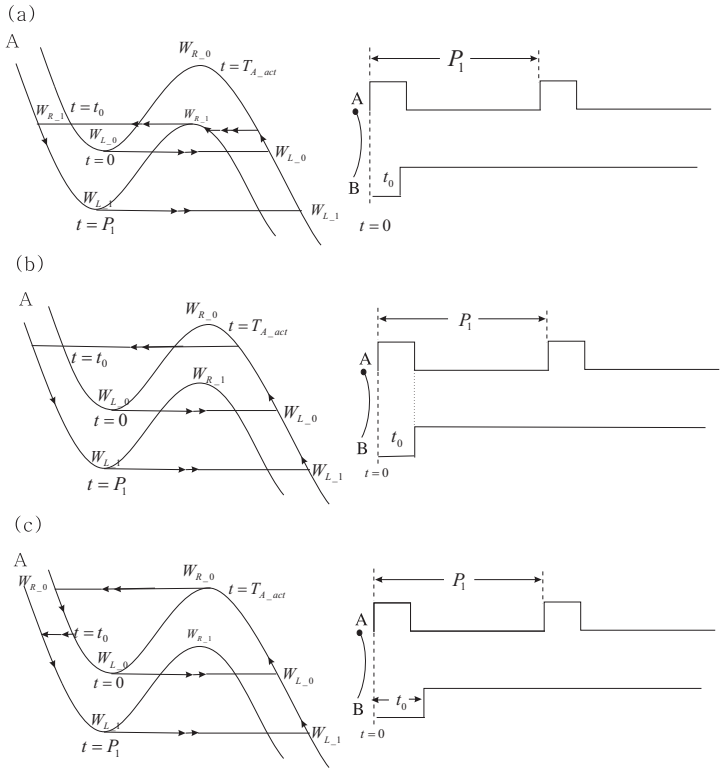

Figure 3.3 Trajectories of A and B in the feed-forward network B inhibiting A. (a) Neuron B fires before A reaches W_{R_1}. The period of A is independent of the relative firing time of B when $t_0 < T_1$, corresponding to Part I in Figure 3.2(b). (b) Neuron B fires after A passes W_{R_1} and before it reaches W_{R_0}. The period of A linearly increases with t_0, corresponding to Part II in Figure 3.2(b). (c) Neuron B fires after A jumps from W_{R_0} to the left branch. The period of A is constant again, independent of the firing time of B for $t_0 > T_3$, corresponding to Part III in Figure 3.2(b). The right panels are schematic plots of voltage traces of A and B for these three cases.

While in the feedback system, B oscillates too, and A always fires when B is active. Schematics of the trajectories of A and B in the feedback network are shown in Figure 3.4.

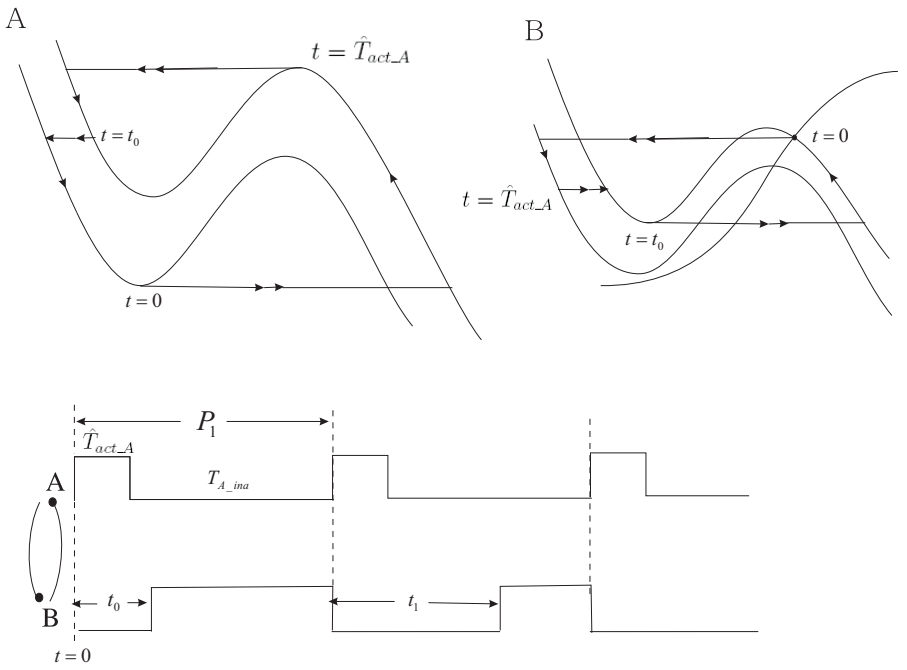

Figure 3.4 In the feedback network, A jumps to the right branch from its inhibited state, i.e., the local minimum of the lower nullcline. B is forced to leave its high-voltage resting potential and jump to the left branch when A fires and spends t_0 time to recover and fires again. The lower panel is the schematic plot of the traces of A and B when they mutually inhibit one another.

In the feed-forward network (Figure 3.3), before A receives inhibition from B, A is on its intrinsic V-nullcline, so at the beginning of a cycle, A jumps from W_{L_0} to the right branch. In the feedback network, since B has a high voltage resting potential, A always jumps from the inhibited state, i.e., from the local minimum of its lower V-nullcline W_{L_1}. Therefore, the time A spends on the right branch of its V-nullcline is different, namely, the active durations of A are different when in the feed-forward network and when in the feedback network. Let T_{act_A} be the active duration of neuron A in the feed-forward network and $\hat{T}_{act\_A}$ be the active duration of neuron A in the feedback network and $\triangle T = \hat{T}_{act\_A} - T_{act\_A}$. So, we have to adjust this difference $\triangle T$ which is the time spent on the right branch for A from the upper left knee ($s = 0$) to the lower left knee ($s = 1$), i.e., from W_{L_0} to W_{L_1}.

After adjusting, the new curve $P_1 = \hat{f}(t_0)$ has the same shape, but different scale with the original curve obtained from the feed-forward network. See Figure 3.5. There are three parts on this curve. On Part I, $\hat{f}(t_0)$ is a constant, on Part II, $\hat{f}(t_0)$

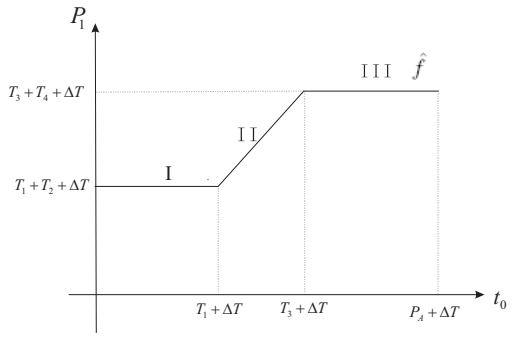

Figure 3.5 Period of A as a function of relative firing time of B in a feedback network.

linearly increases and on Part III, $\hat{f}(t_0)$ is constant again.

Combining the feed-forward information, the map $\pi : P_0 \to P_1$ can be defined as: $P_1 = \pi(P_0) = \hat{f}(P_0 g(P_0))$. The fixed point of this map satisfies $P^* = \pi(P^*)$, i.e., $P^* = \hat{f}(P^* g(P^*))$. Suppose $\hat{f}(t_0) = kt_0 + b,\ k \neq 0$, then $P^* = kP^* g(P^*) + b \Rightarrow g(P^*) = \frac{P^*-b}{kP^*}$. So, the fixed point is the intersection point of the function $g(P)$ and the function $h(P) = \frac{P-b}{kP}$. See Figure 3.6 and Part II in Figure 3.7.

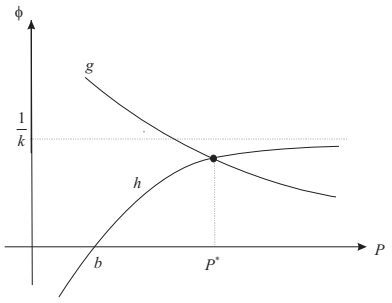

Figure 3.6 Solution of the feedback network for part II of $\hat{f}$ function. The intersection point of g and h corresponds to the solution of the feedback network.

For Part I of $\hat{f}$, $k = 0$, $b = T_1+T_2+\triangle T$, $P_1 = T_1+T_2+\triangle T$, $\forall t_0 \in (0, T_1+\triangle T)$, i.e., $\forall \phi \in (0, \frac{T_1+\triangle T}{T_1+T_2+\triangle T})$, corresponding to Part I in Figure 3.7. Similarly, for Part

III, $k = 0$, $b = T_3 + T_4 + \triangle T$, $P_1 = T_3 + T_4 + \triangle T$, $\forall t_0 \in (T_3 + \triangle T, \tilde{P} + \triangle T)$, i.e., $\forall \phi \in (\frac{T_3+\triangle T}{T_3+T_4+\triangle T}, \frac{\tilde{P}+\triangle T}{T_3+T_4+\triangle T})$, corresponding to Part III in Figure 3.7. Since g is decreasing and h is increasing, there is only one intersection point for these two curves. If $\phi(T_1+T_2+\triangle T) < \frac{T_1+\triangle T}{T_1+T_2+\triangle T}$, i.e., $t_0 < T_1+\triangle T$, the intersection point is on Part I and B fires when A is active (Figure 3.3(a)). If $\phi(T_3 + T_4 + \triangle T) > \frac{T_3+\triangle T}{T_3+T_4+\triangle T}$, i.e., $t_0 > T_3 + \triangle T$, the intersection point is on Part III and B fires when A is inactive (Figure 3.3(c)). Otherwise, the fixed point is on Part II and B fires when A is active (Figure 3.3(b)) and the activity of A and B are anti-phase. If the fixed point is on Part I or Part III, $\hat{f}$ is constant and $\pi' \equiv 0$, thus, the fixed point is stable. Otherwise, the fixed point is on Part II and $P_1 = \pi(P_0) = \hat{f}(t_0)$. Since t_0 is independent of P_0, $\pi' \equiv 0$ and the fixed point is also stable. From simulation by software XPPAUT, we also find the fixed point on any part of the three is stable.

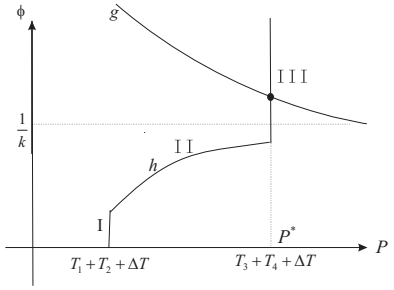

Figure 3.7 Solution of the feedback network of A and B mutually inhibited. The intersection point of these two curves corresponds to the phase-locked activity of the feedback network.

Example

In the reciprocally inhibitory network, the equations for the system are the following.

$$\frac{dV_A}{dt} = -\bar{g}_{Ca} m_\infty(V_A)(V_A - E_{Ca}) - \bar{g}_K W_A(V_A - E_K) - g_L(V_A - E_L) + I_{ext\_A} - \bar{g}_{syn\_B} s_B(V_A - E_{syn})$$

$$\frac{dW_A}{dt} = \begin{cases} \frac{W_\infty(V_A)-W_A}{\tau_{L\_A}} & V_A < Vth \\ \frac{W_\infty(V_A)-W_A}{\tau_{R\_A}} & V_A > Vth \end{cases}$$

$$\begin{aligned} \frac{dV_B}{dt} =& -\bar{g}_{Ca} m_\infty(V_B)(V_B - E_{Ca}) - \bar{g}_K W_B(V_B - E_K) - g_L(V_B - E_L) \\ & + I_{ext\_B} - \bar{g}_{syn\_A} s_A(V_B - E_{syn}) \end{aligned}$$

$$\frac{dW_B}{dt} = \begin{cases} \frac{W_\infty(V_B)-W_B}{\tau_{L\_B}} & V_B < Vth \\ \frac{W_\infty(V_B)-W_B}{\tau_{R\_B}} & V_B > Vth \end{cases}$$

$$\frac{ds_A}{dt} = \begin{cases} -\frac{s}{\tau_{\kappa\_A}} & V_A < Vth \\ -\frac{s}{\tau_{\eta\_A}} & V_A > Vth \end{cases}$$

$$\frac{ds_B}{dt} = \begin{cases} -\frac{s}{\tau_{\kappa\_B}} & V_B < Vth \\ -\frac{s}{\tau_{\eta\_B}} & V_B > Vth \end{cases}$$

The maximal conductances are $\bar{g}_{Ca} = 0.3, \bar{g}_K = 0.6, g_L = 0.15$; the reversal potentials are $E_{Ca} = 100, E_K = -70, E_L = -50, E_{syn} = -70$, and $I_{ext\_A} = 7.5, I_{ext\_B} = 8.5, \bar{g}_{syn\_A} = 0.1, \bar{g}_{syn\_B} = 0.08, \tau_{L\_A} = 450, \tau_{L\_B} = 500, \tau_{R\_A} = 300, \tau_{R\_B} = 25, \tau_{\kappa\_A} = \tau_{\kappa\_B} = 1, 1/\tau_{\eta\_A} \approx 0, 1/\tau_{\eta\_B} \approx 0$.

When A inhibits to B, we obtain the g function as shown in Figure 3.2(a), and $t_0 = 374$. When B inhibits A, the parameters for f function as shown in Figure 3.2(b) are: $T_1 = 113, T_3 = 150, T_1 + T_2 = 1265, T_3 + T_4 = 1525$. After adjusting f, we obtain $\hat{f}$ function as shown in Figure 3.5, and $\triangle T = 43$.

Combining the feed-forward information, we have two intersecting curves as shown in Figure 3.7. The intersection point is on Part III of the $\hat{f}$ function, so the fixed point for the system is $P^* = 1568$ and $\phi^* = \frac{t^*}{P^*} = \frac{374}{1568} \approx 0.2385$. This result is consistent with the result we obtained directly from the simulation by XPPAUT.

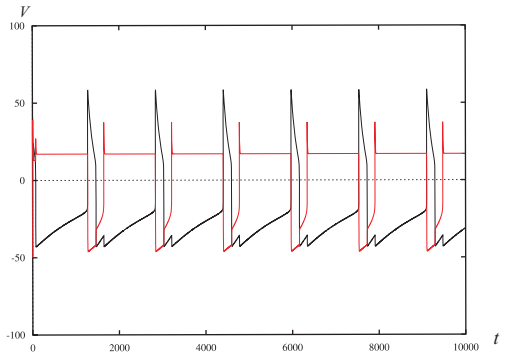

Figure 3.8 Voltage traces of A and B when they are mutually inhibited, obtained from the simulation in XPPAUT. Here, $\phi^* \approx 0.2386$.

3.2 Phase-locked Activity of Two Neurons in a Feedback Network with Synaptic Depression

Model

Synaptic depression is a common form of short-term plasticity in the central and peripheral nervous systems [6, 82]. With synaptic plasticity, the synaptic strength is not a constant, but depends on the available synaptic resources, which is related to the period of the oscillatory neuron. Synaptic depression describes the phenomenon that the synaptic strength decreases as the frequency of the neuron increases. Thus, the dynamics of s is governed by the following equation.

$$\frac{ds}{dt} = \begin{cases} -\frac{s}{\tau_\kappa} & \text{the presynaptic neuron is inactive} \\ -\frac{s}{\tau_\eta} & \text{the presynaptic neuron is active} \end{cases}$$

s is set to the value of d when the presynaptic neuron fires. d represents the fraction of available synaptic resources, which is governed by the following equation [51].

$$\frac{dd}{dt} = \begin{cases} \frac{1-d}{\tau_\alpha} & \text{the presynaptic neuron is inactive} \\ -\frac{d}{\tau_\beta} & \text{the presynaptic neuron is active} \end{cases} \tag{3.4}$$

Now we are considering the reciprocally inhibitory network with depressing synapse from A to B and non-depressing synapse from B to A. For this case, the trajectories of A and B are shown in Figure 3.9, where, P_n is the period of A in the nth cycle, t_n is the relative firing time of B in the $(n+1)$th cycle and s_A^n represents the value of s_A when A fires for the $(n+1)$th time.

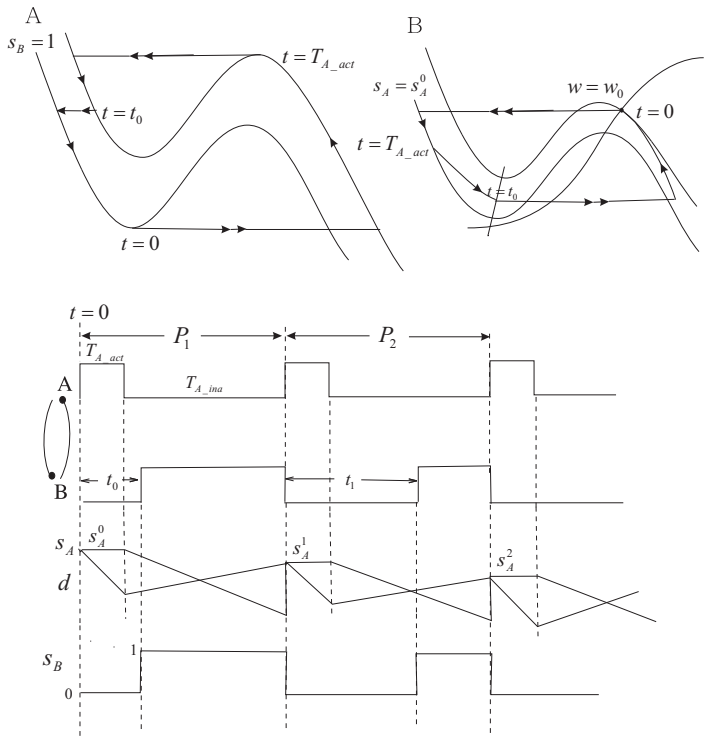

Figure 3.9 Reciprocally inhibitory network with depressing synapse. The upper panel shows the trajectories of neurons A and B in their phase planes. Since the synapse from A to B is depressing, the inhibitory strength B receives when A fires depends on the available synaptic resources at that moment, i.e., s_A^n. The lower panel shows the schematic plot of traces of A and B, as well as the traces of s_A, s_B and d. When A fires, s_A^n is set to the value of d^n, $n = 0, 1, 2, \cdots$. s_B is a square wave because the synapse from B to A is non-depressing.

We will again suppose the phase function of B obtained from the feed-forward network A inhibiting B is $\phi_n = \frac{t_n}{\tilde{P}}$. Since the inhibitory synapse from A to B is depressing, t_n changes with the duration of A (the time when A is active) and the value

of the gating variable s. Previously, in [51], the relationship between the duration of A, the gating variable and the relative firing time of B is shown to be

$$\bar{g}_{syn\_A} s_A^n exp(-(t_n - T_{act\_A}))^+/\tau_{\kappa\_A}) + MW_0 exp(-t_n/\tau_{L\_B}) = g_s^* \tag{3.5}$$

where s_A^n is the value of s when A fires for the $(n+1)$th time. $(t_n - T_{act\_A})^+ = t_n - T_{act\_A}$ if $t_n > T_{act\_A}$ or 0 if $t_n < T_{act\_A}$. T_{act_A} is the time when A is active; and W_0 is the value of W_B when B leaves its high-voltage steady state and jumps to the left branch; M is a positive constant, the proportionality factor that indicates that a jump point with a smaller value of W_B corresponds to stronger inhibition; g_s^* is the critical synaptic conductance below which the synapse is too weak to keep neuron B inactive. Our goal is to examine the convergence of the sequence s_A^n or t_n.

For the system described above, the value of s_A^n varies in the next cycle period. Define G as the relative firing time t_n as a function of s_A^n which can be numerically calculated from Equation (3.5).

Suppose the period function of A, P_1, obtained from the feed-forward network B inhibiting A is $f(t_0)$. Since the synapse from B to A is non-depressing, we can assume that the period function of A is of the same shape as that in the non-depressing case (Figure 3.2(b)). Since the duration of A, T_{act_A}, in the feed-forward network is different from the duration in the feedback network $\hat{T}_{act\_A}$, we have to adjust the curve in Figure 3.2(b), too. The difference is due to the time spent on the right branches of V-nullclines for A to go from the left knee of the nullcline with $s_B = 1$ to that of the nullcline with $s_B = 0$. The time difference $\triangle T = \hat{T}_{act\_A} - T_{act\_A}$ is a constant, measuring the time for A to go from W_{L_1} to W_{L_0} as shown in Figure 3.10.

After adjustment, the new curve $\hat{f}(t_0)$ has the same shape as the original curve obtained from the feed-forward network as shown in Figure 3.5. Also, for the phase function of B, since the duration of A changes, we have to adjust it, replacing T_{act_A}

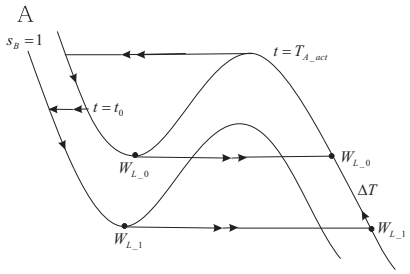

Figure 3.10 Different duration of A between in feed-forward and feedback networks. In the feed-forward network, at the beginning of each cycle, neuron A jumps from W_{L_0} to the right branch, while in the feedback network, A jumps form W_{L_1} to the right branch. $\triangle T$ is the time difference of the duration of A when in the feed-forward network and when in the feedback network.

with $\hat{T}_{act\_A}$ in Equation (3.5). Define $\hat{G}$ as the relative firing time t_n as a function of s_A^n, $t_n = \hat{G}(s_A^n)$. See Figure 3.11.

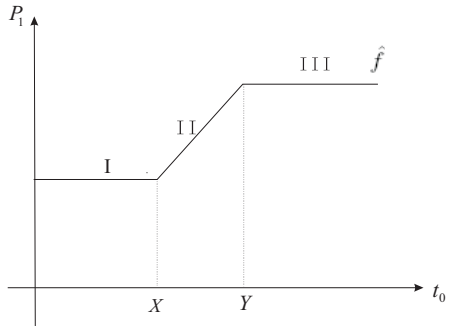

Figure 3.11 Period of A as a function of the relative firing time of B in the feedback network. $X = T_1 + \triangle T$ and $Y = T_3 + \triangle T$, the same as that in Figure 3.5.

From the d governing equation (3.4), $d^{n+1} = 1 - exp(-\frac{P_{n+1} - \hat{T}_{act\_A}}{\tau_{\alpha\_A}})(1 - d^n exp(-\frac{\hat{T}_{act\_A}}{\tau_{\beta\_A}}))$, since when A fires, the value of s_A is reset to the value of d, we obtain the 1-dimensional map

$$s_A^{n+1} = \pi(s_A^n) = 1 - exp(-\frac{P_{n+1} - \hat{T}_{act\_A}}{\tau_{\alpha\_A}})(1 - s_A^n exp(-\frac{\hat{T}_{act\_A}}{\tau_{\beta\_A}})) \qquad (3.6)$$

Suppose $P_{n+1} = k\hat{G}(s_A^n) + b$

The fixed point of s_A^n satisfies

$$s_A^* = 1 - exp(-\frac{k\hat{G}(s_A^*) + b - \hat{T}_{act\_A}}{\tau_{\alpha\_A}})(1 - s_A^* exp(-\frac{\hat{T}_{act\_A}}{\tau_{\beta\_A}}))$$

$\Rightarrow$

$$\hat{G}(s_A^*) = \frac{\hat{T}_{act\_A} - b + \tau_{\alpha\_A} ln \frac{1 - s_A^* e^{-\frac{\hat{T}_{act\_A}}{\tau_{\beta\_A}}}}{1 - s_A^*}}{k} \tag{3.7}$$

Geometrically, s_A^* is the intersection point of $\hat{G}(s_A)$ and the right hand side function of Equation (3.7), $H(s_A) = \frac{\hat{T}_{act\_A} - b + \tau_{\alpha\_A} ln \frac{1 - s_A e^{-\frac{\hat{T}_{act\_A}}{\tau_{\beta\_A}}}}{1 - s_A}}{k}$. See Figure 3.12.

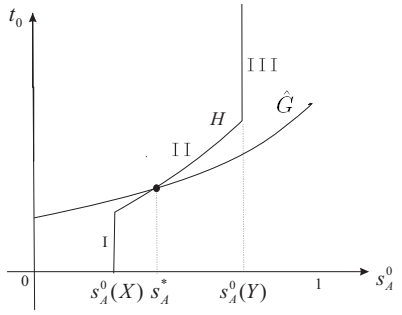

Figure 3.12 The intersection point of these two curves is the solution of feedback inhibitory network with depressing synapse. H is the function on right hand side of Equation (3.7). $\hat{G}$ can be obtained form Equation (3.5).

For Part I or Part III, the period of A, P_1, is a constant and s_A^0 is a constant, too, which corresponds to the vertical parts of the curve as shown in Figure 3.12, where $s_A^0(X) = s_A^0(t_0 = X) = \frac{g_s^* - MW_0 e^{-X/\tau_{L\_B}}}{\bar{g}_{syn\_A} e^{-(X - \hat{T}_A)^+/\tau_{\kappa\_A}}}$ and $s_A^0(Y) = s_A^0(t_0 = Y) = \frac{g_s^* - MW_0 e^{-Y/\tau_{L\_B}}}{\bar{g}_{syn\_A} e^{-(Y - \hat{T}_A)^+/\tau_{\kappa\_A}}}$. Since the slope of $\hat{G}$ is always less than the slope of H on Part II, there exists only one intersection point for these two curves.

From the 1D map (3.6), if the fixed point is on Part I or Part III, P_{n+1} in (3.6) is constant and

$$\pi' = exp(-\frac{\tilde{P} - \hat{T}_{act\_A}}{\tau_{\alpha\_A}}) exp(-\frac{\hat{T}_{act\_A}}{\tau_{\beta\_A}})$$

This value is greater than 0 and less than 1, so the fixed point on Part I or Part III is stable. If the fixed point is on Part II, $P_{n+1} = k\hat{G}(s_A^n) + b$. At the fixed point s_A^*, $\pi'(s_A^*) = exp(-\frac{k\hat{G}(s_A^*) + b - \hat{T}_{act\_A}}{\tau_{\alpha\_A}})[\frac{k\hat{G}'(s_A^*)}{\tau_{\alpha\_A}}(1 - s_A^* exp(-\frac{-\hat{T}_{act\_A}}{\tau_{\beta\_A}})) + exp(-\frac{-\hat{T}_{act\_A}}{\tau_{\beta\_A}})]$

Since the relation between t_n and s_A^n is positive, $\hat{G}'(s_A) > 0$ and $\pi'(s_A) > 0$. When

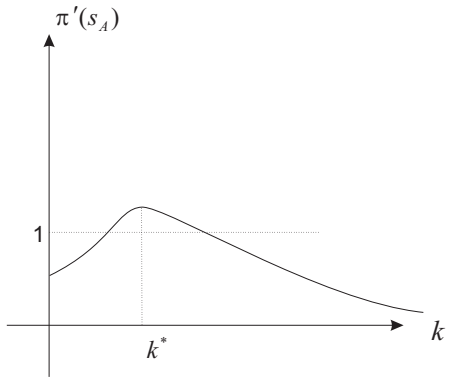

Figure 3.13 Dependency of $\pi'(s_A)$ on k on Part II. There exists a peak value of $\pi'(s_A)$ at k^*.

$k = 0$, $\pi'(s_A) = exp(-\frac{b - \hat{T}_{act\_A}}{\tau_{\alpha\_A}})exp(-\frac{\hat{T}_{act\_A}}{\tau_{\beta\_A}}) < 1$. When $k \to \infty$, $\pi'(s_A) \to 0$. A schematic plot of $\pi'(s_A)$ versus k is shown in Figure 3.13. $\pi'(s_A)$ reaches its maximum at

$$k^* = \frac{\tau_{\alpha\_A}}{\hat{G}(s_A)}[1 - \frac{\hat{G}(s_A)exp(-\frac{\hat{T}_{act\_A}}{\tau_{\beta\_A}})}{\hat{G}'(s_A)(1 - s_A exp(-\frac{\hat{T}_{act\_A}}{\tau_{\beta\_A}}))}]$$

At the steady state $s_A = s_A^*$

$$\pi'(s_A^*)|_{k^*} = (1 - s_A^*)\frac{\hat{G}'(s_A^*)}{\hat{G}(s_A^*)}$$

The instability happens only when $\hat{G}'(s_A^*) > \hat{G}(s_A^*)$ which needs τ_{κ_A} and τ_{L_B} are very large. This will push the fixed point away from Part II to Part III, where the fixed point is stable. So, realistically, the fixed point of the feedback network with synaptic depression remains stable in each part.

Example

Use the same equations as in the example of the non-depressing synapse part and add the d equation (Equation (3.4)) for the depressing synapse from A to B. The maximal conductances are $\bar{g}_{Ca} = 0.3, \bar{g}_K = 0.6, g_L = 0.15$; the reversal potentials are $E_{Ca} = 100, E_K = -70, E_L = -50, E_{syn} = -70$, and $I_{ext\_A} = 7.5, I_{ext\_B} = 7.5, \bar{g}_{syn\_A} = 0.1, \bar{g}_{syn\_B} = 0.08, \tau_{L\_A} = 1200, \tau_{L\_B} = 1500, \tau_{R\_A} = 1000, \tau_{R\_B} = 25, \tau_{\kappa\_A} = 600, \tau_{\kappa\_B} = 200, 1/\tau_{\eta\_A} \approx 0, 1/\tau_{\eta\_B} \approx 0, \tau_\alpha = 1500, \tau_\beta = 1800$.

The adjusted function $\hat{f}$ function from the feed-forward network B inhibiting A is shown in Figure 3.14, where $X = 300, Y = 645$, and the linear function for Part II is $kt_0 + b = 2.1275t_0 + 2861.7$.

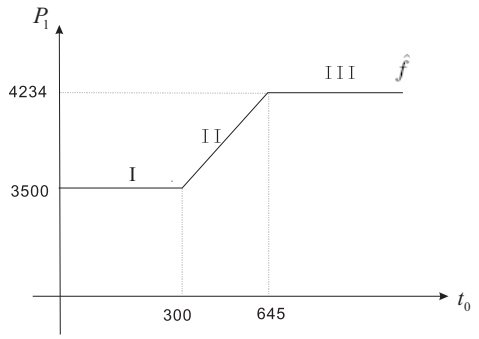

Figure 3.14 Period of A as a function of relative firing time of B in feedback network. $\hat{f}$ is adjusted from f in the feed-forward network.

We obtain the values of the parameters in Equation (3.5) from the feed-forward network A inhibiting B and replace T_{act_A} with $\hat{T}_{act\_A}$. $\hat{T}_{act\_A} = 633.5, M = 0.5687, W_0 = 0.384, g_s^* = 0.091$. With these parameter values, we have the two curves shown in Figure 3.15 and $t_0^* = 453$ which is obtained from Matlab.

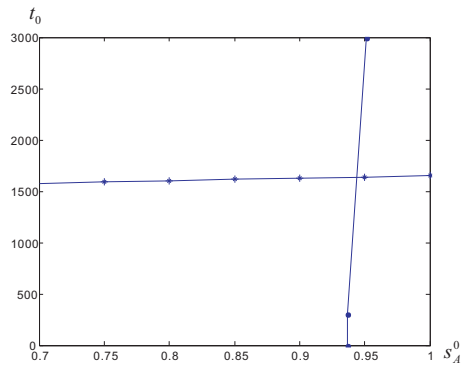

Figure 3.15 The starred curve is the $\hat{G}$ function and the dotted curve is the H function, generated numerically in Matlab. The fixed point is the solution of the feedback network with depressing synapse.

CHAPTER 4

PHASE-LOCKED ACTIVITY OF TRI-PHASIC PYLORIC NETWORK OF CRUSTACEAN STOMATOGASTRIC GANGLION

We apply our method to the pyloric system of the crustacean stomatogastric ganglion (STG). The STG of the crab or lobster has been used to investigate the basic properties of neurons and the synapses between them [58, 23]. In the simplest network model of this system, there are three groups of neurons. The AB neuron and PD neuron are co-active and function as the pacemaker pair of this network. AB sends feed-forward inhibitory synapses to LP and PY. Those two cells mutually inhibit one another and there is a feedback inhibitory synapse from LP to PD. See Figure 4.1. The left panel is a schematic diagram of this network. The right panel is voltages traces of AB, LP and PY taken from experiment. Hooper has shown that the LP and PY neurons fire at the same phases relative to AB firing over a range of frequencies of the pacemaker pair AB/PD [37]. In later studies, Manor et al. [51] and Mouser et al. [62] suggested that synaptic depression could help to maintain these phase relationships. Neither of these studies included the feedback synapse from LP to the pacemaker pair AB/PD which we will do in our study. However, in our model, we simplify AB/PD and assume that the feedback synapse is directly to AB. We will derive a method of combining a set of feed-forward information to infer the activity of the tri-phasic network as a whole. In particular, since AB is the pacemaker of this network, without the feedback synapse from LP to AB, the phase-locked activity of this network is completely determined by the rhythm of AB. We consider this partial network without the LP to AB synapse as a feed-forward network in which AB sends feed-forward inhibitory synapses to LP and PY and those two cells are mutually inhibited. We take as the other feed-forward network the one

in which LP sends a feed-forward inhibitory synapse to AB. We then combine these two pieces feed-forward information to determine activity of the feedback network. First, in section 4.1 we examine the phase-locked activity of the neurons in the partial network without the LP to AB synapse. Then, we investigate how the synapse from LP to AB influences the activity of this network. In sections 4.2 and 4.3, we take this feedback synapse into account and investigate the phase-locked activity of the entire network as well as the effect of this feedback synapse on the activity of this network.

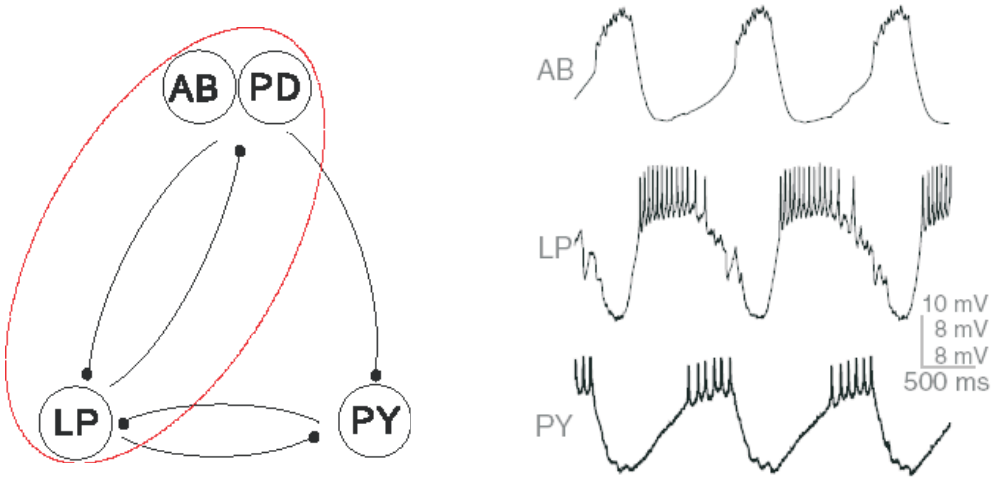

Figure 4.1 Triphasic rhythm of the pyloric network of STG. The left panel is a schematic diagram of the network. AB sends feed-forward inhibitory synapses to LP and PY which mutually inhibits one another and there is a feedback synapse from LP to AB/PD. The right panel is voltages traces of biological AB, LP and PY neurons, reprinted from [62].

4.1 Activity of the Tri-phasic Pyloric Network without the Feedback Synapse from LP to AB/PD

In this section, we consider the feed-forward network comprised of AB, LP and PY, in which AB sends feed-forward inhibitory synapses to LP and PY and these two follower cells are mutually inhibited. Mouser et al. [62] derived the steady state

phases of LP and PY as a function of the period of AB. Here, we derive a map that determines these phases cycle by cycle. This map will then allow us to check the stability of the ensuing phase-locked solutions. Since AB is the pacemaker, the period of this network is determined by the frequency of AB. We denote the active duration of AB as T_{AB} and the period of AB as P which is the period of the network as well. Both are constant in each cycle. In the ith cycle, $i = 1, 2, \cdots$, the delay firing times of LP and PY after AB firing are denoted as t^i_{LP} and t^i_{PY}, respectively, and the active duration of LP and PY are denoted as T^i_{LP} and T^i_{PY}, respectively. Since we incorporate the short-term synaptic depression of LP and PY, in this model, there are two depression variable, d_{LP} for LP and d_{PY} for PY. In the ith cycle, the value of d_{LP} at the moment LP fires is denoted as d^i_{LP} and d^i_{PY} represents the value of d_{PY} when PY fires (Figure 4.2).

Without any synaptic coupling, AB is an oscillator whose phase plane corresponds to the situation in Figure 3.1(c) of Chapter 3, the fixed point on the middle branch of the V-nullcline. LP and PY have high-voltage resting potentials corresponding to the situation as shown in Figure 3.1(b) of Chapter 3, fixed points on the right branches of their V-nullclines in the phase plane. We assume the moment AB fires is the beginning of each cycle, $t = 0$. When AB fires, it sends feed-forward inhibitory synapses to LP and PY, delaying the firing of these two follower neurons. AB remains active for the time T_{AB} during which time both LP and PY are silent. After the delay time t^i_{LP}, LP fires and also sends an inhibitory synapse to PY. At the time $t = t^i_{PY}$, PY escapes from the inhibition of AB and LP and simultaneously sends feedback inhibition to LP, stopping the bursting activity of LP returning it to its silent state. After T^i_{PY} time, AB fires again and inhibits LP and PY, so LP is further inhibited and PY returns the silent state. This time is the end of the ith cycle and also the beginning of the $(i + 1)$th cycle. Here, we assume the firing of PY is later than the firing of LP, i.e., $t^i_{LP} < t^i_{PY}$, due to their intrinsic properties, which is experimentally

shown by Rabbah and Nadim [66]. A schematic plot of the voltage traces of AB, LP and PY is shown in Figure 4.2.

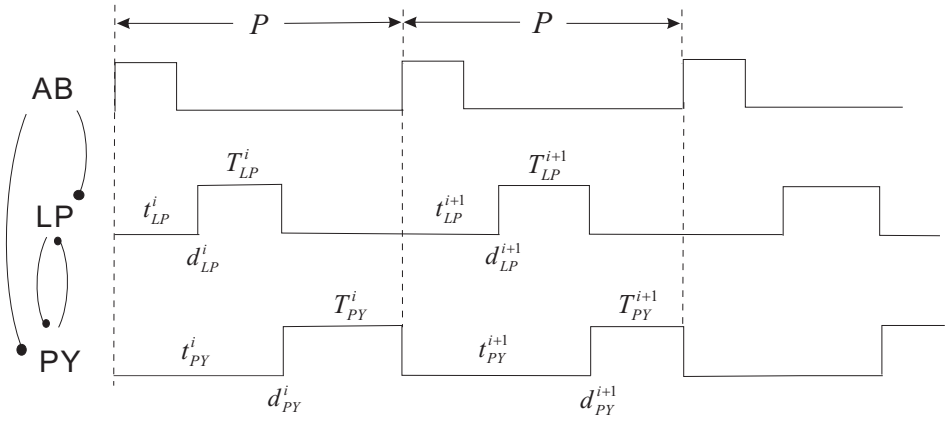

Figure 4.2 Voltage traces of neurons AB, LP and PY in the feed-forward tri-phasic pyloric network of STG. AB is the pacemaker of this network and LP and PY are followers. P is the period of AB. The superscript i denotes the value of the associated variable in the ith cycle. t^i_{LP} and t^i_{PY} are delay firing times of LP and PY, respectively, after AB spikes. T^i_{LP} and T^i_{PY} are active durations of LP and PY, respectively. d^i_{LP} is the value of the depression variable for LP at the moment it fires and d^i_{PY} is the value of the depression variable for PY at the moment it fires.

The neurons in this network are modeled by Morris-Lecar type equations.

$$\begin{aligned}\frac{dV_x}{dt} =& -\bar{g}_{Ca} m_\infty(V_x)(V_x - E_{Ca}) - \bar{g}_K W_x(V_x - E_K) - g_L(V_x - E_L) \\ &+ I_{ext\_x} - I_{syn\_x} \\ \frac{dW_x}{dt} =& \frac{W_\infty(V_x) - W_x}{\tau_{W,x}(V_x)}\end{aligned} \tag{4.1}$$

where x represents AB, LP or PY. V_x is the voltage of x, I_{ext_x} is the applied current, E_L is the resting potential of the leak current and E_{Ca} and E_K are reversal potentials for Ca^{2+} and K^+ currents, respectively. g_L is the conductance for the leak current, $\bar{g}_{Ca}$ is the maximal Ca^{2+} conductance and $\bar{g}_K$ is the maximal K^+ conductance. If there is no synaptic input from other neurons, $I_{syn\_x} = 0$, otherwise, I_{syn_x} represents the inhibitory synaptic currents from the presynaptic neurons. W_x is the recovery

variable of K^+. m_∞ and W_∞ are sigmoidal functions of V_x,

$$\begin{aligned} m_\infty(V_x) &= 0.5(1 + tanh\frac{V_x - V_1}{V_2}) \\ W_\infty(V_x) &= 0.5(1 + tanh\frac{V_x - V_3}{V_4}). \end{aligned}$$

where V_1, V_2, V_3 and V_4 are constants related to the shape of the sigmoidal functions. For simplicity, we assume $W_\infty(V_x) = 0$ and $\tau_{W,x}(V_x) = \tau_{W,x}$, on the left branch of the V-nullcline in the phase plane. The synapse for each neuron is modeled by the following equations.

$$\frac{dd_{AB}}{dt} = \begin{cases} \frac{\hat{d}_{AB}(P,T_{AB}) - d_{AB}}{\tau_\alpha} & V_{AB} < V_{th} \\ \frac{-d_{AB}}{\tau_\beta} & V_{AB} > V_{th} \end{cases} \tag{4.2}$$

$$\frac{ds_{AB}}{dt} = \begin{cases} \frac{-s_{AB}}{\tau_\kappa} & V_{AB} < V_{th} \\ \frac{-s_{AB}}{\tau_\zeta} & V_{AB} > V_{th} \end{cases} \tag{4.3}$$

$$\frac{dd_{PY}}{dt} = \begin{cases} \frac{\hat{d}_{PY}(P,T_{PY}) - d_{PY}}{\tau_a} & V_{PY} < V_{th} \\ \frac{-d_{PY}}{\tau_b} & V_{PY} > V_{th} \end{cases} \tag{4.4}$$

$$\frac{ds_{PY}}{dt} = \begin{cases} \frac{-s_{PY}}{\tau_1} & V_{PY} < V_{th} \\ \frac{-s_{PY}}{\tau_2} & V_{PY} > V_{th} \end{cases} \tag{4.5}$$

$$\frac{dd_{LP}}{dt} = \begin{cases} \frac{\hat{d}_{LP}(P,T_{LP}) - d_{LP}}{\tau_c} & V_{LP} < V_{th} \\ \frac{-d_{LP}}{\tau_d} & V_{LP} > V_{th} \end{cases} \tag{4.6}$$

$$\frac{ds_{LP}}{dt} = \begin{cases} \frac{-s_{LP}}{\tau_3} & V_{LP} < V_{th} \\ \frac{-s_{LP}}{\tau_4} & V_{LP} > V_{th} \end{cases} \tag{4.7}$$

where V_{th} represents the threshold of the active state. s_x is the gating variable for x and d_x is the depression variable. They evolve according to the above equations. When x fires, s_x is set to the value of d_x at that moment. The traces of these two

variables were shown in Figure 3.9 of Chapter 3. When $V_x < V_{th}$, d_x increases towards $\hat{d}_x(P, T_x)$, where $\hat{d}_x(P, T_x)$ is an increasing function of $P - T_x$. Specifically,

$$\begin{aligned} \hat{d}_{AB}(P) &= (1 + tanh((P - P_1)/x_1)/2 \\ \hat{d}_{LP}(P, T_{LP}) &= (1 + tanh((P - T_{LP} - P_2)/x_2)/2 \end{aligned}$$

In these two equations, P_1 determines the half-activation time of $\hat{d}_{AB}$ and x_1 determines the steepness of $\hat{d}_{AB}$. We use this function as $\hat{d}_{AB}$, instead of a constant value, to model the dependency of recovery from depression on the cycle period of the neuron, which provide a better approximation of the two time scales of recovery observed in the pyloric synapses [62]. Similarly, P_2 determines the half-activation time of $\hat{d}_{LP}$ and x_2 determines the steepness of $\hat{d}_{LP}$. We assume $\hat{d}_{PY} = 1$ for simplicity.

In this feed-forward network, AB sends feed-forward inhibitory synapses to LP and PY which mutually inhibit one another. For the LP neuron, it is inhibited by AB and PY, thus,

$$I_{syn\_LP} = \bar{g}_{AB} s_{AB}(V_{LP} - E_{inh}) + \bar{g}_{PY} s_{PY}(V_{LP} - E_{inh})$$

where $\bar{g}_{AB}$ and $\bar{g}_{PY}$ are the maximal synaptic conductances of AB and PY, respectively, and E_{inh} is the reversal potential of the inhibitory synapse. Similarly, the PY neuron receives inhibition from AB and LP, thus,

$$I_{syn\_PY} = \bar{g}_{AB} s_{AB}(V_{PY} - E_{inh}) + \bar{g}_{LP} s_{LP}(V_{PY} - E_{inh})$$

where $\bar{g}_{LP}$ is the maximal conductance of LP.

In the following, we derive a 4D map for the activity of this feed-forward network, based on the delay firing times and depression variable values in a cycle.

First, we examine how the relative firing time of LP in the $(i+1)$th cycle t_{LP}^{i+1} depends on the variables in the ith cycle. As shown in Figure 4.2, at the beginning of the $(i+1)$th cycle, LP is silent, inhibited by AB and PY. The firing of AB sends

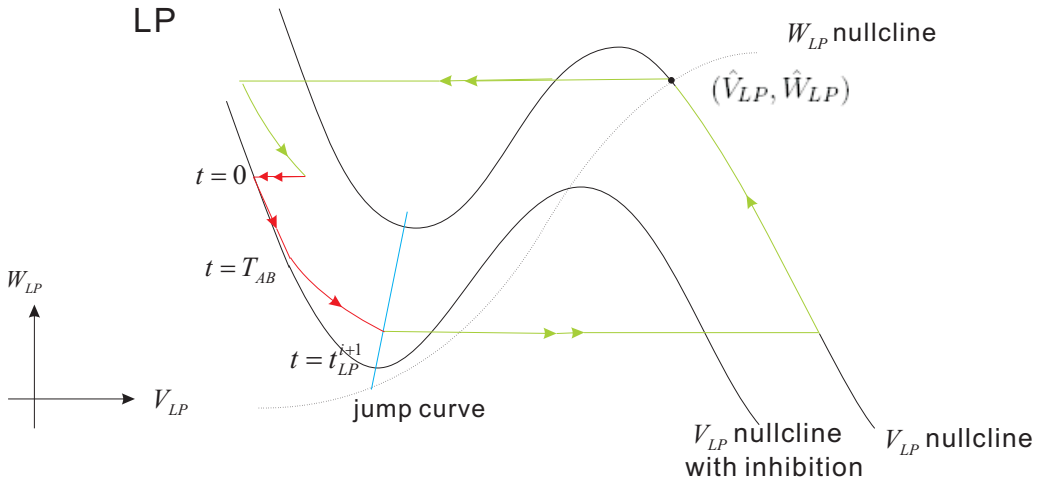

Figure 4.3 Trajectory of LP in the phase plane $V_{LP} - W_{LP}$. Without synaptic input, LP has a high-voltage resting potential. When PY fires, LP jumps to the left branch of the lower V_{LP}-nullcline. When $t = 0$, AB fires and LP gets inhibited more, LP fires until it reaches its jump curve (blue line). The arrowed trajectory shows the trajectory of LP during a cycle. The red part is the trajectory of LP after AB firing and before it turns active, corresponding to the time t_{LP}^{i+1}.

LP an inhibitory synapse with strength $\bar{g}_{AB} s^*_{AB}$, where $s^*_{AB} = d^*_{AB}$, which we assume constant in the feed-forward network. According to Equation (4.3), s_{AB} decays with time constant τ_ζ during the time AB is active, then after the active duration of AB, s_{AB} decays with time constant τ_κ, usually, $\tau_\zeta \gg \tau_\kappa$. The synapse from PY decays with time constant τ_1. LP escapes from the inhibition and becomes active at $t = t_{LP}^{i+1}$. In the phase plane analysis, the trajectory of LP is shown in Figure 4.3. $(\hat{V}_{LP}, \hat{W}_{LP})$ is the fixed point of the dynamical system for LP without synaptic input. When PY fires, LP jumps from $(\hat{V}_{LP}, \hat{W}_{LP})$ to the lower V_{LP}-nullcline and travels along the gradually rising nullclines. When AB fires, i.e., $t = 0$ in the $(i+1)$th cycle, LP is pushed away to a lower nullcline due to the inhibition from AB, then travels downwards along the rising V_{LP}-nullclines until it reaches its jump curve at $t = t_{LP}^{i+1}$. The jump curve is formed by the local minima of the V-nullclines with different synaptic strength values from presynaptic neurons. The cell can jump to the active state when it reaches any local minimum of the V-nullcline, i.e., when it reaches

its jump curve [7, 62]. Therefore, t_{LP}^{i+1} is determined by the synaptic strength from AB neuron, the active duration of AB and the position of LP on the left branch of the V-nullcline at the instant AB fires. The first two factors are fixed if there is no feedback synapse from LP to AB, therefore, t_{LP}^{i+1} is determined by the last factor, the initial position of LP at the beginning of the $(i+1)$the cycle. In the ith cycle, the firing of PY stops the active state of LP and forces LP to jump to the left branch of its V-nullcline. There it evolves in the silent state along the slowly rising nullclines due to the decay of s_{PY}. Therefore, the position of LP when AB fires is determined by d_{PY}^{i}, the synaptic strength of PY when it fires, and T_{PY}^{i}, the duration of PY (Figure 4.2) and $T_{PY}^{i} = P - t_{PY}^{i}$, where P is the period of AB. So, the delay firing time of LP in the $(i+1)$th cycle is determined by the delay firing time of PY in the previous cycle t_{PY}^{i} as well as the synaptic strength from PY d_{PY}^{i}. We use the function h to denote this relation, $t_{LP}^{i+1} = h(t_{PY}^{i}, d_{PY}^{i})$. Now we derive the specific form of this function according to the equations of the model. t_{LP}^{i+1} is the time for LP to evolve from the initial position when $t = 0$ to reach the jump curve. In [7, 62] this curve is assumed to be a linear relation that can be expressed as

$$\bar{g}_{AB} s_{AB} + \bar{g}_{PY} s_{PY} + M_1 W_{LP} = g_{syn1}^{*} \tag{4.8}$$

where M_1 is related to the slope of the LP jump curve and g_{syn1}^{*} is related to the level of inhibitory synaptic input needed to make the V_{LP}-nullcline tangent to the W_{LP}-nullcline. Both are positive numbers and determined by the intrinsic properties of the neuron. At the time $t = t_{LP}^{i+1}$, according to Equations (4.3) and (4.5),

$$\begin{aligned} s_{AB}(t_{LP}^{i+1}) &= d_{AB}^{*} exp(-\frac{T_{AB}}{\tau_\zeta}) exp(-\frac{t_{LP}^{i+1} - T_{AB}}{\tau_\kappa}) \\ s_{PY}(t_{LP}^{i+1}) &= d_{PY}^{i} exp(-\frac{T_{PY}^{i}}{\tau_2}) exp(-\frac{t_{LP}^{i+1}}{\tau_1}) \end{aligned}$$

Since $T^i_{PY} = P - t^i_{PY}$, the second equation can be rewritten as

$$s_{PY}(t^{i+1}_{LP}) = d^i_{PY} exp(-\frac{P - t^i_{PY}}{\tau_2}) exp(-\frac{t^{i+1}_{LP}}{\tau_1})$$

With the assumption that in Equation (4.1), $W_\infty(V_{LP})$=0 and $\tau_{W,LP}(V_{LP})$ is a constant $\tau_{W,LP}$ on the left branch of the V-nullcline,

$$\begin{aligned} W_{LP}(t^{i+1}_{LP}) &= \hat{W}_{LP} exp(-\frac{T^i_{PY} + t^{i+1}_{LP}}{\tau_{W,LP}}) \\ &= \hat{W}_{LP} exp(-\frac{P - t^i_{PY} + t^{i+1}_{LP}}{\tau_{W,LP}}) \end{aligned}$$

So, at the moment LP fires in the $(i+1)$th cycle, (4.8) can be expressed as the following equation

$$\begin{aligned} &\bar{g}_{AB} d^*_{AB} exp(-\frac{T_{AB}}{\tau_\zeta}) exp(-\frac{t^{i+1}_{LP} - T_{AB}}{\tau_\kappa}) + \bar{g}_{PY} d^i_{PY} exp(-\frac{P - t^i_{PY}}{\tau_2}) exp(-\frac{t^{i+1}_{LP}}{\tau_1}) \\ &+ M_1 \hat{W}_{LP} exp(-\frac{P - t^i_{PY} + t^{i+1}_{LP}}{\tau_{W,LP}}) = g^*_{syn1} \end{aligned} \tag{4.9}$$

The partial derivative of the left-hand side function of (4.9) with respect to t^{i+1}_{LP} is not equal to 0, which implies that given the values of t^i_{PY} and d^i_{PY} in the ith cycle, t^{i+1}_{LP} can be obtained from this equation by Implicit Function Theorem. Let $t^{i+1}_{LP} = h(t^i_{PY}, d^i_{PY})$, where h function can not be explicitly expressed, but implicitly reflects the relation between t^i_{PY}, d^i_{PY} and t^{i+1}_{LP}.

The depression variable value of LP in the $(i+1)$th cycle d^{i+1}_{LP} depends on d^i_{LP}, T^i_{LP} and the inactive time of LP in the $i$the cycle $T^i_{PY} + t^{i+1}_{LP}$. From Equation (4.6),

$$d^{i+1}_{LP} = \hat{d}_{LP}(P, T^i_{LP}) - [\hat{d}_{LP}(P, T^i_{LP}) - d^i_{LP} exp(-\frac{T^i_{LP}}{\tau_d})] exp(-\frac{T^i_{PY} + t^{i+1}_{LP}}{\tau_c})$$

where $T^i_{LP} = t^i_{PY} - t^i_{LP}$ and $T^i_{PY} = P - t^i_{PY}$. So,

$$d^{i+1}_{LP} = \hat{d}_{LP}(P, T^i_{LP}) - [\hat{d}_{LP}(P, T^i_{LP}) - d^i_{LP} exp(-\frac{t^i_{PY} - t^i_{LP}}{\tau_d})] exp(-\frac{P - t^i_{PY} + t^{i+1}_{LP}}{\tau_c}) \tag{4.10}$$

where

$$\hat{d}_{LP}(P, T^i_{LP}) = (1 + tanh((P - t^i_{PY} + t^i_{LP} - P_2)/x_2)/2$$

If we write the right hand side of (4.10) as a function l, then $d^{i+1}_{LP} = l(t^i_{LP}, d^i_{LP}, t^i_{PY}, t^{i+1}_{LP})$, where t^{i+1}_{LP} is given by the map h.

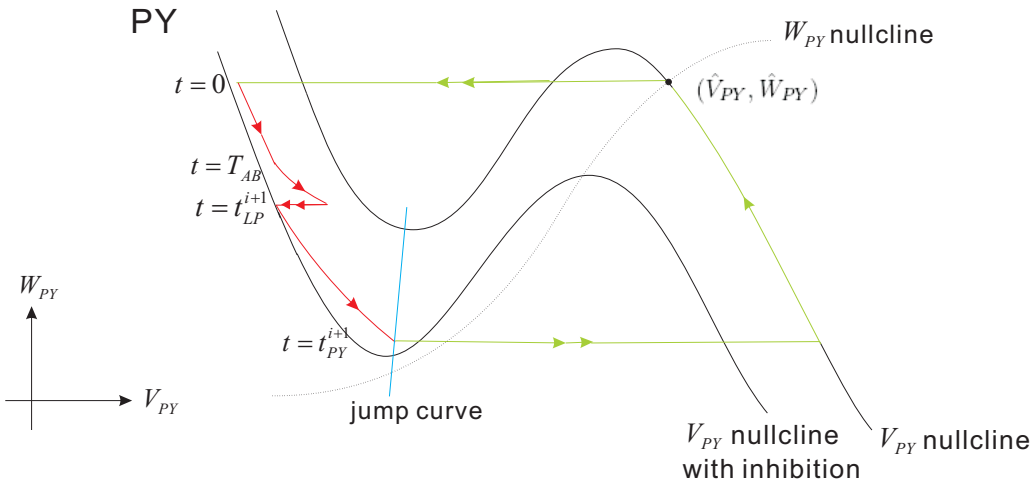

Figure 4.4 Trajectory of PY in the phase plane $V_{PY} - W_{PY}$. Without synaptic input, PY has a high-voltage resting potential. When $t = 0$, AB fires and LP jumps to the left branch of the lower V_{PY}-nullcline. When $t = t^{i+1}_{LP}$, LP fires and PY get inhibited more, PY fires until it reaches its jump curve (blue line). The arrowed trajectory shows the trajectory of PY during a cycle. The red part is the trajectory of PY after AB firing and before it turns active, corresponding to the time t^{i+1}_{PY}.

Now we derive the delay firing time for PY, t^{i+1}_{PY}. The termination of the firing of PY neuron is due to the spiking of AB (Figure 4.2), so PY leaves its high-voltage fixed point $(\hat{V}_{PY}, \hat{W}_{PY})$ when AB fires (Figure 4.4), i.e., at the beginning of the $(i+1)$th cycle. PY is inhibited by AB together with the decreasing synapse from LP before LP's firing. The trajectory is shown in Figure 4.4. At $t = t^{i+1}_{LP}$, LP fires and sends an inhibitory synapse to PY with strength $\bar{g}_{LP} s^{i+1}_{LP} = \bar{g}_{LP} d^{i+1}_{LP}$. This inhibition pushes down the V-nullcline of PY. PY evolves along the gradually increasing V_{PY}-nullcline until it reaches the jump curve, which gives the time t^{i+1}_{PY}. This jump curve is also

expressed as a linear function,

$$\bar{g}_{AB}s_{AB} + \bar{g}_{LP}s_{LP} + M_2 W_{PY} = g^*_{syn2} \tag{4.11}$$

where M_2 and g^*_{syn2} are positive numbers, M_2 related to the slope of the PY jump curve and g^*_{syn2} related to the level of inhibitory synaptic input needed to make the V_{PY}-nullcline tangent to the W_{PY}-nullcline. At $t = t^{i+1}_{PY}$, from Equations (4.3) and (4.7),

$$\begin{aligned} s_{AB}(t^{i+1}_{PY}) &= d^*_{AB} exp(-\frac{T_{AB}}{\tau_\zeta}) exp(-\frac{t^{i+1}_{PY} - T_{AB}}{\tau_\kappa}) \\ s_{LP}(t^{i+1}_{PY}) &= d^{i+1}_{LP} exp(-\frac{T^{i+1}_{LP}}{\tau_4}) \\ &= d^{i+1}_{LP} exp(-\frac{t^{i+1}_{PY} - t^{i+1}_{LP}}{\tau_4}) \end{aligned}$$

At this time,

$$W_{PY}(t^{i+1}_{PY}) = \hat{W}_{PY} exp(-\frac{t^{i+1}_{PY}}{\tau_{W,PY}})$$

Substituting these three equations into (4.11), we obtain the following equation

$$\begin{aligned} &\bar{g}_{AB} d^*_{AB} exp(-\frac{T_{AB}}{\tau_\zeta}) exp(-\frac{t^{i+1}_{PY} - T_{AB}}{\tau_\kappa}) + \bar{g}_{LP} d^{i+1}_{LP} exp(-\frac{t^{i+1}_{PY} - t^{i+1}_{LP}}{\tau_4}) \\ &+ M_2 \hat{W}_{PY} exp(-\frac{t^{i+1}_{PY}}{\tau_{W,PY}}) = g^*_{syn2} \end{aligned} \tag{4.12}$$

This equation implicitly gives the dependence of t^{i+1}_{PY} on the variables t^{i+1}_{LP} and d^{i+1}_{LP}. We express this relation as a function f, $t^{i+1}_{PY} = f(t^{i+1}_{LP}, d^{i+1}_{LP})$, where t^{i+1}_{LP} and d^{i+1}_{LP} are given by the maps h and l, respectively.

The value of the depression variable d_{PY} when PY fires in the $(i+1)$th cycle d^{i+1}_{PY} can be found via Equation (4.4) and the assumption $\hat{d}_{PY} = 1$.

$$d^{i+1}_{PY} = 1 - [1 - d^i_{PY} exp(-\frac{P - t^i_{PY}}{\tau_b})] exp(-\frac{t^{i+1}_{PY}}{\tau_a}) \tag{4.13}$$

We define this relation as a function g and $d_{PY}^{i+1} = g(t_{PY}^i, d_{PY}^i, t_{PY}^{i+1})$, where d_{PY}^{i+1} is given by the map f. Thus,

$$\begin{cases} t_{LP}^{i+1} = h(t_{PY}^i, d_{PY}^i) \\ d_{LP}^{i+1} = l(t_{LP}^i, d_{LP}^i, t_{PY}^i, t_{LP}^{i+1}) \\ t_{PY}^{i+1} = f(t_{LP}^{i+1}, d_{LP}^{i+1}) \\ d_{PY}^{i+1} = g(t_{PY}^i, d_{PY}^i, t_{PY}^{i+1}) \end{cases} \tag{4.14}$$

which can be rewritten as

$$\begin{cases} t_{LP}^{i+1} = h(t_{PY}^i, d_{PY}^i) \\ d_{LP}^{i+1} = l(t_{LP}^i, d_{LP}^i, t_{PY}^i, h(t_{PY}^i, d_{PY}^i)) \\ t_{PY}^{i+1} = f(h(t_{PY}^i, d_{PY}^i), l(t_{LP}^i, d_{LP}^i, t_{PY}^i, h(t_{PY}^i, d_{PY}^i))) \\ d_{PY}^{i+1} = g(t_{PY}^i, d_{PY}^i, f(h(t_{PY}^i, d_{PY}^i), l(t_{LP}^i, d_{LP}^i, t_{PY}^i, h(t_{PY}^i, d_{PY}^i)))) \end{cases}$$

where the functions h, l, f and g are given by (4.9), (4.10), (4.12) and (4.13), respectively.

Therefore, we have derived a 4D map for the activity of the feed-forward network in which AB sends inhibitory synapses to LP and PY which are mutually inhibited. This map is based on the delay firing time of LP and PY as well as the depression variables at the moment LP or PY fires. The fixed point of this map corresponds to the phase-locked activity of the feed-forward tri-phasic pyloric network.

The fixed point of this map $(t^*_{LP}, d^*_{LP}, t^*_{PY}, d^*_{PY})$ can be obtained by numerically solving the following equations.

$$\begin{cases} \bar{g}_{AB} d^*_{AB} exp(-\frac{T_{AB}}{\tau_\zeta}) exp(-\frac{t^*_{LP}-T_{AB}}{\tau_\kappa}) + \bar{g}_{PY} d^*_{PY} exp(-\frac{P-t^*_{PY}}{\tau_2}) exp(-\frac{t^*_{LP}}{\tau_1}) \\ +M_1 \hat{W}_{LP} exp(-\frac{P-t^*_{PY}+t^*_{LP}}{\tau_{W,LP}}) = g^*_{syn1} \\ d^*_{LP} = \hat{d}_{LP}(P, T^*_{LP}) \frac{1-exp(-\frac{P-t^*_{PY}+t^*_{LP}}{\tau_c})}{1-exp(-\frac{t^*_{PY}-t^*_{LP}}{\tau_d}) exp(-\frac{P-t^*_{PY}+t^*_{LP}}{\tau_c})} \\ \bar{g}_{AB} d^*_{AB} exp(-\frac{T_{AB}}{\tau_\zeta}) exp(-\frac{t^*_{PY}-T_{AB}}{\tau_\kappa}) + \bar{g}_{LP} d^*_{LP} exp(-\frac{t^*_{PY}-t^*_{LP}}{\tau_4}) \\ +M_2 \hat{W}_{PY} exp(-\frac{t^*_{PY}}{\tau_{W,PY}}) = g^*_{syn2} \\ d^*_{PY} = \frac{1-exp(-\frac{t^*_{PY}}{\tau_a})}{1-exp(-\frac{P-t^*_{PY}}{\tau_b}) exp(-\frac{t^*_{PY}}{\tau_a})} \end{cases} \tag{4.15}$$

The stability of the fixed point can be examined from the eigenvalues of the Jacobian for the 4D map (4.14).

$$\mathrm{J}= \begin{pmatrix} J_{11} & J_{12} & J_{13} & J_{14} \\ J_{21} & J_{22} & J_{23} & J_{24} \\ J_{31} & J_{32} & J_{33} & J_{34} \\ J_{41} & J_{42} & J_{43} & J_{44} \end{pmatrix} = \begin{pmatrix} \frac{\partial h}{\partial t_{LP}} & \frac{\partial h}{\partial d_{LP}} & \frac{\partial h}{\partial t_{PY}} & \frac{\partial h}{\partial d_{PY}} \\ \frac{\partial l}{\partial t_{LP}} & \frac{\partial l}{\partial d_{LP}} & \frac{\partial l}{\partial t_{PY}} & \frac{\partial l}{\partial d_{PY}} \\ \frac{\partial f}{\partial t_{LP}} & \frac{\partial f}{\partial d_{LP}} & \frac{\partial f}{\partial t_{PY}} & \frac{\partial f}{\partial d_{PY}} \\ \frac{\partial g}{\partial t_{LP}} & \frac{\partial g}{\partial d_{LP}} & \frac{\partial g}{\partial t_{PY}} & \frac{\partial g}{\partial d_{PY}} \end{pmatrix}_{(t^*_{LP}, d^*_{LP}, t^*_{PY}, d^*_{PY})}$$

If the eigenvalues of this matrix are all located inside the unit circle, the fixed point is stable, otherwise, it is unstable. Below we will consider specific parameter values and discuss stability.

4.2 Activity of the Tri-phasic Pyloric Network with the Feedback Synapse from LP to AB/PD

With the feedback synapse from LP to AB, we examine how the relative firing time of LP with respect to the firing of AB affects the period of AB. In the feedback network, the period of AB is not fixed but changes cycle by cycle depending on the different relative firing time of LP. Here we assume the firing of LP affects the inactive

duration of AB, so the active duration T_{AB} is fixed. But, the synaptic strength will change cycle by cycle due to the period variation. The period of AB in the ith cycle is denoted as P^i and the value of the depression variable when AB spikes is denoted as d^i_{AB}, $i = 1, 2, \cdots$. A schematic plot for the voltage traces of AB, LP and PY is shown in Figure 4.5. Because of the existence of the feedback synapse from LP to AB, there are two more variables to be considered in the map, the period of AB P^i and its depression variable d_{AB}.

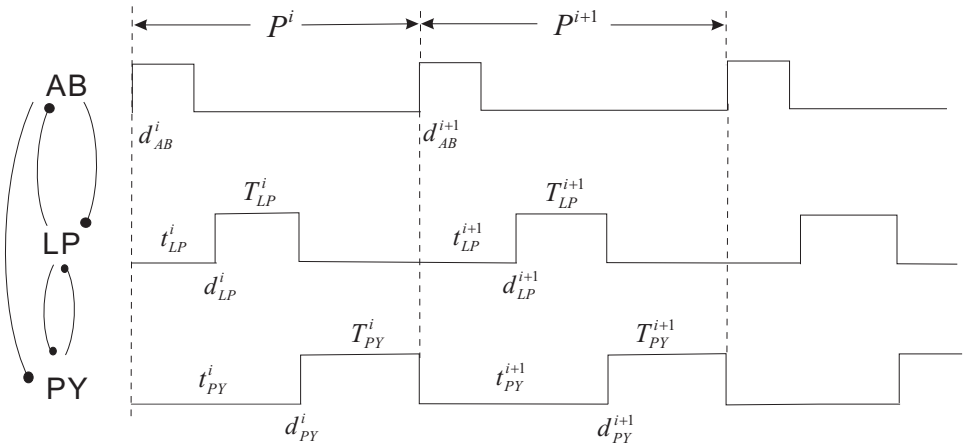

Figure 4.5 Voltage traces of neurons AB, LP and PY in the feedback tri-phasic pyloric network of STG. AB sends inhibitory synapses to LP and PY which mutually inhibited one another and there's a feedback inhibitory synapse from LP to AB. P^i is the period of AB in ith cycle and d^i_{AB} is the depression variable value of AB when it fires. The other notation is the same as in Figure 4.2.

In the feed-forward network, the relative firing time of LP in the $(i+1)$th cycle is determined by the relative firing time of PY and the depression variable of PY in the ith cycle, $t^{i+1}_{LP} = h(t^i_{PY}, d^i_{PY})$. In the feedback network, the inhibitory strength from AB when it fires is $\bar{g}_{AB} d^i_{AB}$ and the active duration of PY is $T^i_{PY} = P^i - t^i_{PY}$. LP fires when it reaches its jump curve (Figure 4.3) and Equation (4.8) is still used

to calculate the delay firing time of LP. At $t = t_{LP}^{i+1}$,

$$\begin{aligned} s_{AB}(t_{LP}^{i+1}) &= d_{AB}^{i+1} exp(-\frac{T_{AB}}{\tau_\zeta}) exp(-\frac{t_{LP}^{i+1} - T_{AB}}{\tau_\kappa}) \\ s_{PY}(t_{LP}^{i+1}) &= d_{PY}^{i} exp(-\frac{T_{PY}^{i}}{\tau_2}) exp(-\frac{t_{LP}^{i+1}}{\tau_1}) \end{aligned}$$

Since $T_{PY}^i = P^i - t_{PY}^i$, the second equation is rewritten as

$$s_{PY}(t_{LP}^{i+1}) = d_{PY}^{i} exp(-\frac{P^i - t_{PY}^{i}}{\tau_2}) exp(-\frac{t_{LP}^{i+1}}{\tau_1})$$

And

$$\begin{aligned} W_{LP}(t_{LP}^{i+1}) &= \hat{W}_{LP} exp(-\frac{T_{PY}^{i} + t_{LP}^{i+1}}{\tau_{W,LP}}) \\ &= \hat{W}_{LP} exp(-\frac{P^i - t_{PY}^{i} + t_{LP}^{i+1}}{\tau_{W,LP}}) \end{aligned}$$

Substitute the functions for $s_{AB}(t_{LP}^{i+1})$, $s_{PY}(t_{LP}^{i+1})$ and $W_{LP}(t_{LP}^{i+1})$ into (4.8),

$$\begin{aligned} &\bar{g}_{AB} d_{AB}^{i+1} exp(-\frac{T_{AB}}{\tau_\zeta}) exp(-\frac{t_{LP}^{i+1} - T_{AB}}{\tau_\kappa}) + \bar{g}_{PY} d_{PY}^{i} exp(-\frac{P^i - t_{PY}^{i}}{\tau_2}) exp(-\frac{t_{LP}^{i+1}}{\tau_1}) \\ &+ M_1 \hat{W}_{LP} exp(-\frac{P^i - t_{PY}^{i} + t_{LP}^{i+1}}{\tau_{W,LP}}) = g_{syn1}^{*} \end{aligned} \tag{4.16}$$

The delay firing time of LP in the $(i+1)$th cycle t_{LP}^{i+1} depends on t_{PY}^i, d_{PY}^i, P^i and d_{AB}^{i+1}. Let $t_{LP}^{i+1} = \tilde{h}(t_{PY}^i, d_{PY}^i, P^i, d_{AB}^{i+1})$, where $\tilde{h}$ implicitly expresses the dependence of t_{LP}^{i+1} on the other four variables.

To determine the value of the depression variable of LP in the $(i+1)$th cycle d_{LP}^{i+1}, the information needed from the previous cycle is t_{LP}^i, $T_{LP}^i = t_{PY}^i - t_{LP}^i$ and the inactive duration of LP $T_{PY}^i + t_{LP}^{i+1} = P^i - t_{PY}^i + t_{LP}^{i+1}$. According to (4.6),

$$d_{LP}^{i+1} = \hat{d}_{LP}(P^i, T_{LP}^i) - [\hat{d}_{LP}(P^i, T_{LP}^i) - d_{LP}^i exp(-\frac{t_{PY}^i - t_{LP}^i}{\tau_d})] exp(-\frac{P^i - t_{PY}^i + t_{LP}^{i+1}}{\tau_c}) \tag{4.17}$$

where

$$\hat{d}_{LP}(P^i, T_{LP}^i) = (1 + tanh((P^i - t_{PY}^i + t_{LP}^i - P_2)/x_2))/2$$

If we write the right hand side function as $\tilde{l}$, then $d_{LP}^{i+1} = \tilde{l}(t_{LP}^i, d_{LP}^i, t_{PY}^i, P^i, t_{LP}^{i+1})$, where t_{LP}^{i+1} is given by $\tilde{h}$.

The synaptic strengths of LP to PY and AB are different, so here we use different maximal synaptic conductances to discriminate between these two types of synapses. $\bar{g}_{LP\to PY}$ is used to denote the maximal synaptic conductance of LP to PY and $\bar{g}_{LP\to AB}$ is denoted as the maximal synaptic conductance of LP to AB. We still use Equation (4.11) to derive the maps for the relative firing time of PY in the $(i+1)$th cycle, t_{PY}^{i+1}. When $t = t_{PY}^{i+1}$,

$$\begin{aligned} s_{AB}(t_{PY}^{i+1}) &= d_{AB}^{i+1} exp(-\frac{T_{AB}}{\tau_\zeta}) exp(-\frac{t_{PY}^{i+1} - T_{AB}}{\tau_\kappa}) \\ s_{LP}(t_{PY}^{i+1}) &= d_{LP}^{i+1} exp(-\frac{t_{PY}^{i+1} - t_{LP}^{i+1}}{\tau_4}) \\ W_{PY}(t_{PY}^{i+1}) &= \hat{W}_{PY} exp(-\frac{t_{PY}^{i+1}}{\tau_{W,PY}}) \end{aligned}$$

So, Equation (4.11) at the time $t = t_{PY}^{i+1}$ is

$$\begin{aligned} &\bar{g}_{AB} d_{AB}^{i+1} exp(-\frac{T_{AB}}{\tau_\zeta}) exp(-\frac{t_{PY}^{i+1} - T_{AB}}{\tau_\kappa}) + \bar{g}_{LP\to PY} d_{LP}^{i+1} exp(-\frac{t_{PY}^{i+1} - t_{LP}^{i+1}}{\tau_4}) \\ &+ M_2 \hat{W}_{PY} exp(-\frac{t_{PY}^{i+1}}{\tau_{W,PY}}) = g_{syn2}^* \end{aligned} \tag{4.18}$$

Let $t_{PY}^{i+1} = \tilde{f}(t_{LP}^{i+1}, d_{LP}^{i+1}, d_{AB}^{i+1})$, where t_{LP}^{i+1} is given by $\tilde{h}$, d_{LP}^{i+1} is given by $\tilde{l}$ and d_{AB}^{i+1} will be determined later.

d_{PY}^{i+1} can be calculated from Equation (4.4).

$$d_{PY}^{i+1} = 1 - [1 - d_{PY}^i exp(-\frac{P^i - t_{PY}^i}{\tau_b})] exp(-\frac{t_{PY}^{i+1}}{\tau_a}) \tag{4.19}$$

Let the right hand side function as $\tilde{g}$, thus, $d_{PY}^{i+1} = \tilde{g}(t_{PY}^i, d_{PY}^i, P^i, t_{PY}^{i+1})$, where t_{PY}^{i+1} is give by the map $\tilde{f}$.

So far, we have derived the maps for the four variables, t_{LP}^{i+1}, d_{LP}^{i+1}, t_{PY}^{i+1} and d_{PY}^{i+1} corresponding to the same variables in the feed-forward network. In the following,

we will derive the maps for the other two variables in the feedback network, P^{i+1} and d_{AB}^{i+1}.

First, we derive the map for d_{AB}^{i+1}. From Equation (4.2), d_{AB}^{i} increases with time constant τ_α to $\hat{d}_{AB}(P^i, T_{AB})$ during AB is active and decreases with time constant τ_β when AB is inactive, so

$$d_{AB}^{i+1} = \hat{d}_{AB}(P^i) - [\hat{d}_{AB}(P^i) - d_{AB}^{i} exp(-\frac{T_{AB}}{\tau_\beta})]exp(-\frac{P^i - T_{AB}}{\tau_\alpha}) \tag{4.20}$$

where

$$\hat{d}_{AB}(P^i) = (1 + tanh((P^i - P_1)/x_1))/2$$

The above function gives the map for d_{AB}^{i+1}, $d_{AB}^{i+1} = \tilde{q}(P^i, d_{AB}^{i})$.

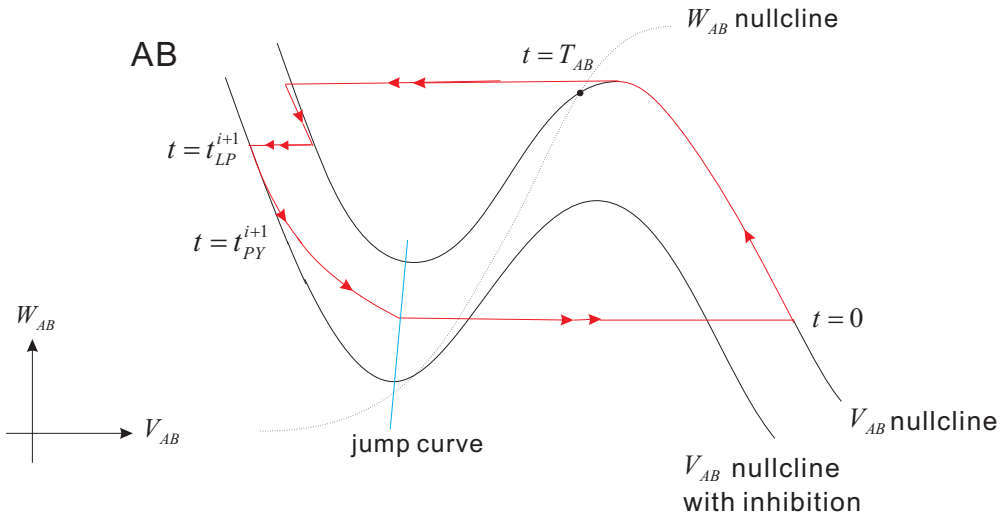

Figure 4.6 Trajectory of AB in the phase plane $V_{AB} - W_{AB}$ in the feedback network with an inhibitory synapse from LP to AB. Without synaptic input, AB is an oscillator. When $t = 0$, AB fires and remains active until $t = T_{AB}$, then AB jumps to the left branch of its V-nullcline. At $t = t_{LP}^{i+1}$, AB jumps to a lower nullcline because of the firing of LP, then AB evolves to reach the jump curve. The red trajectory is a cycle of AB.

Now we derive the map for the last variable P^{i+1}. Since we assume that the feedback synapse from LP to AB only affects the inactive duration of AB, we focus

on examining the trajectory of AB on its left branches of V-nullclines. AB is an oscillator, so in the phase plane, V_{AB}-nullcline and W_{AB} nullcline intersect on the middle branch of the V_{AB}-nullcline (Figure 4.6). When $t = 0$, AB jumps to the active state and spends T_{AB} time on the right branch of the V_{AB}-nullcline to reach the local maximum of V_{AB}-nullcline, $(\hat{V}_{AB}, \hat{W}_{AB})$, then AB jumps to the left branch and travels down according to the W_{AB} equation in (4.1). At $t = t_{LP}^{i+1}$, LP spikes and sends an inhibitory synapse to AB, pushing AB to jump to a lower V_{AB}-nullcline. It takes AB $P^{i+1} - T_{AB}$ time to evolve along the rising V_{AB}-nullclines and reach its jump curve, the blue line in Figure 4.6. The $(i+1)$th cycle ends. The arrowed cycle is the trajectory of AB during $(i+1)$th cycle, which takes P^{i+1} time, i.e., the period of AB in the $(i+1)$th cycle. Let the linear function for the jump curve of AB be

$$\bar{g}_{LP\to AB} s_{LP} + M_3 W_{AB} = g_{syn3}^{*} \tag{4.21}$$

where M_3 is related to the slope of the jump curve and g_{syn3}^{*} is related to the level of inhibition needed to make V_{AB}-nullcline tangent to the W_{AB}-nullcline. Both are positive numbers. At $t = P^{i+1}$, AB jumps to the active state and at that time, by Equations (4.7) and (4.1)

$$\begin{aligned} s_{LP}(P^{i+1}) &= d_{LP}^{i+1} exp(-\frac{T_{LP}^{i+1}}{\tau_4}) exp(-\frac{T_{PY}^{i+1}}{\tau_3}) \\ &= d_{LP}^{i+1} exp(-\frac{t_{PY}^{i+1} - t_{LP}^{i+1}}{\tau_4}) exp(-\frac{P^{i+1} - t_{PY}^{i+1}}{\tau_3}) \\ W_{AB}(P^{i+1}) &= \hat{W}_{AB} exp(-\frac{P^{i+1} - T_{AB}}{\tau_{W,AB}}) \end{aligned}$$

Substitute the above two equations into (4.21), we obtain the equation for the relation between t_{LP}^{i+1}, d_{LP}^{i+1}, t_{PY}^{i+1} and P^{i+1}.

$$\begin{aligned} &\bar{g}_{LP\to AB} d_{LP}^{i+1} exp(-\frac{t_{PY}^{i+1} - t_{LP}^{i+1}}{\tau_4}) exp(-\frac{P^{i+1} - t_{PY}^{i+1}}{\tau_3}) \\ &+ M_3 \hat{W}_{AB} exp(-\frac{P^{i+1} - T_{AB}}{\tau_{W,AB}}) = g_{syn3}^{*} \end{aligned} \tag{4.22}$$

Express P^{i+1} as a function $\tilde{p}$ of t_{LP}^{i+1}, d_{LP}^{i+1} and t_{PY}^{i+1}, $P^{i+1} = \tilde{p}(t_{LP}^{i+1}, d_{LP}^{i+1}, t_{PY}^{i+1})$, where t_{LP}^{i+1} is given by $\tilde{h}$, d_{LP}^{i+1} is given by $\tilde{l}$ and t_{PY}^{i+1} is given by $\tilde{f}$. Thus,

$$\begin{cases} t_{LP}^{i+1} = \tilde{h}(t_{PY}^{i}, d_{PY}^{i}, P^{i}, d_{AB}^{i}) \\ d_{LP}^{i+1} = \tilde{l}(t_{LP}^{i}, d_{LP}^{i}, t_{PY}^{i}, P^{i}, t_{LP}^{i+1}) \\ t_{PY}^{i+1} = \tilde{f}(t_{LP}^{i+1}, d_{LP}^{i+1}, d_{AB}^{i+1}) \\ d_{PY}^{i+1} = \tilde{g}(t_{PY}^{i}, d_{PY}^{i}, P^{i}, t_{PY}^{i+1}) \\ d_{AB}^{i+1} = \tilde{q}(P^{i}, d_{AB}^{i}) \\ P^{i+1} = \tilde{p}(t_{LP}^{i+1}, d_{LP}^{i+1}, t_{PY}^{i+1}) \end{cases} \tag{4.23}$$

where the functions $\tilde{h}$, $\tilde{l}$, $\tilde{f}$, $\tilde{g}$, $\tilde{q}$ and $\tilde{p}$ are given by (4.16), (4.17), (4.18), (4.19), (4.20) and (4.22), respectively. Although there are some variables in the $(i+1)$th cycle appearing in the functions on the right hand side, they all can be substituted by the functions only including the terms in the ith cycle, e.g., the term t_{LP}^{i+1} in $\tilde{l}$ can be replaced by $\tilde{h}$ which only includes the variables in the ith cycle. Therefore, for the network with the feedback inhibitory synapse from LP to AB, we have derived a 6D map based on the delay firing times of LP and PY, the period of AB and the depression variable for each neuron. The fixed point of this map corresponds to the phase-locked activity of the feedback tri-phasic pyloric network.

The fixed point of this 6D map $(t_{LP}^{*}, d_{LP}^{*}, t_{PY}^{*}, d_{PY}^{*}, d_{AB}^{*}, P^{*})$ can be obtained by numerically solving the following equations, which are the corresponding steady state

equations.

$$
\begin{cases}
\bar{g}_{AB} d^*_{AB} exp(-\frac{T_{AB}}{\tau_\zeta}) exp(-\frac{t^*_{LP}-T_{AB}}{\tau_\kappa}) + \bar{g}_{PY} d^*_{PY} exp(-\frac{P^*-t^*_{PY}}{\tau_2}) exp(-\frac{t^*_{LP}}{\tau_1}) \\
+M_1 \hat{W}_{LP} exp(-\frac{P^*-t^*_{PY}+t^*_{LP}}{\tau_{W,LP}}) = g^*_{syn1} \\
d^*_{LP} = \hat{d}_{LP}(P^*, T^*_{LP}) \frac{1-exp(-\frac{P^*-t^*_{PY}+t^*_{LP}}{\tau_c})}{1-exp(-\frac{t^*_{PY}-t^*_{LP}}{\tau_d}) exp(-\frac{P^*-t^*_{PY}+t^*_{LP}}{\tau_c})} \\
\bar{g}_{AB} d^*_{AB} exp(-\frac{T_{AB}}{\tau_\zeta}) exp(-\frac{t^*_{PY}-T_{AB}}{\tau_\kappa}) + \bar{g}_{LP} d^*_{LP} exp(-\frac{t^*_{PY}-t^*_{LP}}{\tau_4}) \\
+M_2 \hat{W}_{PY} exp(-\frac{t^*_{PY}}{\tau_{W,PY}}) = g^*_{syn2} \\
d^*_{PY} = \frac{1-exp(-\frac{t^*_{PY}}{\tau_a})}{1-exp(-\frac{P^*-t^*_{PY}}{\tau_b}) exp(-\frac{t^*_{PY}}{\tau_a})} \\
d^*_{AB} = \hat{d}_{AB}(P^*) \frac{1-exp(-\frac{P^*-T_{AB}}{\tau_\alpha})}{1-exp(-\frac{T_{AB}}{\tau_\beta}) exp(-\frac{P^*-T_{AB}}{\tau_\alpha})} \\
\bar{g}_{LP\to AB} d^*_{LP} exp(-\frac{t^*_{PY}-t^*_{LP}}{\tau_4}) exp(-\frac{P^*-t^*_{PY}}{\tau_3}) \\
+M_3 \hat{W}_{AB} exp(-\frac{P^*-T_{AB}}{\tau_{W,AB}}) = g^*_{syn3}
\end{cases}
\tag{4.24}
$$

The stability of the fixed point can be examined from the eigenvalues of the Jacobian for the 6D map (4.23).

$$
J = \begin{pmatrix}
J_{11} & J_{12} & J_{13} & J_{14} & J_{15} & J_{16} \\
J_{21} & J_{22} & J_{23} & J_{24} & J_{25} & J_{26} \\
J_{31} & J_{32} & J_{33} & J_{34} & J_{35} & J_{36} \\
J_{41} & J_{42} & J_{43} & J_{44} & J_{45} & J_{46} \\
J_{51} & J_{52} & J_{53} & J_{54} & J_{55} & J_{66} \\
J_{61} & J_{62} & J_{63} & J_{64} & J_{65} & J_{66}
\end{pmatrix}
$$

$$= \begin{pmatrix} \frac{\partial h}{\partial t_{LP}} & \frac{\partial h}{\partial d_{LP}} & \frac{\partial h}{\partial t_{PY}} & \frac{\partial h}{\partial d_{PY}} & \frac{\partial h}{\partial d_{AB}} & \frac{\partial h}{\partial P} \\ \frac{\partial l}{\partial t_{LP}} & \frac{\partial l}{\partial d_{LP}} & \frac{\partial l}{\partial t_{PY}} & \frac{\partial l}{\partial d_{PY}} & \frac{\partial l}{\partial d_{AB}} & \frac{\partial l}{\partial P} \\ \frac{\partial f}{\partial t_{LP}} & \frac{\partial f}{\partial d_{LP}} & \frac{\partial f}{\partial t_{PY}} & \frac{\partial f}{\partial d_{PY}} & \frac{\partial f}{\partial d_{AB}} & \frac{\partial f}{\partial P} \\ \frac{\partial g}{\partial t_{LP}} & \frac{\partial g}{\partial d_{LP}} & \frac{\partial g}{\partial t_{PY}} & \frac{\partial g}{\partial d_{PY}} & \frac{\partial g}{\partial d_{AB}} & \frac{\partial g}{\partial P} \\ \frac{\partial q}{\partial t_{LP}} & \frac{\partial q}{\partial d_{LP}} & \frac{\partial q}{\partial t_{PY}} & \frac{\partial q}{\partial d_{PY}} & \frac{\partial q}{\partial d_{AB}} & \frac{\partial q}{\partial P} \\ \frac{\partial p}{\partial t_{LP}} & \frac{\partial p}{\partial d_{LP}} & \frac{\partial p}{\partial t_{PY}} & \frac{\partial p}{\partial d_{PY}} & \frac{\partial p}{\partial d_{AB}} & \frac{\partial p}{\partial P} \end{pmatrix}$$

If the eigenvalues of this matrix are all located inside the unit circle, the fixed point is stable, otherwise, it is unstable. If the fixed point in the feedback network is the same as that in the feed-forward network, each entry of the 4×4 submatrix consisting of the first four rows and columns in the above 6×6 matrix has the same value as the corresponding entry of the 4×4 matrix for the feed-forward network.

4.3 Effect of the Inhibitory Feedback Synapse from LP to AB/PD

In the feed-forward network without the inhibitory synapse from LP to AB, we examine how the period of the pacemaker AB affects the phase of LP or PY, which is defined as the proportion of the relative firing time to the network period. Figure 4.7 is an example of the relation between the period of AB and the phases of LP and PY. The magenta solid curve shows the dependence of the phase of LP on the period of AB, obtained by directly solving Equation (4.15) for the fixed point. The cyan solid curve shows the dependence of the phase of PY on the period of AB from solving Equation (4.15). The red dotted curve and the green starred curve are obtained from the iteration of the map (4.14). The red curve shows the phase of LP and the green curve shows the phase of PY. They overlap with the magenta solid curve and the cyan solid curve, respectively, in most of the domain, except in a small range, $1205 \leq P \leq 1317$. In this range, the map does converge to a fixed number, but

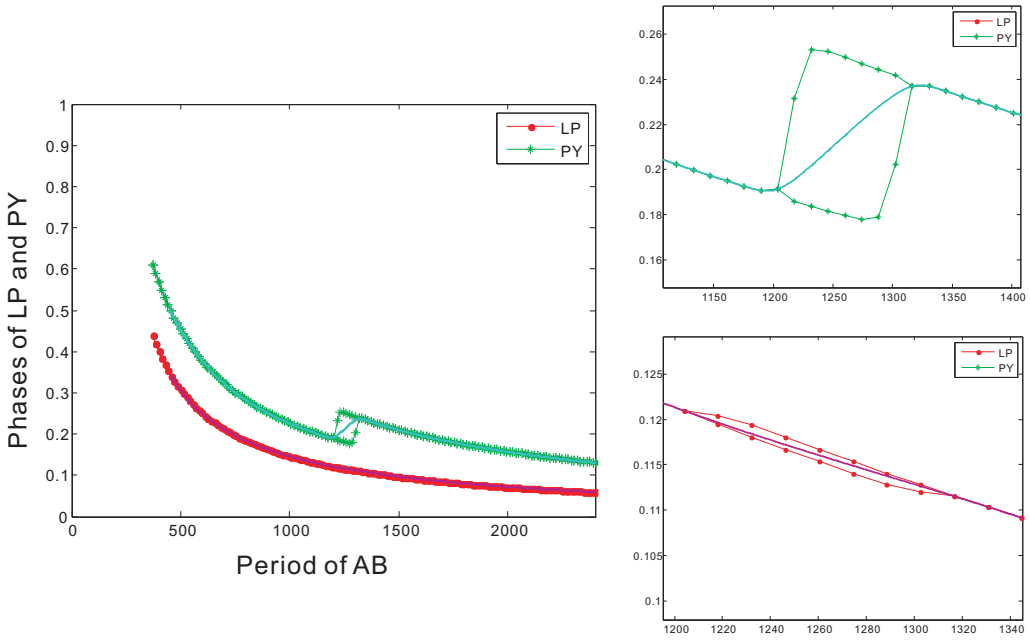

Figure 4.7 The relationship between the phases of LP and PY and the period of AB in the feed-forward network. The solid curves are obtained from directly solving Equation (4.15), the magenta curve for the phase of LP and the cyan curve for the phase of PY. The dotted and starred curves are obtained from iteration of map (4.14), the red dotted curve is for the phase of LP and the green starred curve is for the phase of PY. Note that the feed-forward synapses from AB to LP and PY are non-depressing. When $1205 \leq P \leq 1317$, the map does not converge, corresponding to a period-2 phase-locked solution. The upper right panel of the zoom-in of this part is for the phase of LP and the lower right panel of the zoom-in of this part is for the phase of PY.

alternates between two numbers, which implies a period-2 phase-locked solution for the network. Later we will prove that the fixed point in this region is not stable by calculating the eigenvalues of the Jacobian for the map and showing one of the four eigenvalues is outside of the unit circle.

In the feedback network, we use the same parameter values as in the feed-forward network and increase the synaptic strength from LP to AB, $\bar{g}_{LP\to AB}$. The period-2 region becomes smaller with a stronger synapse and disappears when $\bar{g}_{LP\to AB}$ is big enough. Figure 4.8 shows the dependence of the phases on the period for $\bar{g}_{LP\to AB} = 20$ and $\bar{g}_{LP\to AB} = 27$. When $\bar{g}_{LP\to AB} = 20$, the period-2 region is much smaller than in

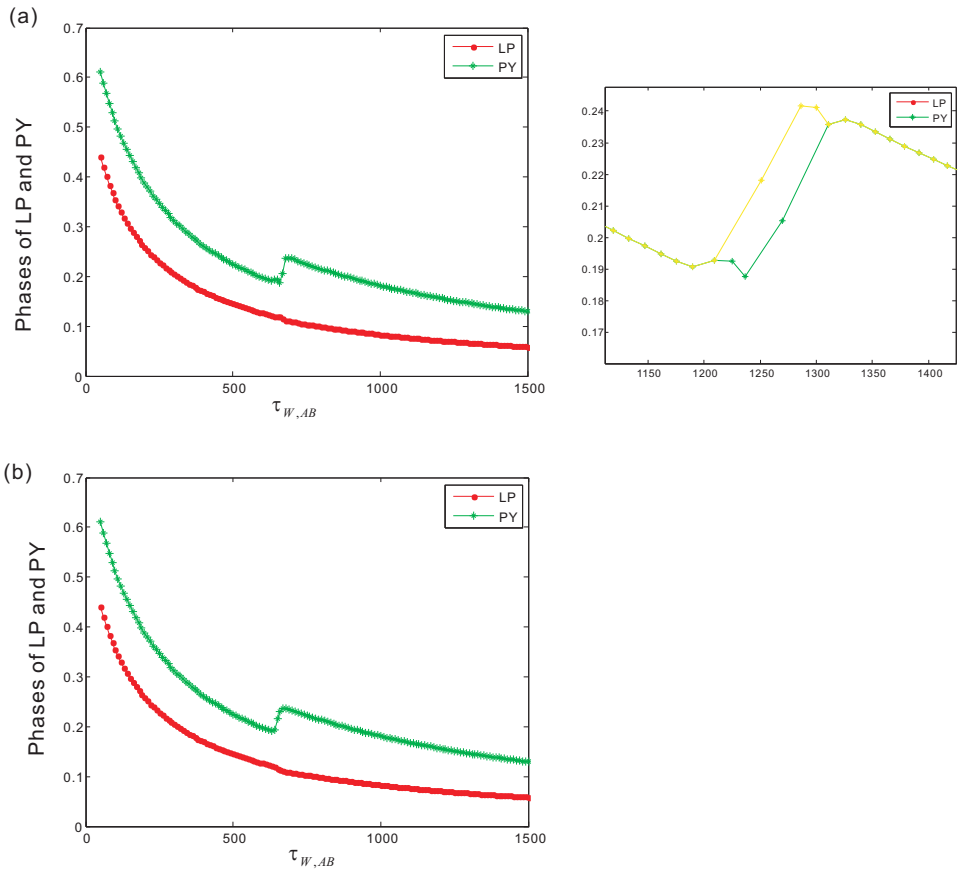

Figure 4.8 The relationship between the phases of LP and PY and the period of AB in the feed-forward network. (a) When $\bar{g}_{LP\to AB} = 20$, the period-2 region is much smaller than in Figure 4.7. The right panel is the zoom-in of the period-2 region. (b) When $\bar{g}_{LP\to AB} = 27$, there is no period-2 region. The different line styles are the same as the description in Figure 4.7.

Figure 4.7 where $\bar{g}_{LP\to AB} = 0$ and when $\bar{g}_{LP\to AB}$ increases to 27, the map converges in the entire domain. So the unstable fixed point in the feed-forward network is stabilized in the feedback network if the feedback synapse from LP to AB is strong enough.

Setting the synapse of AB is depressing in the network without the feedback synapse from LP to AB, we obtained the dependency of the phase of PY on the period of AB as shown in Figure 4.9(a). The synaptic depression of AB affects the phase of LP when the period is short. The phase curve of LP becomes to be of cubic shape,

which is consistent with the results shown in [51]. But there still exists a period-2 region, since the presence of this region is induced by the synaptic depression of LP and the interaction of LP and PY. In the feedback network with the synapse form LP to AB, this period-2 region gradually shrinks and disappears. As shown in Figure 4.9(b), where $\bar{g}_{LP\to LP} = 27$, the period-2 region almost vanishes and the neurons are period-1 phase-locked with each other in the entire period domain. As an extensive work, we are going to increase the time constants for AB to move the cubic part to overlap with the period-2 region. We will investigate the activity of the tri-phasic network under the interaction between the synaptic depression of AB and that of LP.

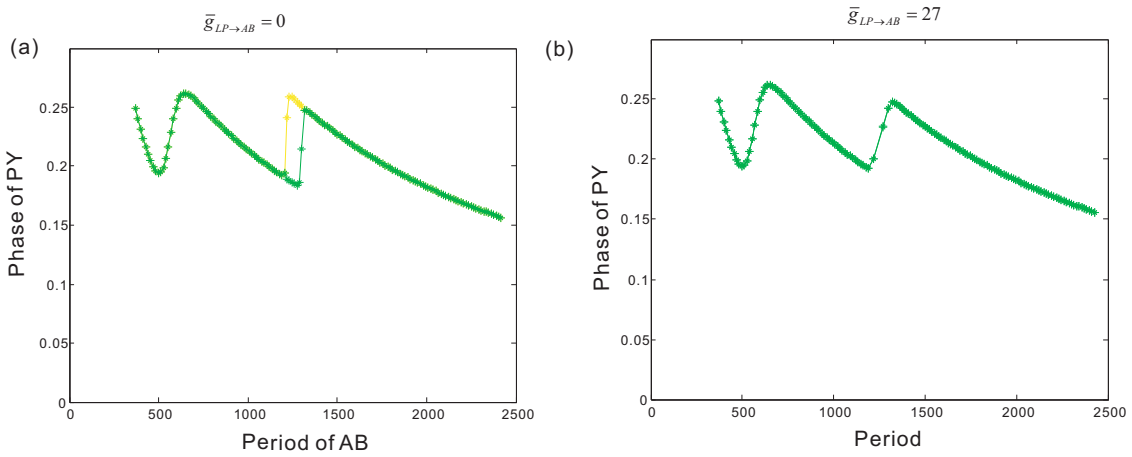

Figure 4.9 The relationship between the phase of PY and the period of AB in the feed-forward and feedback networks. (a) In the feed-forward network without the synapse from LP to AB, where $\bar{g}_{LP\to AB} = 0$, there exists a period-2 region over the period of AB. (b) In the feedback network with the synapse from LP to AB, when $\bar{g}_{LP\to AB} = 27$, there is no period-2 region.

In the following, we provide a proof for the stabilization of the fixed point from the feed-forward network to the feedback network for a specific set of parameter values. We choose the parameters as follows:

$T_{AB} = 300$, $\tau_{W,AB} = 360$, $\tau_{W,LP} = 102$, $\tau_{W,PY} = 126$, $\hat{W}_{AB} = 1$, $\hat{W}_{LP} = 1$, $\hat{W}_{PY} = 1$, $M_1 = 3.12$, $M_2 = 3.12$, $M_3 = 3.12$, $g^*_{syn1} = 3.12$, $g^*_{syn2} = 1.5$, $g^*_{syn3} = 0.76$, $\tau_\zeta =$

600000, $\tau_\kappa = 120$, $\tau_1 = 60$, $\tau_2 = 1350$, $\tau_3 = 330$, $\tau_4 = 60$, $\tau_a = 1350$, $\tau_b = 240$, $\tau_c = 60$, $\tau_d = 60$, $P_2 = 1140$, $x_2 = 10$. The synapse of AB in non-depressing. $d^*_{AB} = 0.38$, $\bar{g}_{AB} = 1.4$, $\bar{g}_{PY} = 11$, $\bar{g}_{LP\to PY} = 13$. In the feed-forward network, $\bar{g}_{LP\to AB} = 0$, while in the feedback network, $\bar{g}_{LP\to AB}$ is a positive number. We change the period of AB by varying $\tau_{W,AB}$, the time constant for W_{AB} on the left side of the threshold.

The entries in the 4×4 Jacobian for the 4D map and those in the 6×6 Jacobian for the 6D map are the following.

$$J_{11} = 0$$

$$J_{12} = 0$$

$$\begin{aligned} J_{13} =& [\frac{1}{\tau_2}\bar{g}_{PY}d^*_{PY}exp(-\frac{P^*-t^*_{PY}}{\tau_2})exp(-\frac{t^*_{LP}}{\tau_1}) + \frac{1}{\tau_{W,LP}}M_1\hat{W}_{LP}exp(-\frac{P^*-t^*_{PY}+t^*_{LP}}{\tau_{W,LP}})] \\ & /[\frac{1}{\tau_\kappa}\bar{g}_{AB}d^*_{AB}exp(-\frac{T_{AB}}{\tau_\zeta})exp(-\frac{t^*_{LP}-T_{AB}}{\tau_\kappa}) \\ & + \frac{1}{\tau_1}\bar{g}_{PY}d^*_{PY}exp(-\frac{P^*-t^*_{PY}}{\tau_2})exp(-\frac{t^*_{LP}}{\tau_1}) \\ & + \frac{1}{\tau_{W,LP}}M_1\hat{W}_{LP}exp(-\frac{P^*-t^*_{PY}+t^*_{LP}}{\tau_{W,LP}})] \end{aligned}$$

$$\begin{aligned} J_{14} =& [\bar{g}_{PY}exp(-\frac{P^*-t^*_{PY}}{\tau_2})exp(-\frac{t^*_{LP}}{\tau_1})]/[\frac{1}{\tau_\kappa}\bar{g}_{AB}d^*_{AB}exp(-\frac{T_{AB}}{\tau_\zeta})exp(-\frac{t^*_{LP}-T_{AB}}{\tau_\kappa}) \\ & + \frac{1}{\tau_1}\bar{g}_{PY}d^*_{PY}exp(-\frac{P^*-t^*_{PY}}{\tau_2})exp(-\frac{t^*_{LP}}{\tau_1}) \\ & + \frac{1}{\tau_{W,LP}}M_1\hat{W}_{LP}exp(-\frac{P^*-t^*_{PY}+t^*_{LP}}{\tau_{W,LP}})] \end{aligned}$$

$$\begin{aligned} J_{21} =& \frac{\partial\hat{d}_{LP}}{\partial t_{LP}} - [\frac{\partial\hat{d}_{LP}}{\partial t_{LP}} - \frac{1}{\tau_d}d^*_{LP}exp(-\frac{t^*_{PY}-t^*_{LP}}{\tau_d})]exp(-\frac{P^*-t^*_{PY}+t^*_{LP}}{\tau_c}) \\ & \text{where } \frac{\partial\hat{d}_{LP}}{\partial t_{LP}} = sech^2(\frac{P^*-t^*_{PY}+t^*_{LP}-P_2}{x_2})/(2x^2) \end{aligned}$$

$$J_{22} = exp(-\frac{t^*_{PY}-t^*_{LP}}{\tau_d})exp(-\frac{P^*-t^*_{PY}+t^*_{LP}}{\tau_c})$$

$$\begin{aligned} J_{23} =& \frac{\partial\hat{d}_{LP}}{\partial t_{PY}} - [\frac{\partial\hat{d}_{LP}}{\partial t_{PY}} + \frac{1}{\tau_d}d^*_{LP}exp(-\frac{t^*_{PY}-t^*_{LP}}{\tau_d})]exp(-\frac{P^*-t^*_{PY}+t^*_{LP}}{\tau_c}) \\ & - \frac{1}{\tau_c}[\hat{d}_{LP} - d^*_{LP}exp(-\frac{t^*_{PY}-t^*_{LP}}{\tau_d})](1-J_{13})exp(-\frac{P^*-t^*_{PY}+t^*_{LP}}{\tau_c}) \\ & \text{where } \frac{\partial\hat{d}_{LP}}{\partial t_{PY}} = -sech^2(\frac{P^*-t^*_{PY}+t^*_{LP}-P_2}{x_2})/(2x_2) \end{aligned}$$

$$
\begin{aligned}
J_{24} =& \frac{1}{\tau_c}[\hat{d}_{LP} - d^*_{LP} exp(-\frac{t^*_{PY} - t^*_{LP}}{\tau_d})] J_{14} exp(-\frac{P^* - t^*_{PY} + t^*_{LP}}{\tau_c}) \\
J_{31} =& [\bar{g}_{LP} J_{21} exp(-\frac{t^*_{PY} - t^*_{LP}}{\tau_4})] / [\frac{1}{\tau_\kappa} \bar{g}_{AB} d^*_{AB} exp(-\frac{T_{AB}}{\tau_\zeta}) exp(-\frac{t^*_{PY} - T_{AB}}{\tau_\kappa}) \\
& + \frac{1}{\tau_4} \bar{g}_{LP} d^*_{LP} exp(-\frac{P^* - t^*_{PY}}{\tau_2}) exp(-\frac{t^*_{LP}}{\tau_1}) \\
& + \frac{1}{\tau_{W,LP}} M_1 \hat{W}_{LP} exp(-\frac{P^* - t^*_{PY} + t^*_{LP}}{\tau_{W,LP}})] \\
J_{32} =& [\bar{g}_{LP \to PY} J_{22} exp(-\frac{t^*_{PY} - t^*_{LP}}{\tau_4})] / [\frac{1}{\tau_\kappa} \bar{g}_{AB} d^*_{AB} exp(-\frac{T_{AB}}{\tau_\zeta}) exp(-\frac{t^*_{PY} - T_{AB}}{\tau_\kappa}) \\
& + \frac{1}{\tau_4} \bar{g}_{LP \to PY} d^*_{LP} exp(-\frac{t^*_{PY} - t^*_{LP}}{\tau_4}) + \frac{1}{\tau_{W,PY}} M_2 \hat{W}_{PY} exp(-\frac{t^*_{PY}}{\tau_{W,PY}})] \\
J_{33} =& [\bar{g}_{LP \to PY} J_{23} exp(-\frac{t^*_{PY} - t^*_{LP}}{\tau_4}) + \frac{1}{\tau_4} \bar{g}_{LP \to PY} d^*_{LP} J_{13} exp(-\frac{P^* - t^*_{PY}}{\tau_2}) exp(-\frac{t^*_{LP}}{\tau_1})] \\
& / [\frac{1}{\tau_\kappa} \bar{g}_{AB} d^*_{AB} exp(-\frac{T_{AB}}{\tau_\zeta}) exp(-\frac{t^*_{PY} - T_{AB}}{\tau_\kappa}) \\
& + \frac{1}{\tau_4} \bar{g}_{LP \to PY} d^*_{LP} exp(-\frac{P^* - t^*_{PY}}{\tau_2}) exp(-\frac{t^*_{LP}}{\tau_1}) \\
& + \frac{1}{\tau_{W,LP}} M_1 \hat{W}_{LP} exp(-\frac{P^* - t^*_{PY} + t^*_{LP}}{\tau_{W,LP}})] \\
J_{34} =& [\bar{g}_{LP \to PY} J_{24} exp(-\frac{t^*_{PY} - t^*_{LP}}{\tau_4}) + \frac{1}{\tau_4} \bar{g}_{LP \to PY} d^*_{LP} J_{14} exp(-\frac{P^* - t^*_{PY}}{\tau_2}) exp(-\frac{t^*_{LP}}{\tau_1})] \\
& / [\frac{1}{\tau_\kappa} \bar{g}_{AB} d^*_{AB} exp(-\frac{T_{AB}}{\tau_\zeta}) exp(-\frac{t^*_{PY} - T_{AB}}{\tau_\kappa}) \\
& + \frac{1}{\tau_4} \bar{g}_{LP \to PY} d^*_{LP} exp(-\frac{P^* - t^*_{PY}}{\tau_2}) exp(-\frac{t^*_{LP}}{\tau_1}) \\
& + \frac{1}{\tau_{W,LP}} M_1 \hat{W}_{LP} exp(-\frac{P^* - t^*_{PY} + t^*_{LP}}{\tau_{W,LP}})] \\
J_{41} =& \frac{1}{\tau_a}[1 - d^*_{PY} exp(-\frac{P^* - t^*_{PY}}{\tau_b})] J_{31} exp(-\frac{-t^*_{PY}}{\tau_a}) \\
J_{42} =& \frac{1}{\tau_a}[1 - d^*_{PY} exp(-\frac{P^* - t^*_{PY}}{\tau_b})] J_{32} exp(-\frac{-t^*_{PY}}{\tau_a}) \\
J_{43} =& \frac{1}{\tau_b} d^*_{PY} exp(-\frac{P^* - t^*_{PY}}{\tau_b}) exp(-\frac{-t^*_{PY}}{\tau_a}) \\
& + \frac{1}{\tau_a}[1 - d^*_{PY} exp(-\frac{P^* - t^*_{PY}}{\tau_b})] J_{33} exp(-\frac{-t^*_{PY}}{\tau_a}) \\
J_{44} =& exp(-\frac{P^* - t^*_{PY}}{\tau_b}) exp(-\frac{-t^*_{PY}}{\tau_a}) + \frac{1}{\tau_a}[1 - d^*_{PY} exp(-\frac{P^* - t^*_{PY}}{\tau_b})] J_{34} exp(-\frac{-t^*_{PY}}{\tau_a})
\end{aligned}
$$

These entries are for the 4×4 Jacobian of the 4D map as well as the 4×4 submatrix for the 6×6 Jacobian of the 6D map. The other twenty entries only appearing in the 6×6 matrix are the following.

$$
\begin{aligned}
J_{15} =&\bar{g}_{AB}J_{11}exp(-\frac{T_{AB}}{\tau_\zeta})exp(-\frac{t^*_{LP}-T_{AB}}{\tau_\kappa})\\
&/[\frac{1}{\tau_\kappa}\bar{g}_{AB}d^*_{AB}exp(-\frac{T_{AB}}{\tau_\zeta})exp(-\frac{t^*_{LP}-T_{AB}}{\tau_\kappa})\\
&+\frac{1}{\tau_1}\bar{g}_{PY}d^*_{PY}exp(-\frac{P^*-t^*_{PY}}{\tau_2})exp(-\frac{t^*_{LP}}{\tau_1})\\
&+\frac{1}{\tau_{W,LP}}M_1\hat{W}_{LP}exp(-\frac{P^*-t^*_{PY}+t^*_{LP}}{\tau_{W,LP}})]\\
J_{16} =&[\bar{g}_{AB}J_{56}exp(-\frac{T_{AB}}{\tau_\zeta})exp(-\frac{t^*_{LP}-T_{AB}}{\tau_\kappa})\\
&-\frac{1}{\tau_2}\bar{g}_{PY}d^*_{PY}exp(-\frac{P^*-t^*_{PY}}{\tau_2})exp(-\frac{t^*_{LP}}{\tau_1})-\frac{1}{\tau_{W,LP}}M_1\hat{W}_{LP}exp(-\frac{P^*-t^*_{PY}+t^*_{LP}}{\tau_{W,LP}})]\\
&/[\frac{1}{\tau_\kappa}\bar{g}_{AB}d^*_{AB}exp(-\frac{T_{AB}}{\tau_\zeta})exp(-\frac{t^*_{LP}-T_{AB}}{\tau_\kappa})\\
&+\frac{1}{\tau_1}\bar{g}_{PY}d^*_{PY}exp(-\frac{P^*-t^*_{PY}}{\tau_2})exp(-\frac{t^*_{LP}}{\tau_1})\\
&+\frac{1}{\tau_{W,LP}}M_1\hat{W}_{LP}exp(-\frac{P^*-t^*_{PY}+t^*_{LP}}{\tau_{W,LP}})]\\
J_{25} =&\frac{1}{\tau_c}-[\hat{d}^*_{LP}-d^*_{LP}exp(-\frac{t^*_{PY}-t^*_{LP}}{\tau_d})]J_{15}exp(-\frac{P^*-t^*_{PY}+t^*_{LP}}{\tau_c})\\
&\text{where } \hat{d}^*_{LP}=(1+tanh(\frac{P^*-t^*_{PY}+t^*_{LP}-P_2}{x_2}))/2\\
J_{26} =&\frac{\partial\hat{d}_{LP}}{\partial P}[1-exp(-\frac{P^*-t^*_{PY}+t^*_{LP}}{\tau_c})]\\
&+\frac{1}{\tau_c}[\hat{d}_{LP}-d^*_{LP}exp(-\frac{t^*_{PY}-t^*_{LP}}{\tau_d})](1+J_{16})exp(-\frac{P^*-t^*_{PY}+t^*_{LP}}{\tau_c})\\
&\text{where } \frac{\partial\hat{d}_{LP}}{\partial P}=sech^2(\frac{P^*-t^*_{PY}+t^*_{LP}-P_2}{x_2})/(2x_2)\\
J_{35} =&[\bar{g}_{AB}J^*_{55}exp(-\frac{T_{AB}}{\tau_\zeta})exp(-\frac{t^*_{PY}-T_{AB}}{\tau_\kappa})\\
&+\bar{g}_{LP\to PY}J^*_{25}exp(-\frac{t^*_{PY}-t^*_{LP}}{\tau_4})+\frac{1}{\tau_4}\bar{g}_{LP\to PY}d^*_{LP}J_{15}exp(-\frac{t^*_{PY}-t^*_{LP}}{\tau_4})]\\
&/[\frac{1}{\tau_\kappa}\bar{g}_{AB}d^*_{AB}exp(-\frac{T_{AB}}{\tau_\zeta})exp(-\frac{t^*_{PY}-T_{AB}}{\tau_\kappa})\\
&+\frac{1}{\tau_4}\bar{g}_{LP\to PY}d^*_{LP}exp(-\frac{t^*_{PY}-t^*_{LP}}{\tau_4})+\frac{1}{\tau_{W,PY}}M_2\hat{W}_{PY}exp(-\frac{t^*_{PY}}{\tau_{W,PY}})]
\end{aligned}
$$

$$
\begin{aligned}
J_{36} =&[\bar{g}_{AB} J^*_{56} exp(-\frac{T_{AB}}{\tau_\zeta}) exp(-\frac{t^*_{PY} - T_{AB}}{\tau_\kappa}) \\
&+ \bar{g}_{LP\to PY} J^*_{26} exp(-\frac{t^*_{PY} - t^*_{LP}}{\tau_4}) + \frac{1}{\tau_4} \bar{g}_{LP\to PY} d^*_{LP} J_{16} exp(-\frac{t^*_{PY} - t^*_{LP}}{\tau_4})] \\
&/[\frac{1}{\tau_\kappa} \bar{g}_{AB} d^*_{AB} exp(-\frac{T_{AB}}{\tau_\zeta}) exp(-\frac{t^*_{PY} - T_{AB}}{\tau_\kappa}) \\
&+ \frac{1}{\tau_4} \bar{g}_{LP\to PY} d^*_{LP} exp(-\frac{t^*_{PY} - t^*_{LP}}{\tau_4}) + \frac{1}{\tau_{W,PY}} M_2 \hat{W}_{PY} exp(-\frac{t^*_{PY}}{\tau_{W,PY}})] \\
J_{45} =&\frac{1}{\tau_a}[1 - d^*_{PY} exp(-\frac{P^* - t^*_{PY}}{\tau_b})] J_{35} exp(-\frac{-t^*_{PY}}{\tau_a}) \\
J_{46} =&-\frac{1}{\tau_b} d^*_{PY} exp(-\frac{P^* - t^*_{PY}}{\tau_b}) exp(-\frac{-t^*_{PY}}{\tau_a}) \\
&+ \frac{1}{\tau_a}[1 - d^*_{PY} exp(-\frac{P^* - t^*_{PY}}{\tau_b})] J_{36} exp(-\frac{-t^*_{PY}}{\tau_a}) \\
J_{51} =&0 \\
J_{52} =&0 \\
J_{53} =&0 \\
J_{54} =&0 \\
J_{55} =&exp(-\frac{T_{AB}}{\tau_\beta}) exp(-\frac{P^* - T_{AB}}{\tau_\alpha}) \\
J_{56} =&\frac{\partial \hat{d}_{AB}}{\partial P}[1 - exp(-\frac{P^* - T_{AB}}{\tau_\alpha})] \\
&+ \frac{1}{\tau_\alpha}[\hat{d}_{AB} - d^*_{AB} exp(-\frac{T_{AB}}{\tau_\beta})] exp(-\frac{P^* - T_{AB}}{\tau_\alpha}) \\
&\text{where } \frac{\partial \hat{d}_{AB}}{\partial P} = sech^2(\frac{P^* - P_1}{x_1})/(2x_1) \\
J_{61} =&[\bar{g}_{LP\to AB} J_{21} exp(-\frac{t^*_{PY} - t^*_{LP}}{\tau_4}) exp(-\frac{P^* - t^*_{PY}}{\tau_3}) \\
&- \frac{1}{\tau_4} \bar{g}_{LP\to AB} (J_{31} - J_{11})^* exp(-\frac{t^*_{PY} - t^*_{LP}}{\tau_4}) exp(-\frac{P^* - t^*_{PY}}{\tau_3}) \\
&+ \frac{1}{\tau_3} \bar{g}_{LP\to AB} d^*_{LP} J_{31} exp(-\frac{t^*_{PY} - t^*_{LP}}{\tau_4}) exp(-\frac{P^* - t^*_{PY}}{\tau_3})] \\
&/[\frac{1}{\tau_3} \bar{g}_{LP\to AB} d^*_{LP} J_{35} exp(-\frac{t^*_{PY} - t^*_{LP}}{\tau_4}) exp(-\frac{P^* - t^*_{PY}}{\tau_3}) \\
&+ \frac{1}{\tau_{W,AB}} M_3 \hat{W}_{AB} exp(-\frac{P^* - T_{AB}}{\tau_{W,AB}})]
\end{aligned}
$$

$$
\begin{aligned}
J_{62} =&[\bar{g}_{LP\to AB}J_{22}exp(-\frac{t^*_{PY}-t^*_{LP}}{\tau_4})exp(-\frac{P^*-t^*_{PY}}{\tau_3}) \\
&-\frac{1}{\tau_4}\bar{g}_{LP\to AB}(J_{32}-J_{12})^*exp(-\frac{t^*_{PY}-t^*_{LP}}{\tau_4})exp(-\frac{P^*-t^*_{PY}}{\tau_3}) \\
&+\frac{1}{\tau_3}\bar{g}_{LP\to AB}d^*_{LP}J_{32}exp(-\frac{t^*_{PY}-t^*_{LP}}{\tau_4})exp(-\frac{P^*-t^*_{PY}}{\tau_3})] \\
&/[\frac{1}{\tau_3}\bar{g}_{LP\to AB}d^*_{LP}J_{35}exp(-\frac{t^*_{PY}-t^*_{LP}}{\tau_4})exp(-\frac{P^*-t^*_{PY}}{\tau_3}) \\
&+\frac{1}{\tau_{W,AB}}M_3\hat{W}_{AB}exp(-\frac{P^*-T_{AB}}{\tau_{W,AB}})] \\
J_{63} =&[\bar{g}_{LP\to AB}J_{23}exp(-\frac{t^*_{PY}-t^*_{LP}}{\tau_4})exp(-\frac{P^*-t^*_{PY}}{\tau_3}) \\
&-\frac{1}{\tau_4}\bar{g}_{LP\to AB}(J_{33}-J_{13})^*exp(-\frac{t^*_{PY}-t^*_{LP}}{\tau_4})exp(-\frac{P^*-t^*_{PY}}{\tau_3}) \\
&+\frac{1}{\tau_3}\bar{g}_{LP\to AB}d^*_{LP}J_{33}exp(-\frac{t^*_{PY}-t^*_{LP}}{\tau_4})exp(-\frac{P^*-t^*_{PY}}{\tau_3})] \\
&/[\frac{1}{\tau_3}\bar{g}_{LP\to AB}d^*_{LP}J_{35}exp(-\frac{t^*_{PY}-t^*_{LP}}{\tau_4})exp(-\frac{P^*-t^*_{PY}}{\tau_3}) \\
&+\frac{1}{\tau_{W,AB}}M_3\hat{W}_{AB}exp(-\frac{P^*-T_{AB}}{\tau_{W,AB}})] \\
J_{64} =&[\bar{g}_{LP\to AB}J_{24}exp(-\frac{t^*_{PY}-t^*_{LP}}{\tau_4})exp(-\frac{P^*-t^*_{PY}}{\tau_3}) \\
&-\frac{1}{\tau_4}\bar{g}_{LP\to AB}(J_{34}-J_{14})^*exp(-\frac{t^*_{PY}-t^*_{LP}}{\tau_4})exp(-\frac{P^*-t^*_{PY}}{\tau_3}) \\
&+\frac{1}{\tau_3}\bar{g}_{LP\to AB}d^*_{LP}J_{34}exp(-\frac{t^*_{PY}-t^*_{LP}}{\tau_4})exp(-\frac{P^*-t^*_{PY}}{\tau_3})] \\
&/[\frac{1}{\tau_3}\bar{g}_{LP\to AB}d^*_{LP}J_{35}exp(-\frac{t^*_{PY}-t^*_{LP}}{\tau_4})exp(-\frac{P^*-t^*_{PY}}{\tau_3}) \\
&+\frac{1}{\tau_{W,AB}}M_3\hat{W}_{AB}exp(-\frac{P^*-T_{AB}}{\tau_{W,AB}})] \\
J_{65} =&[\bar{g}_{LP\to AB}J_{25}exp(-\frac{t^*_{PY}-t^*_{LP}}{\tau_4})exp(-\frac{P^*-t^*_{PY}}{\tau_3}) \\
&-\frac{1}{\tau_4}\bar{g}_{LP\to AB}(J_{35}-J_{15})^*exp(-\frac{t^*_{PY}-t^*_{LP}}{\tau_4})exp(-\frac{P^*-t^*_{PY}}{\tau_3}) \\
&+\frac{1}{\tau_3}\bar{g}_{LP\to AB}d^*_{LP}J_{35}exp(-\frac{t^*_{PY}-t^*_{LP}}{\tau_4})exp(-\frac{P^*-t^*_{PY}}{\tau_3})] \\
&/[\frac{1}{\tau_3}\bar{g}_{LP\to AB}d^*_{LP}J_{35}exp(-\frac{t^*_{PY}-t^*_{LP}}{\tau_4})exp(-\frac{P^*-t^*_{PY}}{\tau_3}) \\
&+\frac{1}{\tau_{W,AB}}M_3\hat{W}_{AB}exp(-\frac{P^*-T_{AB}}{\tau_{W,AB}})]
\end{aligned}
$$

$$
\begin{aligned}
J_{66} =&[\bar{g}_{LP\to AB} J_{26} exp(-\frac{t^*_{PY} - t^*_{LP}}{\tau_4}) exp(-\frac{P^* - t^*_{PY}}{\tau_3}) \\
&- \frac{1}{\tau_4}\bar{g}_{LP\to AB}(J_{36} - J_{16})^* exp(-\frac{t^*_{PY} - t^*_{LP}}{\tau_4}) exp(-\frac{P^* - t^*_{PY}}{\tau_3}) \\
&+ \frac{1}{\tau_3}\bar{g}_{LP\to AB} d^*_{LP} J_{36} exp(-\frac{t^*_{PY} - t^*_{LP}}{\tau_4}) exp(-\frac{P^* - t^*_{PY}}{\tau_3})] \\
&/[\frac{1}{\tau_3}\bar{g}_{LP\to AB} d^*_{LP} J_{35} exp(-\frac{t^*_{PY} - t^*_{LP}}{\tau_4}) exp(-\frac{P^* - t^*_{PY}}{\tau_3}) \\
&+ \frac{1}{\tau_{W,AB}} M_3 \hat{W}_{AB} exp(-\frac{P^* - T_{AB}}{\tau_{W,AB}})]
\end{aligned}
$$

For the parameter values from the biological model, the Jacobian for the above example is in the form of

$$
J = \begin{pmatrix}
0 & 0 & J_{13} & J_{14} & 0 & J_{16} \\
J_{21} & 0 & J_{23} & J_{24} & 0 & J_{26} \\
J_{31} & 0 & J_{33} & J_{34} & 0 & J_{36} \\
J_{41} & 0 & J_{43} & J_{44} & 0 & J_{46} \\
0 & 0 & 0 & 0 & 0 & 0 \\
J_{61} & 0 & J_{63} & J_{64} & 0 & J_{66}
\end{pmatrix}
$$

$J_{11} = J_{12} = 0$ because t^{i+1}_{LP} is independent of t^i_{LP} and d^i_{LP}. The fifth row is a zero vector because the synapse of AB is non-depressing. The fifth column is zero for the same reason. The value of each element in the second column is almost zero because the time constants for d_{LP}, τ_c and τ_d are much smaller than other time constants and the depression of LP affects the other variables very slightly.

To find the eigenvalues of this matrix, note

$$|\lambda I - J| = \begin{vmatrix} \lambda & 0 & -J_{13} & -J_{14} & 0 & -J_{16} \\ -J_{21} & \lambda & -J_{23} & -J_{24} & 0 & -J_{26} \\ -J_{31} & 0 & \lambda - J_{33} & -J_{34} & 0 & -J_{36} \\ -J_{41} & 0 & -J_{43} & \lambda - J_{44} & 0 & -J_{46} \\ 0 & 0 & 0 & 0 & \lambda & 0 \\ -J_{61} & 0 & -J_{63} & -J_{64} & 0 & \lambda - J_{66} \end{vmatrix}$$

$$= -J_{61}\lambda \begin{vmatrix} 0 & -J_{13} & -J_{14} & -J_{16} \\ \lambda & -J_{23} & 0 & -J_{26} \\ 0 & \lambda - J_{33} & -J_{34} & -J_{36} \\ 0 & -J_{43} & \lambda - J_{44} & -J_{46} \end{vmatrix} - J_{63}\lambda \begin{vmatrix} \lambda & 0 & -J_{14} & -J_{16} \\ -J_{21} & \lambda & 0 & -J_{26} \\ -J_{31} & 0 & -J_{34} & -J_{36} \\ -J_{41} & 0 & \lambda - J_{44} & -J_{46} \end{vmatrix}$$

$$+J_{64}\lambda \begin{vmatrix} \lambda & 0 & -J_{13} & -J_{16} \\ -J_{21} & \lambda & -J_{23} & -J_{26} \\ -J_{31} & 0 & \lambda - J_{33} & -J_{36} \\ -J_{41} & 0 & -J_{43} & -J_{46} \end{vmatrix} + (\lambda - J_{66})\lambda \begin{vmatrix} \lambda & 0 & -J_{13} & -J_{14} \\ -J_{21} & \lambda & -J_{23} & 0 \\ -J_{31} & 0 & \lambda - J_{33} & -J_{34} \\ -J_{41} & 0 & -J_{43} & \lambda - J_{44} \end{vmatrix}$$

We write this entire determinant as a function of λ, $f_b(\lambda)$. The last term is the characteristic polynomial of the 4×4 Jacobian for the feed-forward network, written

as a function of λ, $f_f(\lambda)$. Then,

$$\begin{aligned} f_b(\lambda) = \lambda\{ & J_{61}\lambda[-J_{13}J_{34}J_{46} - J_{16}(\lambda - J_{33})(\lambda - J_{44}) - J_{43}J_{14}J_{36} \\ & - J_{16}J_{34}J_{43} - J_{14}J_{46}(\lambda - J_{33}) - J_{13}J_{36}(\lambda - J_{44})] \\ & - J_{63}\lambda[J_{36}J_{46}\lambda - J_{31}J_{16}(\lambda - J_{44}) - J_{41}J_{14}J_{36} \\ & + J_{16}J_{34}J_{41} - J_{14}J_{31}J_{46} + J_{36}\lambda(\lambda - J_{44})] \\ & + J_{64}\lambda[-J_{46}\lambda(\lambda - J_{33}) - J_{31}J_{43}J_{16} - J_{41}J_{13}J_{36} \\ & - J_{16}J_{41}(\lambda - J_{33}) + J_{13}J_{31}J_{46} - J_{36}J_{43}\lambda] \\ & + (\lambda - J_{66})f_f(\lambda)\} \end{aligned}$$

where,

$$f_f(\lambda) = \begin{vmatrix} \lambda & 0 & -J_{13} & -J_{14} \\ -J_{21} & \lambda & -J_{23} & 0 \\ -J_{31} & 0 & \lambda - J_{33} & -J_{34} \\ -J_{41} & 0 & -J_{43} & \lambda - J_{44} \end{vmatrix} = \lambda Cu(\lambda)$$

where $Cu(\lambda)$ is a cubic function,

$$Cu(\lambda) = \begin{vmatrix} \lambda & -J_{13} & -J_{14} \\ -J_{31} & \lambda - J_{33} & -J_{34} \\ -J_{41} & -J_{43} & \lambda - J_{44} \end{vmatrix}$$

Then,

$$fb(\lambda) = \lambda^2[A\lambda^2 + B\lambda + C + (\lambda - J_{66})Cu(\lambda)] \tag{4.25}$$

where

$$
\begin{aligned}
A =& - J_{61}J_{16} - J_{63}J_{36} - J_{64}J_{46} \\
B =& J_{61}J_{16}J_{33} + J_{61}J_{16}J_{44} - J_{61}J_{14}J_{46} - J_{61}J_{13}J_{36} - J_{63}J_{34}J_{46} \\
& - J_{63}J_{31}J_{16} + J_{63}J_{36}J_{44} + J_{64}J_{46}J_{33} - J_{64}J_{16}J_{41} - J_{64}J_{36}J_{43} \\
C =& J_{61}(-J_{13}J_{34}J_{46} - J_{16}J_{33}J_{44} - J_{43}J_{14}J_{36} + J_{16}J_{34}J_{43} + J_{14}J_{46}J_{33} + J_{13}J_{36}J_{44}) \\
& - J_{63}(-J_{31}J_{16}J_{44} - J_{41}J_{14}J_{36} + J_{16}J_{34}J_{41} + J_{14}J_{31}J_{46}) \\
& + J_{64}(-J_{31}J_{43}J_{16} - J_{41}J_{13}J_{36} + J_{16}J_{41}J_{33} + J_{13}J_{31}J_{46})
\end{aligned}
$$

From (4.25), $\lambda = 0$ is a double root for $f_b(\lambda) = 0$ which is inside the unit circle. Let

$$\tilde{f}_b(\lambda) = A\lambda^2 + B\lambda + C + (\lambda - J_{66})Cu(\lambda)$$

We will prove how the unstable fixed point in the feed-forward network is stabilized by the feedback synapse from LP to AB, as shown in the period-2 region. In the feed-forward network, $A = B = C = J_{66} = 0$, $f_f(\lambda) = \tilde{f}_b(\lambda) = \lambda Cu(\lambda)$. The fixed point is unstable. Two roots of $Cu(\lambda)$ are near zero and the other unstable one is less than -1. A schematic plot of the function $\tilde{f}_b(\lambda)$ is shown in Figure 4.10 (the black curve). We are proving as $\bar{g}_{LP\to AB}$ increases, the curve of $\tilde{f}_b(\lambda)$ moves downwards and rightwards and a saddle node bifurcation occurs near 0, which implies there are a pair of complex conjugate roots near 0 as $\bar{g}_{LP\to AB}$ continue increasing. At this stage, the curve of $\tilde{f}_b(\lambda)$ looks like the red curve in Figure 4.10, so for $\tilde{f}_b(\lambda) = 0$, there are two small complex conjugate roots inside the unit circle and two real roots, the intersection points of the curve with the abscissa. To force these two roots inside the region $(-1, 1)$, we need the conditions $\tilde{f}_b(-1) > 0$ and $\tilde{f}_b(1) > 0$ to be satisfied. The following shows the process of the detailed proof.

Let

$$\begin{aligned} k(\lambda) &= (\lambda - J_{66})Cu(\lambda) \\ &= (\lambda - J_{66})(\lambda - \lambda_1)(\lambda - \lambda_2)(\lambda - \lambda_3) \end{aligned}$$

where $J_{66} > 0, 0 < \lambda_1 < \lambda_2 \ll 1$ and $\lambda_3 < -1$. The rough plot of this fourth order polynomial is shown in Figure 4.10. J_{66} may be less then λ_1, greater than λ_2 or between λ_1 and λ_2 (black curve in Figure 4.9).

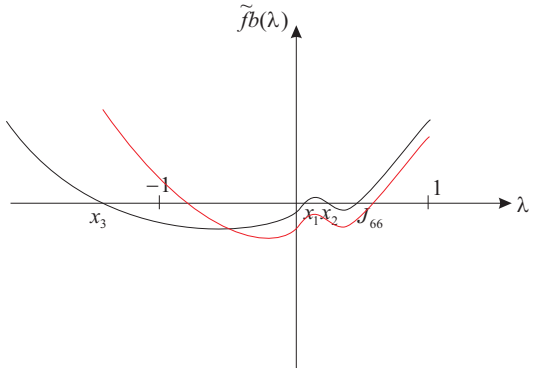

Figure 4.10 Schematic plot of the function $\tilde{f}_b(\lambda)$ ($k(\lambda)$ in the feed-forward network. $J_{66} > 0, 0 < \lambda_1 < \lambda_2 \ll 1$ and $\lambda_3 < -1$. Black curve is for the feed-forward case where $\bar{g}_{LP\to AB} = 0$. Red curve is for the feedback case where $\bar{g}_{LP\to AB} \neq 0$ and sufficiently large.

We investigate how $\bar{g}_{LP\to AB}$ changes the values of A, B and C and change the slope and location of $k(\lambda)$ to force all roots to lie inside the unit circle. In order to consider the same fixed point when increasing $\bar{g}_{LP\to AB}$, we decrease the value of $\tau_{W,AB}$. So, in the Jacobian matrix, two parameters change their values, $\bar{g}_{LP\to AB}$ and $\tau_{W,AB}$ which are only involved in the new entries in the 6×6 Jacobian. Further, J_{16}, J_{26}, J_{36}, J_{46} and J_{56} are independent of these two parameters. J_{61}, J_{63}, J_{64} and J_{66} have linear relation with $\bar{g}_{LP\to AB}$ and the change of $\tau_{W,AB}$ does not affect these values

too much. For example, in the expression for J_{61},

$$\begin{aligned}
J_{61} =&[\bar{g}_{LP\to AB}J_{21}exp(-\frac{t^*_{PY}-t^*_{LP}}{\tau_4})exp(-\frac{P^*-t^*_{PY}}{\tau_3}) \\
&-\frac{1}{\tau_4}\bar{g}_{LP\to AB}(J_{31}-J_{11})^*exp(-\frac{t^*_{PY}-t^*_{LP}}{\tau_4})exp(-\frac{P^*-t^*_{PY}}{\tau_3}) \\
&+\frac{1}{\tau_3}\bar{g}_{LP\to AB}d^*_{LP}J_{31}exp(-\frac{t^*_{PY}-t^*_{LP}}{\tau_4})exp(-\frac{P^*-t^*_{PY}}{\tau_3})] \\
&/[\frac{1}{\tau_3}\bar{g}_{LP\to AB}d^*_{LP}J_{35}exp(-\frac{t^*_{PY}-t^*_{LP}}{\tau_4})exp(-\frac{P^*-t^*_{PY}}{\tau_3}) \\
&+\frac{1}{\tau_{W,AB}}M_3\hat{W}_{AB}exp(-\frac{P^*-T_{AB}}{\tau_{W,AB}})] \\
=&\frac{J_{21}-\frac{1}{\tau_4}d^*_{LP}(J_{31}-J_{11})+\frac{1}{\tau_3}d^*_{LP}J_{31}}{\frac{1}{\tau_3}d^*_{LP}+\frac{M_3\hat{W}_{AB}exp(-\frac{P^*-T_{AB}}{\tau_{W,AB}})}{\tau_{W,AB}\bar{g}_{LP\to AB}exp(-\frac{t^*_{PY}-t^*_{LP}}{\tau_4})exp(-\frac{P^*-t^*_{PY}}{\tau_3})}}
\end{aligned}$$

where $\frac{1}{\tau_3}d^*_{LP}$ is much smaller than $\frac{M_3\hat{W}_{AB}exp(-\frac{P^*-T_{AB}}{\tau_{W,AB}})}{\tau_{W,AB}\bar{g}_{LP\to AB}exp(-\frac{t^*_{PY}-t^*_{LP}}{\tau_4})exp(-\frac{P^*-t^*_{PY}}{\tau_3})}$, so

$$J_{61}\approx\tau_{W,AB}\bar{g}_{LP\to AB}\frac{J_{21}-\frac{1}{\tau_4}d^*_{LP}(J_{31}-J_{11})+\frac{1}{\tau_3}d^*_{LP}J_{31}}{M_3\hat{W}_{AB}exp(-\frac{P^*-T_{AB}}{\tau_{W,AB}})}exp(-\frac{t^*_{PY}-t^*_{LP}}{\tau_4})exp(-\frac{P^*-t^*_{PY}}{\tau_3})$$

The same reasoning holds for J_{63}, J_{64} and J_{66}. A, B and C are also linear functions of $\bar{g}_{LP\to AB}$.

Let $A=k_A\bar{g}_{LP\to AB}$, $B=k_B\bar{g}_{LP\to AB}$, $C=k_C\bar{g}_{LP\to AB}$, $J_{66}=k_{66}\bar{g}_{LP\to AB}$ and $\tilde{f}_b(\lambda)\doteq z(\bar{g}_{LP\to AB},\lambda)=k_A\bar{g}_{LP\to AB}\lambda^2+k_B\bar{g}_{LP\to AB}\lambda+k_C\bar{g}_{LP\to AB}+(\lambda-\lambda_1)(\lambda-\lambda_2)(\lambda-\lambda_3)(\lambda-k_{66}\bar{g}_{LP\to AB})$. There is a saddle-node bifurcation when $\bar{g}_{LP\to AB}=g^*$, where (g^*,λ^*) satisfies

$$\begin{cases} z(g^*,\lambda^*)=0 \\ \frac{\partial z}{\partial\lambda}(g^*,\lambda^*)=0 \end{cases}$$

which is equivalent to

$$\begin{aligned}
&-\lambda^*(k_A\lambda^{*2}+k_B\lambda^*+k_C)[(\lambda^*-\lambda_2)(\lambda^*-\lambda_3)\\
&+(\lambda^*-\lambda_1)(\lambda^*-\lambda_3)+(\lambda^*-\lambda_1)(\lambda^*-\lambda_2)]\\
&+(k_A\lambda^{*2}-k_C)(\lambda^*-\lambda_1)(\lambda^*-\lambda_2)(\lambda^*-\lambda_3)\\
&+k_{66}(\lambda^*-\lambda_1)^2(\lambda^*-\lambda_2)^2(\lambda^*-\lambda_3)^2=0
\end{aligned} \tag{4.26}$$

We use asymptotic methods to prove λ^* is close to 0. For the choice of parameters, $k_A = 0.14965$, $k_B = -0.00526$, $k_C = -0.000033829$ and $k_{66} = 0.07674$. They are $O(1)$, $O(\epsilon)$, $O(\epsilon^2)$ and $O(1)$, respectively, where $\epsilon = 0.01$. Also, we find $\lambda_1 = O(\epsilon)$, $\lambda_2 = O(\epsilon)$, $\lambda_3 = O(1)$. Let $k_A = C_A$, $k_B = C_B\epsilon$, $k_C = C_C\epsilon^2$, $\lambda_1 = C_1\epsilon$, $\lambda_2 = C_2\epsilon$ and $\lambda_3 = C_3$, where $C_A, C_B, C_C, C_1, C_2, C_3 = O(1)$.

Let $\lambda^* = x_1 + \epsilon x_2 + \epsilon^2 x_3 + \cdots$. Substituting into Equation (4.26), we find $x_1 = 0$ and $x_2 = [C_{66}C_3(C_1 + C_2) - C_B]/[2(C_A + C_{66}C_3)]$. Thus, $\lambda^* = \epsilon x_2 + \epsilon^2 x_3 + \cdots$, which implies λ^* is close to 0. Thus, two small real roots λ_1 and λ_2 of $\tilde{f}_b(\lambda)$ coincide as λ^* when $\bar{g}_{LP\to AB} = g^*$, then as $\bar{g}_{LP\to AB}$ increases more, λ_1 and λ_2 become to be two complex conjugate roots of $\tilde{f}_b(\lambda)$ with a sufficiently small modulus (red curve in Figure 4.10). So, the condition for all roots of $\tilde{f}_b(\lambda)$ to be within the unit circle is $\tilde{f}_b(-1) > 0$ and $\tilde{f}_b(1) > 0$, which implies that the negative real root is greater than -1 and the positive real root is less than 1.

In the following, we will derive the conditions based on the values of A, B and C.

$$\begin{aligned}
Cu(\lambda) &= \begin{vmatrix} \lambda & -J_{13} & -J_{14} \\ -J_{31} & \lambda - J_{33} & -J_{34} \\ -J_{41} & -J_{43} & \lambda - J_{44} \end{vmatrix} \\
&= \lambda^3 - (J_{33}+J_{44})\lambda^2 + (J_{33}J_{44} - J_{34}J_{43} - J_{13}J_{31} - J_{14}J_{41})\lambda \\
&\quad + J_{13}J_{31}J_{44} - J_{13}J_{34}J_{41} - J_{14}J_{31}J_{43} + J_{14}J_{41}J_{33}
\end{aligned}$$

Since we find $Cu(\lambda)$ has two roots near 0, $\lambda^3 - (J_{33} + J_{44})\lambda^2 \approx 0 \Rightarrow \lambda \approx J_{33} + J_{44}$. Moreover, it can be observed that $0 < J_{44} \ll 1$, therefore, $\lambda \approx J_{33}$ and $Cu(\lambda) \approx \lambda^2(\lambda - J_{33})$. Then,

$$\tilde{f}b(\lambda) \approx A\lambda^2 + B\lambda + C + (\lambda - J_{66})\lambda^2(\lambda - J_{33})$$

To satisfy $\tilde{f}_b(-1) > 0$, we need

$$B < A + C + 1 + J_{33} + J_{66} + J_{33}J_{66} \tag{4.27}$$

For $\tilde{f}_b(1) > 0$,

$$B > -A - C - 1 + J_{33} + J_{66} - J_{33}J_{66} \tag{4.28}$$

But in the feed-forward network $\bar{g}_{LP\to AB} = 0$ and $A = B = C = J_{66} = 0$. In this specific case, (4.27) is $0 < 1 + J_{33}$ which is not satisfied since $J_{33} < -1$. (4.28) turns out to be $0 > -1 + J_{33}$ which is satisfied. Using the linear relationship of A, B, C and J_{66} with $\bar{g}_{LP\to AB}$, (4.27) can be written as $\bar{g}_{LP\to AB}(k_B - k_A - k_C - k_{66} - J_{33}k_{66}) < 1 + J_{33}$. Since $k_B - k_A - k_C - k_{66} - J_{33}k_{66} < 0$, when $\bar{g}_{LP\to AB}$ increases, the left hand side of the inequality decreases. Therefore, when $\bar{g}_{LP\to AB}$ is sufficiently large, (4.27) and (4.28) are satisfied and all roots of $\tilde{f}_b(\lambda)$ are within the unit circle, and the fixed point is stabilized. Thus, we have the following conjecture:

Conjecture: There exists a value $g^*_{LP\to AB}$, such that, for $\bar{g}_{LP\to AB} > g^*_{LP\to AB}$, the fixed point of the 6D map (4.23) is stable.

To conclude, when the feedback synapse from LP to AB is strong enough, the unstable fixed point of the 4D map (4.14) for the feed-forward network is stabilized and the period-2 region in the feed-forward network vanishes. Therefore, the fixed point in the entire region of the period is stable, then the tri-phasic network exhibits phase-locked activity.

CHAPTER 5

USING SPIKE TIME RESPONSE CURVES OF NEURONS TO INFER ACTIVITY OF FEEDBACK NEURONAL NETWORKS

We consider a network consisting of two heterogenous neurons which are both oscillators with tonic spiking patterns but having slightly different intrinsic periods. The period of a postsynaptic neuron is mainly affected by the relative firing time of the presynaptic neuron and the synaptic strength at the time it spikes. The spike time response curve (STRC) describes how the period of the postsynaptic neuron is affected by a single spike from the presynaptic neuron [3]. We will use STRCs to measure the period change of the postsynaptic neuron in response to the firing of the presynaptic neuron. The synaptic strength at the time the presynaptic neuron fires is constant if the synapse is non-depressing and varies with the period of the neuron if the synapse is depressing. We will consider these two situations respectively and also construct the relationship between the phase-locked activities of the network with these two different synapses.

5.1 Phase-locked Activity of Two Neurons in a Feed-forward Network

First, we examine the conditions for the phased-locked activity of the two neurons, A and B, in the feed-forward network of A inhibiting B where the synapse from A to B is non-depressing.

Denote $\tilde{P}$ and $\tilde{T}$ as the intrinsic periods of neuron A and neuron B, respectively (Figure 5.1). T_i is the new period of neuron B in the ith cycle due to the input from neuron A. t_i is the delay firing time of B after the last spike of A and τ_i is the relative firing time of A after B fires. The phase of neuron A is defined as $\theta = \tau/\tilde{T}$ or $\theta_i = \tau_i/\tilde{T}$ in the ith cycle. Similarly, the phase of neuron B is defined as $\phi = t/\tilde{P}$ or $\phi_i = t_i/\tilde{P}$

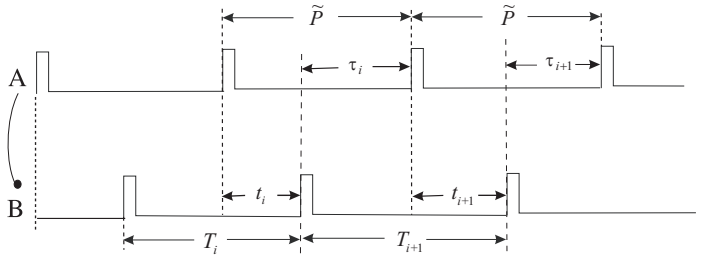

Figure 5.1 Feed-forward network of neuron A inhibiting neuron B, exhibiting 1:1 firing.

in the ith cycle. Using mathematical convention, the STRC of neuron B is defined as $\frac{\tilde{T}-T}{\tilde{T}}$ which can be represented as a function of the phase of A, $z_B(\theta) = \frac{\tilde{T}-T}{\tilde{T}}$. In the $(i+1)$th cycle of B, T_{i+1} is affected by τ_i or θ_i and $T_{i+1} = \tilde{T}(1 - z_B(\theta_i))$. Then, $\theta_{i+1} = \frac{\tau_{i+1}}{\tilde{T}} = \frac{\tilde{P}-t_{i+1}}{\tilde{T}} = \frac{\tilde{P}-(T_{i+1}-\tau_i)}{\tilde{T}} = \frac{\tilde{P}}{\tilde{T}} - 1 + \theta_i + z_B(\theta_i)$. The phase-locked activity of this feed-forward network corresponds to a stable fixed point of this map, i.e., $\theta^* = \frac{\tilde{P}}{\tilde{T}} - 1 + \theta^* + z_B(\theta^*)$ or $z_B(\theta^*) = 1 - \frac{\tilde{P}}{\tilde{T}}$. If $|1 + z'_B(\theta^*)| < 1$ or $-2 < z'_B(\theta^*) < 0$, this fixed point is stable.

Since the map is constructed under the 1:1 firing situation, the conditions to guarantee 1:1 firing should be examined. Two situations that break 1:1 firing are shown in Figure 5.2. T_{i+1} should not be too small (Figure 5.2(a)) or too large (Figure 5.2(b)). To avoid these two cases, we need $T_{i+1} + \tilde{T} > \tau_i + \tilde{P}$ and $T_{i+1} < \tau_i + \tilde{P}$. In terms of the phase of A and STRC of B, the conditions for 1:1 firing are $1 - \theta - \frac{\tilde{P}}{\tilde{T}} < z_B(\theta) < 2 - \theta - \frac{\tilde{P}}{\tilde{T}}$.

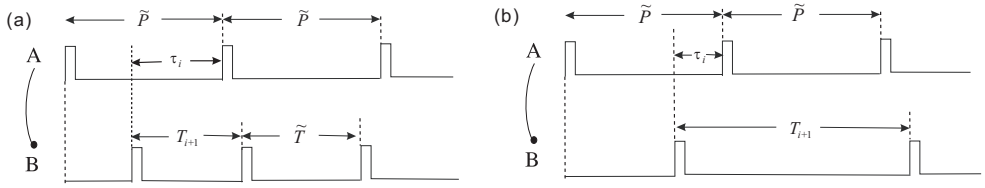

Figure 5.2 Firing pattern that are not 1:1 (a) One A firing and two subsequent B firings. (b) One B firing and two subsequent A firings.

Combining the 1:1 condition with the stability condition for the fixed point, to obtain 1:1 phased-locked activity in the feed-forward network of A inhibiting B, the STRC of neuron B needs to satisfy: $1 - \theta^* - \frac{\tilde{P}}{\tilde{T}} < z_B(\theta^*) < 2 - \theta^* - \frac{\tilde{P}}{\tilde{T}}$ and $-2 < z'_B(\theta^*) < 0$, where $z_B(\theta^*) = 1 - \frac{\tilde{P}}{\tilde{T}}$. Geometrically, the fixed point is the intersection point of the STRC of neuron B and the horizontal line $1 - \frac{\tilde{P}}{\tilde{T}}$ in the $z_B - \theta$ plane (Figure 5.3). The STRC of B at the fixed point θ^* should be located in the bounded region by the two lines $z_B = 1 - \theta - \frac{\tilde{P}}{\tilde{T}}$ and $z_B = 2 - \theta - \frac{\tilde{P}}{\tilde{T}}$. Moreover, the slope of the STRC at θ^* should be negative but greater -2.

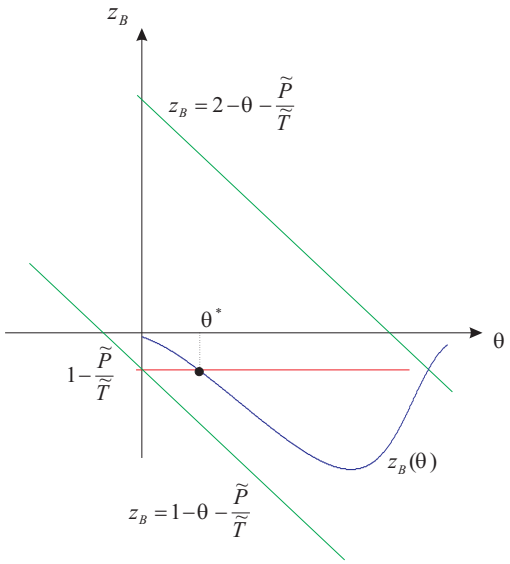

Figure 5.3 Conditions on the STRC of neuron B for the 1:1 phase-locked activity of the feed-forward network. The intersection of the curve $z_B(\theta)$ with the line $1 - \frac{\tilde{P}}{\tilde{T}}$ determine fixed point θ^* corresponding to the phase of the solution.

5.2 Phase-locked Activity of Two Neurons in a Feedback Network with No Synaptic Depression

Here, we consider the feedback network in which neurons A and B are mutually inhibited with non-depressing synapses. Different from Figure 5.1, in the feedback

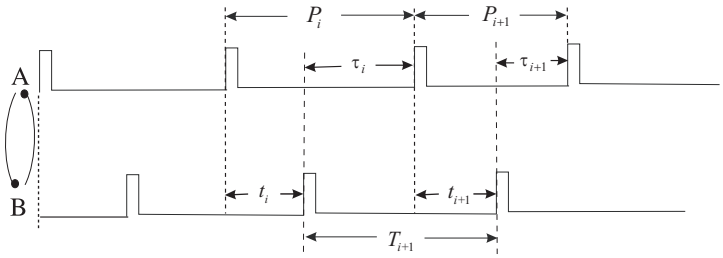

Figure 5.4 Feedback network of neurons A and B inhibiting each other with non-depressing synapses.

network, the period of neuron A is not a constant, but varies due to the firing time of neuron B as shown in Figure 5.4. The new period of A in each cycle is denoted as P_i, $i = 1, 2, \cdots$. In the ith cycle of neuron A, the phase of neuron B, $\phi_i = t_i/\tilde{P}$, determines the period of A, P_i. This effect can be measured by the STRC of A, $\frac{\tilde{P}-P_i}{\tilde{P}} = z_A(\phi_i)$, where z_A is the STRC function of neuron A. On the other hand, the spiking of A at the phase $\theta_i = \tau_i/\tilde{T}$ determines the period of B, T_{i+1}, which is similarly expressed by the STRC of B, $\frac{\tilde{T}-T_{i+1}}{\tilde{T}} = z_B(\theta_i)$. Hence,

$$\begin{aligned}
\theta_{i+1} &= \frac{\tau_{i+1}}{\tilde{T}} \\
&= \frac{P_{i+1} - t_{i+1}}{\tilde{T}} \\
&= \frac{\tilde{P}(1 - z_A(\phi_{i+1})) - \tilde{P}\phi_{i+1}}{\tilde{T}} \\
&= \frac{\tilde{P}}{\tilde{T}}(1 - \phi_{i+1} - z_A(\phi_{i+1}))
\end{aligned}$$

and

$$\begin{aligned}\phi_{i+1} &= \frac{t_{i+1}}{\tilde{P}} \\ &= \frac{T_{i+1} - \tau_i}{\tilde{P}} \\ &= \frac{\tilde{T}(1 - z_B(\theta_i)) - \tilde{T}\theta_i}{\tilde{P}} \\ &= \frac{\tilde{T}}{\tilde{P}}(1 - \theta_i - z_B(\theta_i))\end{aligned}$$

Substitute this relation into the above θ function, a 1D map for θ_i is obtained.

$$\theta_{i+1} = \pi(\theta_i) = \frac{\tilde{P}}{\tilde{T}}(1 - z_A(\frac{\tilde{T}}{\tilde{P}}(1 - \theta_i - z_B(\theta_i)))) - 1 + \theta_i + z_B(\theta_i) \tag{5.1}$$

The fixed point of this map satisfies:

$$\frac{\tilde{P}}{\tilde{T}}(1 - z_A(\frac{\tilde{T}}{\tilde{P}}(1 - \theta^* - z_B(\theta^*)))) - 1 + z_B(\theta^*) = 0 \tag{5.2}$$

The stability condition of the fixed point is $|\pi'(\theta^*)| < 1 \Leftrightarrow |(1+z'_A(\phi^*))(1+z'_B(\theta^*))| < 1$, where $\phi^* = \frac{\tilde{T}}{\tilde{P}}(1 - \theta^* - z_B(\theta^*))$. These results are equivalent to the results in [20].

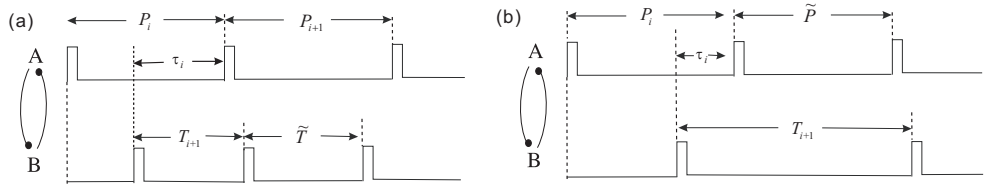

Figure 5.5 Firing patterns that are not 1:1. (a) A fires once, followed by two subsequent firings of B. (b) One firing of B and two subsequent firings of A.

In a manner similar to that in the feed-forward network, the conditions for 1:1 phase-locked activity should be considered. Figure 5.5 shows the two phase-locked situations that are not 1:1 in which the inhibition from neuron B delays the firing of A too much (Figure 5.5(a)) and that the inhibition from A delays the firing of B too much (Figure 5.5(b)). To avoid the case in Figure 5.5(a), we need the condition

$\tau_i + P_{i+1} < T_{i+1} + \tilde{T}$. Use the phase notations, $\tau_i + P_{i+1} < T_{i+1} + \tilde{T} \Leftrightarrow z_A(\phi_{i+1}) > 1 - \frac{\tilde{T}}{\tilde{P}}(2 - \theta_i - z_B(\theta_i))$. Since $\phi_{i+1} = \frac{\tilde{T}}{\tilde{P}}(1 - \theta_i - z_B(\theta_i))$, $z_A(\phi_{i+1}) > 1 - \frac{\tilde{T}}{\tilde{P}} - \phi_{i+1}$. So, to obtain a 1:1 phase-locked solution, the fixed point $\phi^* = \frac{\tilde{T}}{\tilde{P}}(1 - \theta^* - z_B(\theta^*))$ should satisfy $z_A(\phi^*) > 1 - \frac{\tilde{T}}{\tilde{P}} - \phi^*$. Geometrically, at the fixed point, the STRC of A, $z_A(\phi)$, should be above the line $z_A = 1 - \frac{\tilde{T}}{\tilde{P}} - \phi$ as shown in Figure 5.6(a). To avoid the case in Figure 5.5(b), we need the condition $T_{i+1} < \tau_i + \tilde{P} \Leftrightarrow z_B(\theta_i) > 1 - \frac{\tilde{P}}{\tilde{T}} - \theta_i$, or locally, $z_B(\theta^*) > 1 - \frac{\tilde{P}}{\tilde{T}} - \theta^*$, i.e., the STRC of B, $z_B(\theta)$, should be above the line $z_B = 1 - \frac{\tilde{P}}{\tilde{T}} - \theta$ at the fixed point (Figure 5.6(b)).

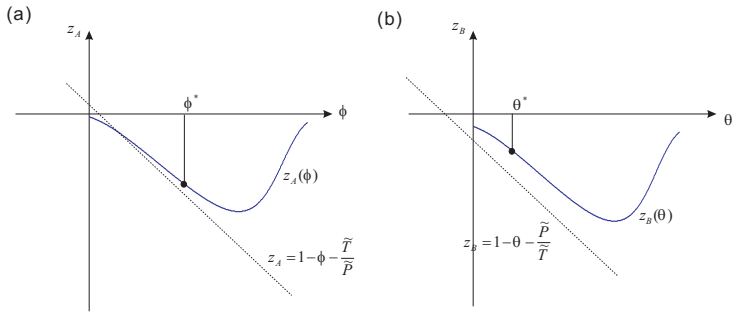

Figure 5.6 Conditions on the STRCs of neurons for the 1:1 phase-locked activity of the feedback network. (a) The STRC of A should be above the dashed line $z_A = 1 - \frac{\tilde{T}}{\tilde{P}} - \phi$. (b) The STRC of B should be above the dashed line $z_B = 1 - \frac{\tilde{P}}{\tilde{T}} - \theta$.

5.3 Phase-locked Activity of Two Neurons in a Feedback Network with Synaptic Depression

In this section, we consider the network involving short-term synaptic depression. Assume in the feedback network of two mutually inhibitory neurons A and B, the synapse from B to A is still non-depressing, while the synapse from A to B is depressing. With non-depressing synapse, the synaptic strength from A to B at the time A fires is determined by the gating variable s (red trace in Figure 5.7) representing the fraction of open synaptic channels. In Figure 5.7, when A fires, s

is set to a constant, without loss of generality, say 1, then s decays to 0 with some time constant. With depressing synapse, when A fires, s is not set to a constant, but the value of the depression variable d (green trace in Figure 5.7) which represents the fraction of available synaptic resources when the neuron fires. It is reset by a fraction f $(0 < f < 1)$ at the instant that A fires and recovers towards 1 with time constant τ_d after A fires.

$$\begin{cases} \dot{d} = \frac{1-d}{\tau_d} & \text{after neuron A fires} \\ d^+ = f \cdot d^- & \text{when neuron A spikes} \end{cases} \tag{5.3}$$

The value of the depression variable at the moment neuron A fires changes with the period of A. The longer the period of A, the larger the value d recovers to 1, as do the s value and the synaptic strength. Thus, the change in the period of A leads to different delay firing time of B.

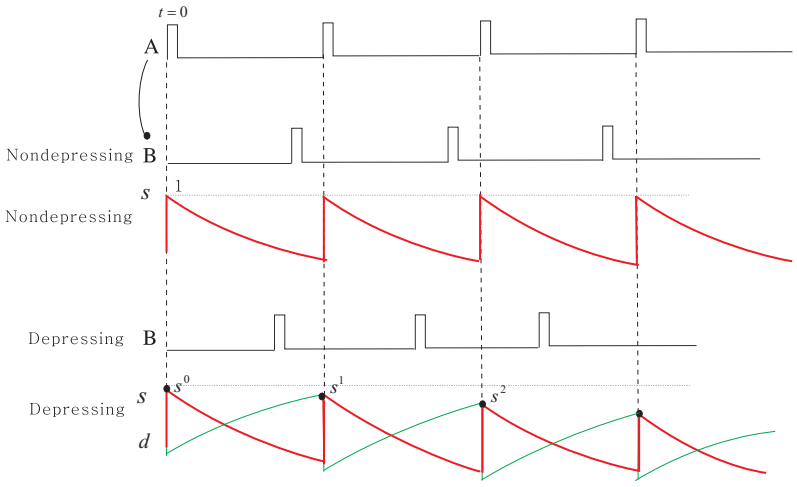

Figure 5.7 Non-depressing synapse and depressing synapse.

The 1D map derived from the non-depressing synapse case in section 5.2 should be revised due to the synaptic depression from neuron A to neuron B. Since the synaptic strength changes cycle by cycle, besides depending on the relative firing time of A, the new period of B also depends on the value of the depression variable

at the moment A spikes (Figure 5.8). Therefore, the STRC of B is a two variable function, $z_B(\theta, d)$, due to the synaptic depression of neuron A. The STRC of A, z_A stays the same as in the previous map because the synapse from B to A is still non-depressing. Hence,

$$\theta_{i+1} = \frac{\tilde{P}}{\tilde{T}}(1 - z_A(\frac{\tilde{T}}{\tilde{P}}(1 - \theta_i - z_B(\theta_i, d_i)))) - 1 + z_B(\theta_i, d_i) + \theta_i.$$

Now, we are deriving the map for the value of the depression variable when A fires in each cycle, d_i, $i = 1, 2, \cdots$. According to Equation (3), $d_{i+1} = 1 - (1 - d_i)exp(-\frac{P_{i+1}}{\tau_d})$ and $P_{i+1} = \tilde{P}(1 - z_A(\frac{\tilde{T}}{\tilde{P}}(1 - \theta_i - z_B(\theta_i, d_i))))$. Thus,

$$d_{i+1} = 1 - (1 - fd_i)exp(-\frac{\tilde{P}}{\tau_d}(1 - z_A(\frac{\tilde{T}}{\tilde{P}}(1 - \theta_i - z_B(\theta_i, d_i))))).$$

So, for a feedback network with synaptic depression, to examine the phase-locked activity of neurons, there is a 2D map based on θ, the phase of neuron A and d, the value of its depression variable.

$$\begin{cases} \theta_{i+1} = \pi_1(\theta_i, d_i) = \frac{\tilde{P}}{\tilde{T}}(1 - z_A(\frac{\tilde{T}}{\tilde{P}}(1 - \theta_i - z_B(\theta_i, d_i)))) - 1 + z_B(\theta_i, d_i) + \theta_i \\ d_{i+1} = \pi_2(\theta_i, d_i) = 1 - (1 - fd_i)exp(-\frac{\tilde{P}}{\tau_d}(1 - z_A(\frac{\tilde{T}}{\tilde{P}}(1 - \theta_i - z_B(\theta_i, d_i))))) \end{cases} \tag{5.4}$$

The fixed points of this 2D map (θ^*, d^*) satisfy the equations:

$$\begin{cases} \frac{\tilde{P}}{\tilde{T}}(1 - z_A(\frac{\tilde{T}}{\tilde{P}}(1 - \theta^* - z_B(\theta^*, d^*)))) - 1 + z_B(\theta^*, d^*) = 0 \\ z_A(\frac{\tilde{T}}{\tilde{P}}(1 - \theta^* - z_B(\theta^*, d^*))) = 1 - \frac{\tau_d}{\tilde{P}} ln(\frac{1 - fd^*}{1 - d^*}) \end{cases} \tag{5.5}$$

The stability of the obtained fixed points can be investigated by the Jacobian of the 2D map.

$$\text{J}= \begin{pmatrix} A_{11} & A_{12} \\ A_{21} & A_{22} \end{pmatrix} = \begin{pmatrix} \frac{\partial \pi_1}{\partial \theta} & \frac{\partial \pi_1}{\partial d} \\ \frac{\partial \pi_2}{\partial \theta} & \frac{\partial \pi_2}{\partial d} \end{pmatrix}_{(\theta^*, d^*)}$$

If the two eigenvalues of this matrix are within the unit circle, i.e., eigenvalues λ_1 and λ_2 satisfy $|\lambda_1| < 1$ and $|\lambda_2| < 1$ or $2 > 1 + det(A) > |tr(A)|$, where $det(A) = A_{11}A_{22} - A_{12}A_{21}, tr(A) = A_{11} + A_{22}$, then the fixed point is stable. We next consider a specific model to investigate this further.

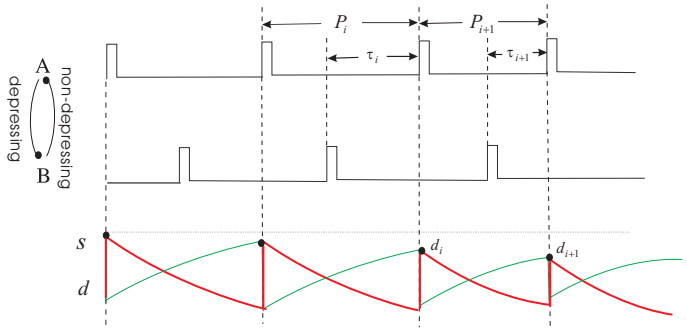

Figure 5.8 Feedback network with depressing synapse from neuron A to neuron B.

5.4 Quadratic Integrate-and-fire (QIF) Model

To verify the validity of our method and examine the role of the synaptic depression, we use the Quadratic Integrate-and-fire Model to generate the STRCs and investigate the solutions of the maps given in (1) and (4).

Quadratic Integrate-and-fire Model [31]:

$$\begin{cases} \frac{dV}{dt} = 1 + V^2 + a \cdot \delta(t - t_s) \\ V^+ = Vr, \text{ when } V = Vt (Vr < Vt) \end{cases} \tag{5.6}$$

where Vt is the threshold and Vr is the resting potential. As soon as the voltage V reaches the threshold Vt, V is reset to the resting potential Vr. At the time $t = t_s$,

a perturbation a is given a the voltage V. If a is positive, V is added by the amount of a, corresponding an excitatory synapse. If a is negative, V is subtracted by the amount of $|a|$, which delays the next firing of the neuron and represents an inhibitory synapse. The intrinsic period of the neuron is $T = arctanVt - arctanVr$ and the new period with a perturbation given at the time $t = t_s$ or at the phase θ ($t_s = T\theta$) is $T = arctanVt - arctan(tan(T\theta + arctanVr) + a) + T\theta$. So the STRC of the neuron can be analytically calculated:

$$STRC(\theta) = \frac{arctan(tan(T\theta + arctanVr) + a) - arctanVr}{T} - \theta \qquad (5.7)$$

If the perturbation is small, the STRCs generated by this model are typical Type I phase response curves (PRCs) [26] as shown in Figure 5.9.

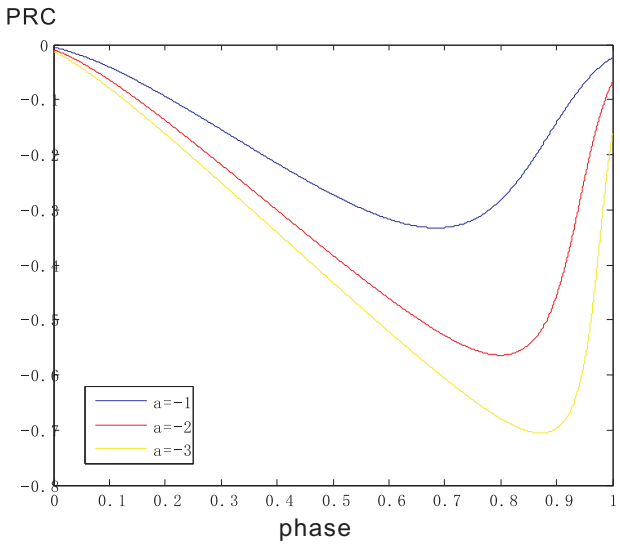

Figure 5.9 STRCs (PRCs) generated by Quadratic Integrate-and-fire Model.

5.4.1 Apply Quadratic Integrate-and-fire Model to a Feedback Network with No Synaptic Depression

From section 5.2, the 1D map for the phase-locked activity of a feedback network with no synaptic depression is:

$$\theta_{i+1} = \pi(\theta_i) = \frac{\tilde{P}}{\tilde{T}}(1 - z_A(\frac{\tilde{T}}{\tilde{P}}(1 - \theta_i - z_B(\theta_i)))) - 1 + \theta_i + z_B(\theta_i)$$

Using QIF, the STRCs of neurons A and B can be analytically expressed.

$$z_A(\phi) = \frac{arctan(tan(\tilde{P}\phi + arctanVr_A) + a_B) - arctanVr_A}{\tilde{P}} - \phi$$

$$z_B(\theta) = \frac{arctan(tan(\tilde{T}\theta + arctanVr_B) + a_A) - arctanVr_A}{\tilde{T}} - \theta$$

The phased-locked activity can be found by looking for the fixed point of this map which is the intersection point of the curve $\pi(\theta)$ (blue curve in Figure 5.10) and the line θ (red line in Figure 5.10) as shown in Figure 10. If the slope of the curve $\pi(\theta)$ at the intersection point is greater than -1 and less than 1, i.e., $|\pi(\theta^*)| < 1$, the fixed point is stable.

The fixed point θ^* must also satisfy the 1:1 firing condition $z_A(\phi^*) > 1 - \frac{\tilde{T}}{\tilde{P}} - \phi^*$ and $z_B(\theta^*) > 1 - \frac{\tilde{P}}{\tilde{T}} - \theta^*$. Here we assume the intrinsic frequency of neuron A is less than that of neuron B, i.e., $\tilde{P} > \tilde{T}$, and the synapse is inhibitory $a < 0$. Under this assumption, at $\phi = 0$, $z_A(0) < 0$ and $1 - \frac{\tilde{T}}{\tilde{P}}$ (Figure 5.11(a)), thus, there must exist an intersection point ϕ_1 of the curve $z_A(\phi)$ with the line $1 - \frac{\tilde{T}}{\tilde{P}} - \phi$. To satisfy the condition $z_A(\phi^*) > 1 - \frac{\tilde{T}}{\tilde{P}} - \phi^*$, the fixed point ϕ^* should be greater than ϕ_1, $\phi^* > \phi_1$, where $\phi_1 = \frac{arctan(tan(\tilde{P}-\tilde{T}+arctanVr_A)-a_B)-arctanVr_A}{\tilde{P}}$. Using the relation $\phi^* = \frac{\tilde{T}}{\tilde{P}}(1 - \theta^* - z_B(\theta^*))$ and Equation (5.2), we proved that the condition $\phi^* > \phi_1$ is equivalent to $\theta^* < 1$. Therefore, if we find a valid value of θ^*, $0 \leq \theta^* < 1$, the conditions $\phi^* > \phi_1$ and $z_A(\phi^*) > 1 - \frac{\tilde{T}}{\tilde{P}} - \phi^*$ are automatically satisfied. On the

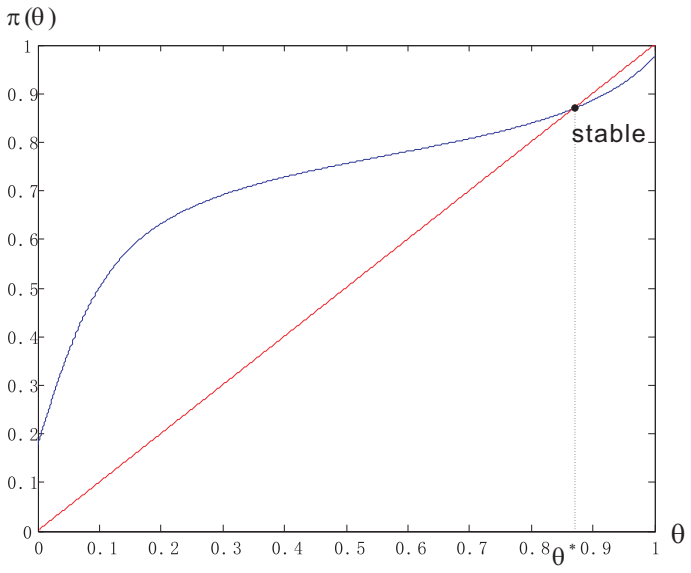

Figure 5.10 Phase-locked solution of the feedback network with no synaptic depression. The intersection of the curve $\pi(\theta)$ with the line θ determines the fixed point θ^* corresponding to the phase locked solution.

STRC of neuron B, the fixed point θ^* should satisfy $z_B(\theta^*) > 1 - \frac{\tilde{P}}{\tilde{T}} - \theta^*$ (Figure 5.11(b)). At $\theta = 0$, $z_B(0) < 0$ and $1 - \frac{\tilde{P}}{\tilde{T}} < 0$, so there are two possibilities for the locations of $z_B(\theta)$ and $1 - \frac{\tilde{P}}{\tilde{T}} - \theta$. One possibility is $1 - \frac{\tilde{P}}{\tilde{T}} < z_B(0)$ (the lower dashed line in Figure 5.11(b)), then $z_B(\theta)$ and $1 - \frac{\tilde{P}}{\tilde{T}} - \theta$ don't intersect and the curve is always above the line. $z_B(\theta) > 1 - \frac{\tilde{P}}{\tilde{T}} - \theta$ holds for all $0 \leq \theta < 1$. If $1 - \frac{\tilde{P}}{\tilde{T}} > z_B(0)$, there exists an intersection point θ_1 of $z_B(\theta)$ with $1 - \frac{\tilde{P}}{\tilde{T}} - \theta$ (the upper dashed line in Figure 5.11(b)). To obtain 1:1 phase-locked solution, the fixed point θ^* should satisfy $\theta^* \geq \theta_1$, where $\theta_1 = \frac{arctan(tan(\tilde{T}-\tilde{P}+arctanVr_B)-a_A)-arctanVr_B}{\tilde{T}}$. Whether $z_B(\theta)$ and $1 - \frac{\tilde{P}}{\tilde{T}} - \theta$ intersect depends on the inhibitory synaptic strength from neuron A to B, the value of a_A, $a_A < 0$. When the synapse is weak, $a_A > a_1$, where $a_1 = tan(\tilde{T} - \tilde{P} + arctanVr_B) - Vr_B$, $1 - \frac{\tilde{P}}{\tilde{T}} < z_B(0)$ and $z_B(\theta) > 1 - \frac{\tilde{P}}{\tilde{T}} - \theta$ for all $0 \leq \theta < 1$. Otherwise, if $a_A < a_1$, $1 - \frac{\tilde{P}}{\tilde{T}} > z_B(0)$ and the condition $\theta^* \geq \theta_1$ is needed. These results are summarized in the following propositions.

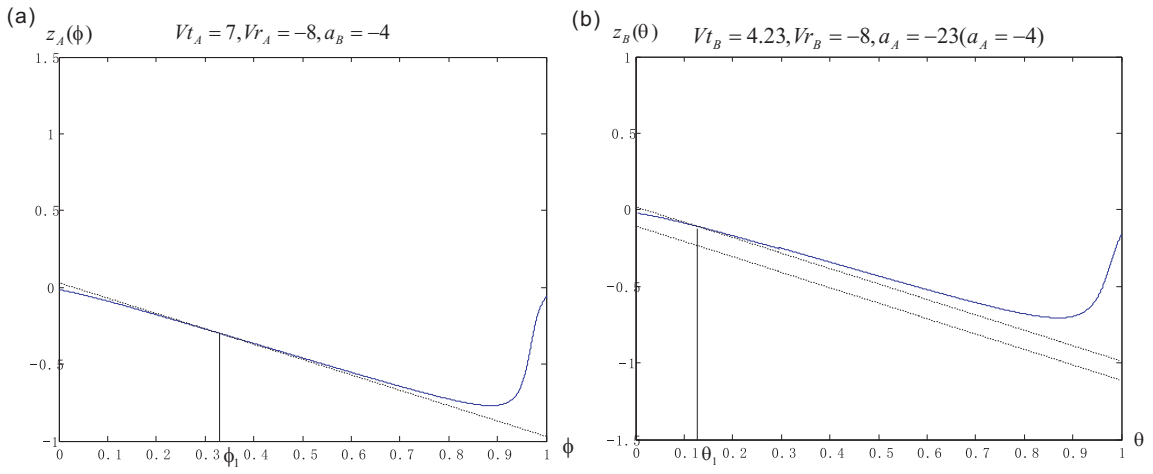

Figure 5.11 Conditions on the STRCs of neurons for the 1:1 phase-locked activity of the feedback network. (a) The fixed point ϕ^* should be greater than ϕ_1. (b) The fixed point θ^* should be greater than θ_1.

Proposition 1: If there exists a fixed point $\theta^* \in [0, 1)$ for the 1D map (5.1) and $a_A > a_1$, where $a_1 = tan(\tilde{T} - \tilde{P} + arctanVr_B) - Vr_B$, θ^* corresponds to a 1:1 phase-locked solution of the feedback network.

Proposition 2: If there exists a fixed point $\theta^* \in [0, 1)$ for the 1D map (1), $a_A < a_1$ and $\theta^* \geq \theta_1$, where $\theta_1 = \frac{arctan(tan(\tilde{T} - \tilde{P} + arctanVr_B) - a_A) - arctanVr_B}{\tilde{T}}$, θ^* corresponds to a 1:1 phase-locked solution of the feedback network.

Examples

(1). The parameter values for neurons A and B: $Vt_A = 7$, $Vr_A = -8$, $Vt_B = 4.23$, $Vr_B = -8$. The synapse from A to B $a_A = -10$ and the synapse from B to A $a_B = -8$. So, $a_1 = -21.3077$. From the 1D map or the fixed point obtained from the geometric method, the intersection of the curve and the line in Figure 5.12(a), the phase of A at the steady state in the feedback network is $\theta^* = 0.9982 \in [0, 1)$. Since $a_A > a_1$, from Proposition 1, θ^* is the 1:1 phase-locked solution. From simulation in

the software XPPAUT, Figure 5.12(b) shows the voltage traces of two neurons at the steady state, which is consistent with the analytical result.

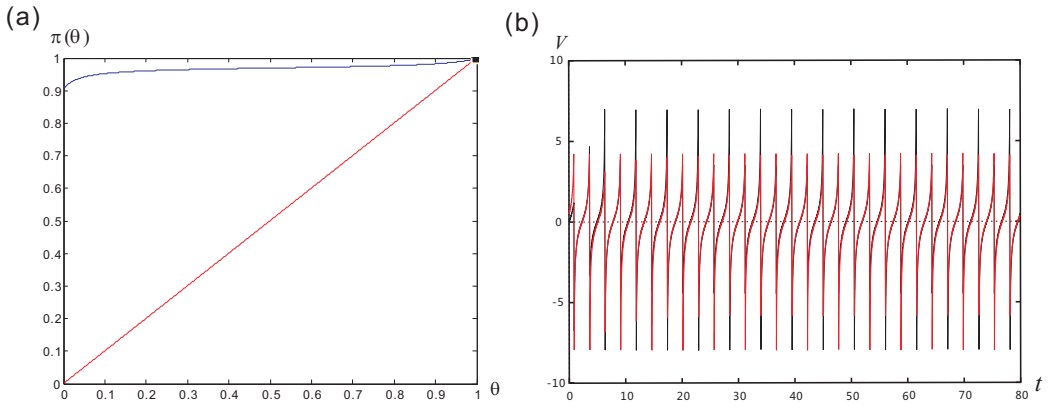

Figure 5.12 An example for the 1:1 phase-locked activity of the feedback network. (a) Solution from 1D map. (b) Voltage traces of neurons A and B from simulation in XPPAUT.

Note that we define θ as the proportion of the relative firing time of A to the intrinsic period of B, i.e., $\theta^* = \frac{\tau^*}{\tilde{T}}$, while in the feedback network, the period is T^* which is different from $\tilde{T}$. That's why the solution θ^* seems inconsistent with what we visibly see in Figure 5.12(b), where the two neurons exhibit near anti-phase locking. We define $\hat{\theta}^* = \frac{\tau^*}{T^*}$. From the analytical solution, $\tau^* = 2.7800$ and $T^* = 5.5206$, thus, $\hat{\theta}^* = 0.5036$. From simulation in XPP, we also find that $\hat{\theta}^* = 0.5036$.

(2). Use the same intrinsic parameter values for the two neurons, but change the synaptic strength value $a_A = -30$ and $a_B = -4$. Since a_1 is independent of the synaptic connection, it keeps the same value as in (5.1), $a_1 = -21.3077$ and $\theta_1 = 0.7382$. From the 1D map, the fixed point $\theta^* = 0.0573 \in [0, 1)$. Here $a_A < a_1$, but $\theta^* < \theta_1$. According to Proposition 2, θ^* is not a 1:1 phase-locked solution. This prediction can be verified by the simulation result in Figure 5.13(b), where A and B are 2:1 phase-locked.

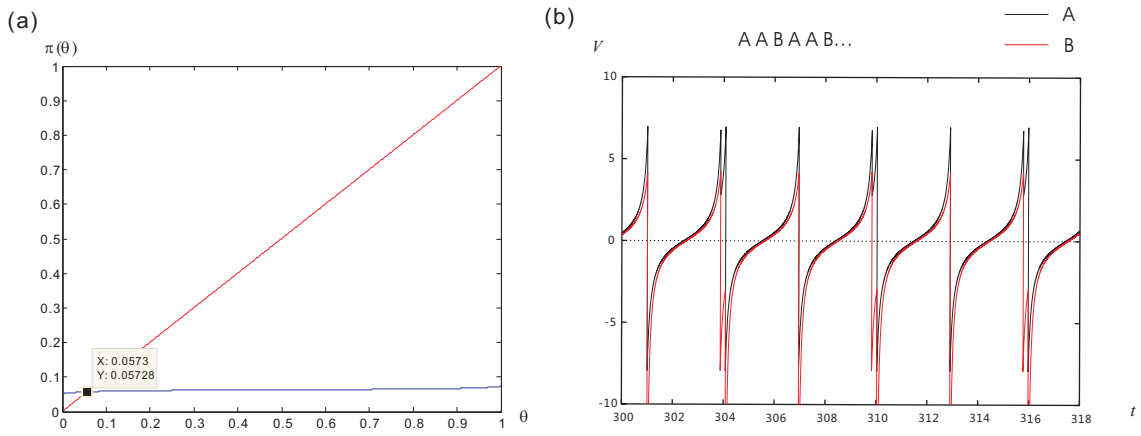

Figure 5.13 An example for the activity of the feedback network in which neurons A and B are not 1:1 phase-locked. (a) Solution from 1D map. (b) Voltage traces of neurons A and B from simulation in XPPAUT.

5.4.2 Apply Quadratic Integrate-and-fire Model to a Feedback Network with Synaptic Depression

In the feedback network without synaptic depression, the phase-locked activity of neurons is obtained from the fixed point of a 1D map (5.1), which is the intersection point of the curve $\pi(\theta)$ and the line θ (Figure 5.10). In the feedback network with synaptic depression, the phase-locked activity of two neurons can be determined by a 2D map (5.4) and the fixed point of this map satisfies Equation (5.5). Using the specific QIF model, the STRC of neuron A is the same as Equation (5.7), while the STRC of B is a two variable function $z_B(\theta, d)$. Without synaptic depression, the STRC of B can be represented as Equation (5.7). With synaptic depression, the synaptic strength from A to B is the product of maximum synaptic strength a_A and the available synaptic resources, i.e., the value of d. Therefore,

$$z_B(\theta, d) = \frac{arctan(tan(\tilde{T}\theta + arctanVr_B) + a_A d) - arctanVr_A}{\tilde{T}} - \theta \qquad (5.8)$$

Plotting the two equations (5.5) in $\theta - d$ plane (Figure 5.14), there are two curves, the red curve corresponding to the first equation and the blue corresponding to the second equation. The intersection of these two curves is the fixed point of the 2D

map.

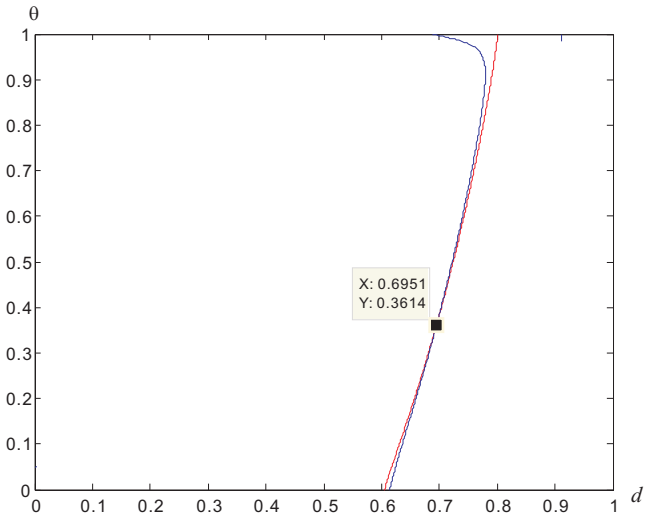

Figure 5.14 Phase-locked solution of the feedback network with synaptic depression. The intersection of the two curves determines the fixed point (θ^*, d^*) corresponding to the phase locked solution.

Example

Take the parameter values: $Vt_A = 7$, $Vr_A = -8$, $Vt_B = 4.23$, $Vr_B = -8$, $a_A = -12$, $a_B = -4$, $f = 0.5$, $\tau_d = 5$. From the fixed point of the 2D map or the intersection of the two curves plotted by Equation (5.5), the two neurons are locked at the phase $\theta^* \approx 0.3614$, $d^* \approx 0.6951$ as shown in Figure 5.15(a), the intersection of the red curve and the blue curve. From simulation by XPPAUT, we obtained the same result (Figure 5.15(b)), $\theta^* \approx 0.3614$, $d^* \approx 0.6951$. The green dots in Figure 5.15(a) are obtained from XPPAUT, representing the values of (θ_i, d_i) in each cycle at the moment neuron A spikes. This sequence quickly converges to the fixed point from some initial value.

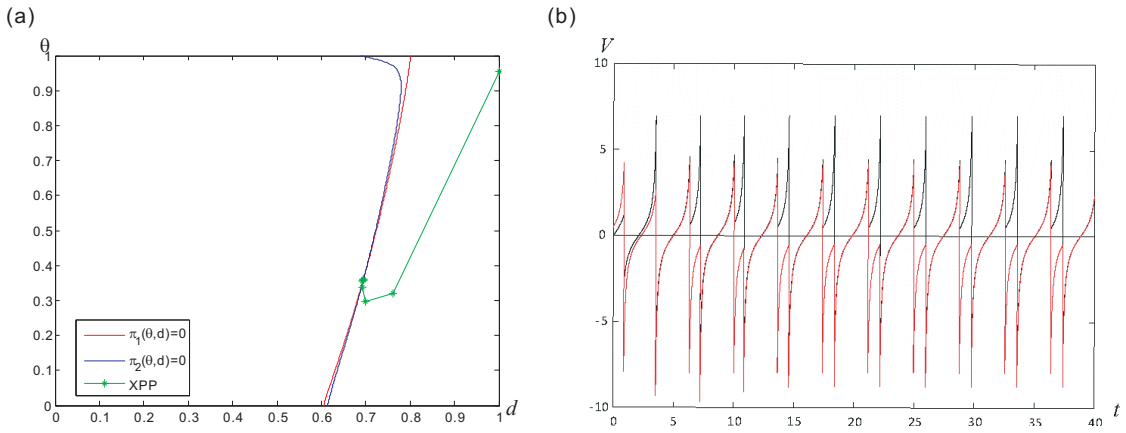

Figure 5.15 An example for the 1:1 phase-locked activity of the feedback network with synaptic depression. (a) Solution from 2D map. (b) Voltage traces of neurons A and B from simulation in XPPAUT.

5.4.3 Relationship between the Phase-locked Activities of the Feedback Network with and without Synaptic Depression

Since the 2D map (5.4) for the feedback network with synaptic depression is very complicated, we will try to find the relationship between the 1D map without synaptic depression and the 2D map with synaptic depression. Then, we will analyze the phase-locked activity of the feedback network with depression through the 1D map, instead of analyzing the 2D map directly.

When the synapse is non-depressing, at the steady state, the phase of A, θ^* decreases with increasing inhibitory synaptic strength from neuron A to neuron B (Figure 5.16(a)). As shown in the upper panel of Figure 5.16(b), when the inhibitory synaptic strength is small, it does not delay the firing of B too much and B fires right after the firing of A. The θ value is near 1. On the other hand, when the synaptic strength is large, the firing of B is delayed a lot, right before the next firing of A and θ value is close to 0, as shown in the lower panel of Figure 5.16(b).

To distinguish the parameter notation for the synaptic strength in the non-depressing synapse case and in the depressing synapse case, in the following, we denote the synaptic strength in the network without synaptic depression or in the 1D

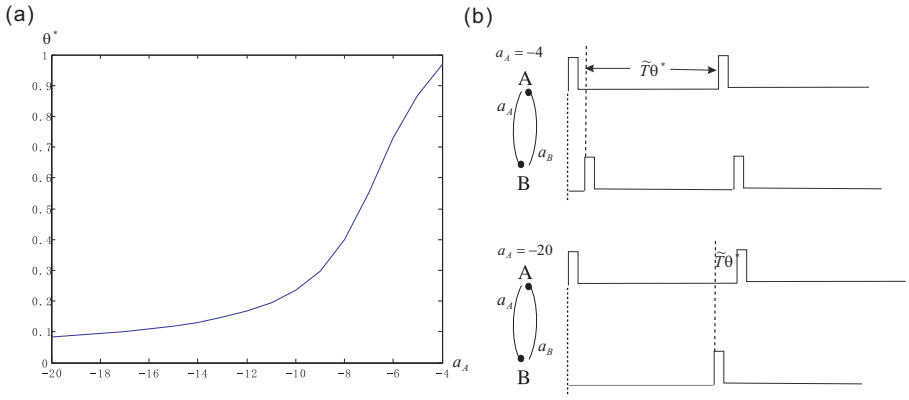

Figure 5.16 Relation between the phase of A and the inhibitory synaptic strength from A to B in the feedback network without synaptic depression. (a) From the 1D map (1), the phase of A decreases with increasing synaptic strength. (b) Schematic plot of the relation between the phase of A and the synaptic strength from A to B.

map as $\bar{a}_A$ and denote the maximal synaptic strength in the network with synaptic depression or in the 2D map as a_A. In the feedback network with depression, the synaptic strength when A fires is the product of the maximal synaptic strength and the value of the depression variable, i.e., $a_A d^*$, which yields the same phase-locked activity in the network without depression, if $\bar{a}_A = a_A d^*$. This proposition is verified in Figure 5.17(a). The blue curve represents the relationship between θ^* and $\bar{a}_A$ in the $\theta^* - \bar{a}_A$ plane obtained from the 1D map (5.1). There always exists a pair of (a_A, d^*) in the 2D map corresponding to the same θ^* value for the 1D map and they satisfy the relation $\bar{a}_A = a_A d^*$ except in a very small region near $\theta^* = 1$. The red curve in Figure 5.17(a) is the relationship between θ^* and $a_A d^*$, obtained from the 2D map (5.4) which overlaps the blue curve for the 1D map in almost the entire domain except a small region near $\theta^* = 1$ which is zoomed in Figure 5.17(b). To explain this, first, we construct the relationship between a_A, d^* and $\bar{a}_A$. Compare the first equation in Equations (5.5) for the fixed point of the 2D map with Equations (5.2) for the fixed point of the 1D map, the only difference is that with a depressing synapse, the STRC of neuron B is a two variable function $z_B(\theta^*, d^*)$ instead of $z_B(\theta^*)$. Here,

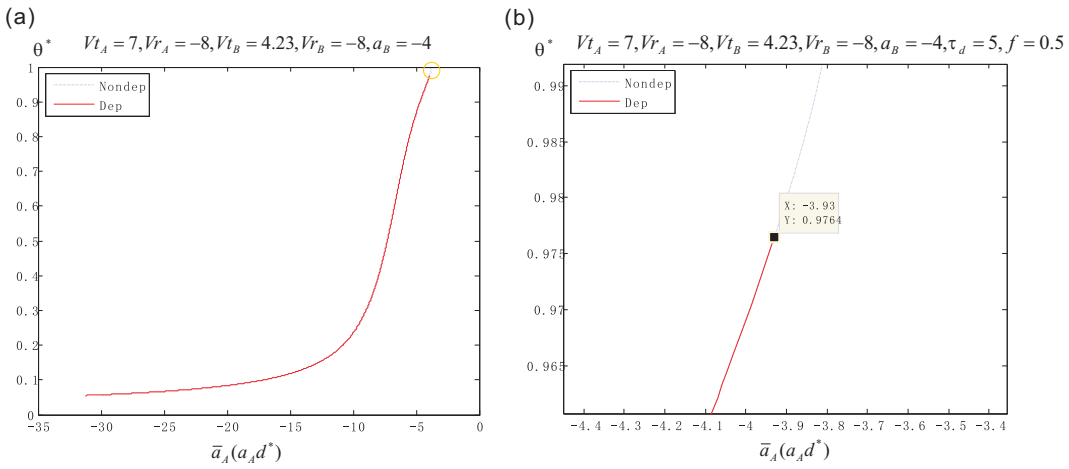

Figure 5.17 Comparison of the result from the 1D map and that from the 2D map. (a) The relation curve of θ^* and $a_A d^*$ from the 2D map overlaps the relation curve of θ^* and $\bar{a}_A$ from the 1D map, where $\bar{a}_A = a_A d^*$, except a small region near $\theta^* = 1$. (b) Zoom-in of the inconsistent part of (a).

$$z_B(\theta^*) = \frac{arctan(tan(\tilde{T}\theta^* + arctanVr_B) + \bar{a}_A) - arctanVr_A}{\tilde{T}} - \theta^*$$
$$z_B(\theta^*, d^*) = \frac{arctan(tan(\tilde{T}\theta^* + arctanVr_B) + a_A d^*) - arctanVr_A}{\tilde{T}} - \theta^*$$

Therefore, to obtain the same phase θ^*, we need $\bar{a}_A = a_A d^*$. Rewrite the first equation in (5.5) as

$$z_A(\frac{\tilde{T}}{\tilde{P}}(1 - \theta^* - z_B(\theta^*, d^*))) = 1 - \frac{\tilde{T}}{\tilde{P}}(1 - z_B(\theta^*, d^*)).$$

Combining with the second equation in (5.5), d^* should satisfy

$$1 - \frac{\tilde{T}}{\tilde{P}}(1 - z_B(\theta^*, d^*)) = 1 - \frac{\tau_d}{\tilde{P}} ln \frac{1 - fd^*}{1 - d^*}$$

$$\Leftrightarrow \qquad ln\frac{1 - fd^*}{1 - d^*} = \frac{\tilde{T}}{\tau_d}(1 - z_B(\theta^*, d^*))$$
$$= \frac{\tilde{T}}{\tau_d}(1 - z_B(\theta^*)|\bar{a}_A)$$

$$\Leftrightarrow \qquad d^* = \frac{exp(\frac{\tilde{T}}{\tau_d}(1 - z_B(\theta^*)|\bar{a}_A) - 1}{exp(\frac{\tilde{T}}{\tau_d}(1 - z_B(\theta^*)|\bar{a}_A) - f}$$

So, for a synaptic strength $\bar{a}_A$ in the feedback network without synaptic depression, there is a fixed point θ^* of the 1D map. To obtain the same fixed point θ^* in the 2D map, d^* and a_A should satisfy the following two equations:

$$d^* = \frac{exp(\frac{\tilde{T}}{\tau_d}(1 - z_B(\theta^*)|\bar{a_A}) - 1}{exp(\frac{\tilde{T}}{\tau_d}(1 - z_B(\theta^*)|\bar{a_A}) - f} \tag{5.9}$$

$$a_A = \frac{\bar{a}_A}{d^*} \tag{5.10}$$

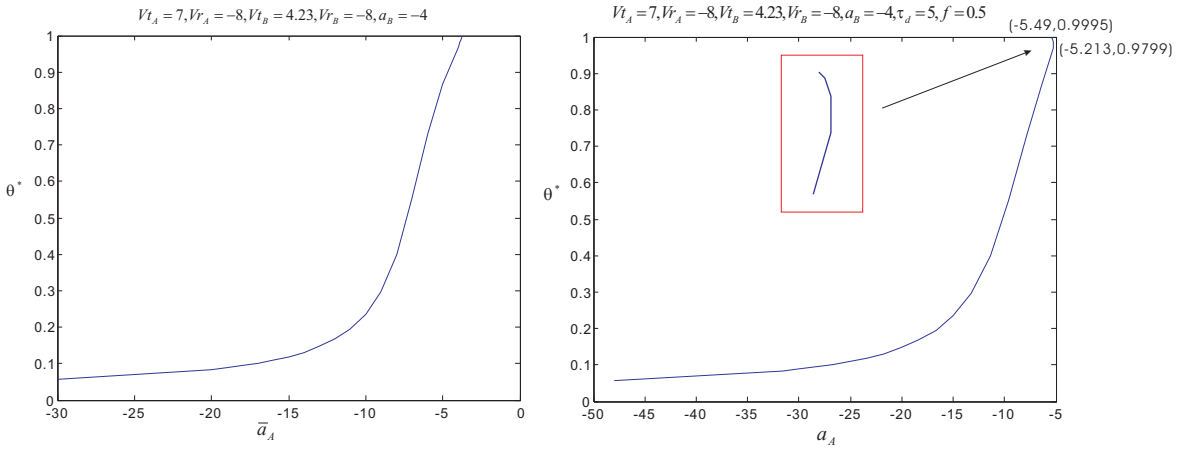

Figure 5.18 Comparison of the 1D map and the 2D map. (a) The relation curve of θ^* and $\bar{a}_A$ from the 1D map. (b) The relation curve of θ^* and a_A obtained from equations (5.9) and (5.10). The inset is the enlargement of the right end part, where each a_A value corresponds to two θ^* values. The fixed point corresponding to the bigger θ^* value is stable, while that corresponding to the smaller one is unstable.

In Figure 5.18(a), the curve is obtained from the 1D map (5.1), showing the relation between θ^* and $\bar{a}_A$. Figure 5.18(b) is the dependence of θ^* on the synaptic strength a_A in the depressing synapse case which is obtained from the above relation formulae (5.9) and (5.10). The right end part of the curve bends up due to the decreasing of d^*, meaning that for the a_A values in this part, there are two fixed

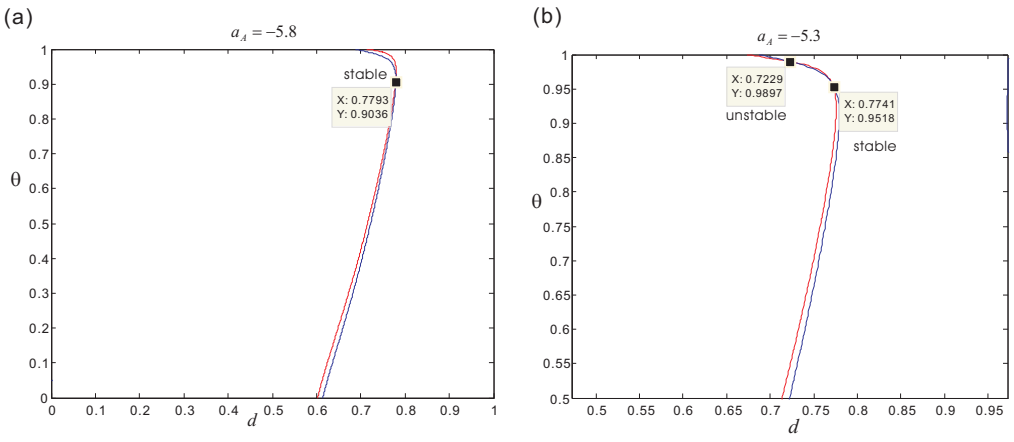

Figure 5.19 Plotting of the two curves from Equations (5.5). (a) When $a_A = -5.8$, there is one intersection point. (b) When $a_A = -5.3$, there are two intersection points.

points, θ_1^* and θ_2^*, $\theta_1^* < \theta_2^*$. Through checking the stability, we found the smaller value θ_1^* is stable and the bigger value θ_2^* is unstable. This explains why we can not obtain phase-locked activities in the region where θ^* is close to 1 (Figure 5.17(b)). In Figure 5.19, we directly plot the curves for (5.5) and find the intersection points. When $a_A < -5.49$, there is one intersection of the two curves (Figure 5.19(a)). When $a_A > -5.49$, there are two intersections and the bigger θ^* value is unstable (Figure 5.19(b)). This domain of a_A corresponds to the enlarged part in Figure 5.18(b) where one a_A value corresponds to two θ^* values. With increasing a_A value or decreasing strength $|a_A|$, the two intersection points get closer and finally the curves become tangent and then don't intersect with each other. In Figure 5.20(a), $a_A = -5.3706$ and there are two intersections. When a_A value increases to -5.2390, the upper intersection moves down and the lower intersection moves up and they are getting closer. This phenomenon is also shown in the curves from Formulae (5.9) and (5.10) in Figure 5.18(b). These analytical results can be verified by the simulations in XPPAUT. Figure 5.21(a) shows the dependency of θ^* on the synaptic strength of A, a_A. θ^* decreases as $|a_A|$ increases and neurons A and B are not phase-locked when

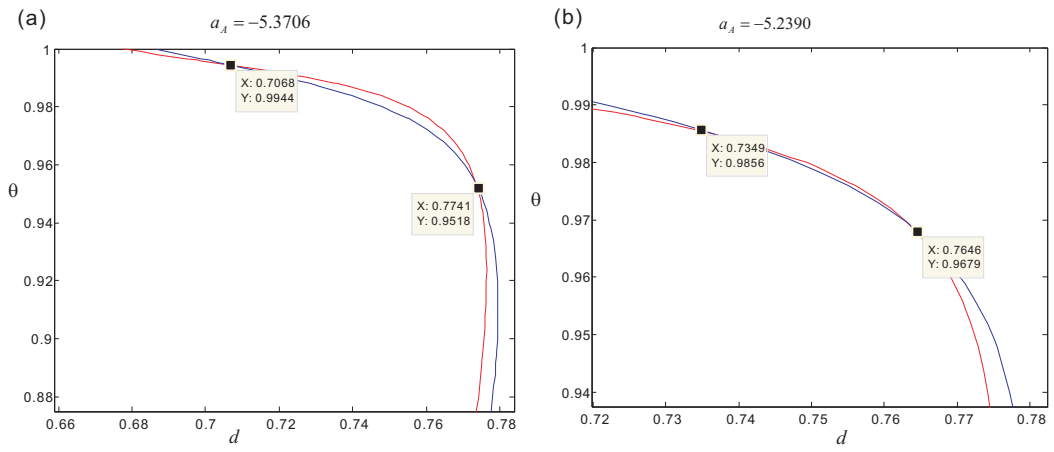

Figure 5.20 The intersection points get closer with increasing a_A value. (a) $a_A = -5.3706$. (b) $a_A = -5.2390$.

$a_A > -5.21$. Figure 5.21(b) is the voltage traces of A and B when $a_A = -5.209$, which shows they are not phase-locked.

To conclude, we have the following propositions.

Proposition 1: In the feedback network of A and B with no synaptic depression, there exists a synaptic strength $\bar{a}_A^*$, such that, when $\bar{a}_A < \bar{a}_A^*$, the two neurons are phase-locked. Moreover,

$$\lim_{\bar{a}_A \to \bar{a}_A^*} \theta^* = 1$$

Proposition 2: In the feedback network with depression in the synapse from A to B, there exists a synaptic strength a_A^*, such that, when $a_A < a_A^*$, the two neurons are phase-locked. Moreover,

$$\lim_{a_A \to a_A^*} \theta^* = b$$

where $b < 1$.

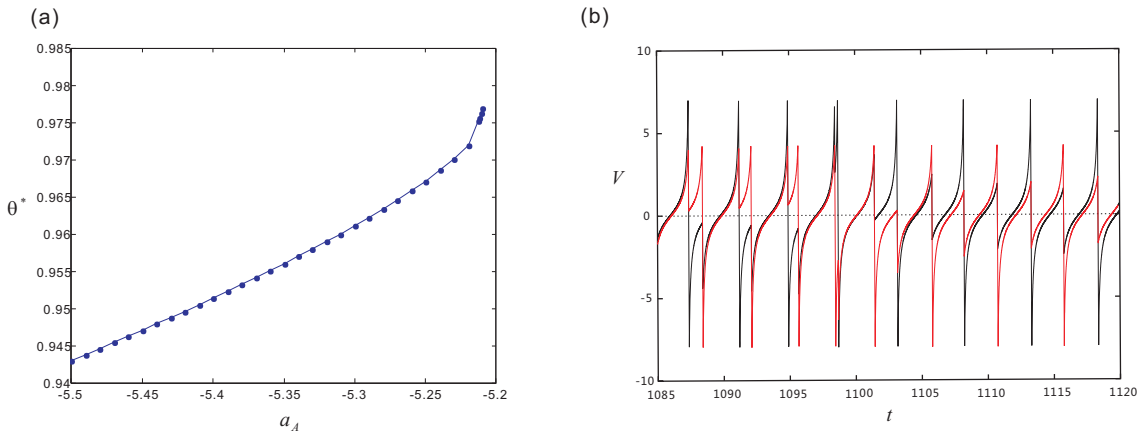

Figure 5.21 Simulation results from XPPAUT. (a) The dependency of the phase of A, θ^* on the synaptic strength of A, a_A. (b) The voltage traces of A and B when $a_A = -5.209$. The black trace is for neuron A and the red trace is for neuron B.

5.5 Morris-Lecar Model

In this section, we apply our method to the Morris-Lecar biological model. The equations for neuron A or B are the following.

$$\begin{aligned}
\frac{dV}{dt} &= -\bar{g}_{Ca} m_\infty(V)(V - E_{Ca}) - \bar{g}_K W(V - E_K) - g_L(V - E_L) + I_{ext} \\
\frac{dW}{dt} &= \lambda(V)(W_\infty(V) - W) \\
\frac{ds_A}{dt} &= \frac{1-s}{\tau_1} Heav(V - V_{th}) - \frac{s}{\tau_2} Heav(V_{th} - V) \\
m_\infty(V) &= 0.5(1 + tanh\frac{V - V_1}{V_2}) \\
W_\infty(V) &= 0.5(1 + tanh\frac{V - V_3}{V_4}) \\
\lambda(V) &= \phi cosh\frac{V - V_3}{2V_4}
\end{aligned}$$

If there is an inhibitory synaptic input from the presynaptic neuron, another term $I_{syn} = -\bar{g}_{syn} s(V - E_{syn})$ is added to the right hand side of the first equation, the V equation. This model can generate oscillatory spiking patterns as shown in Figure

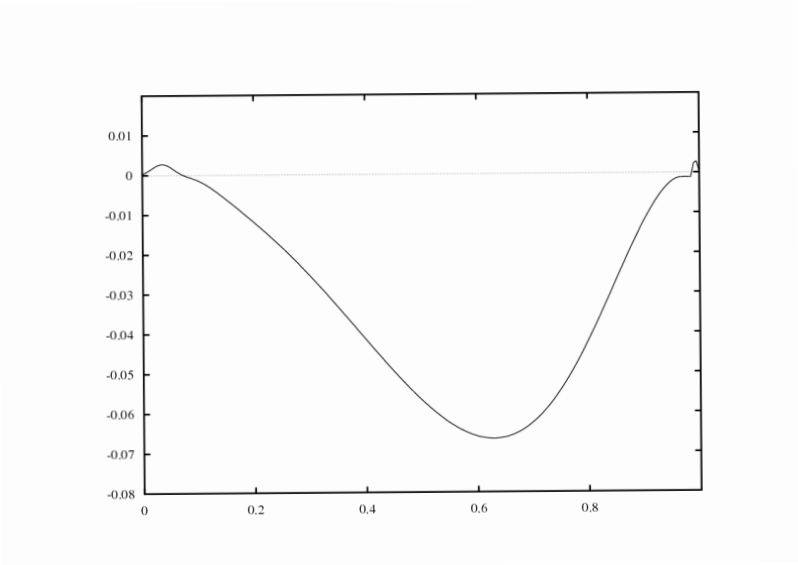

Figure 5.22 A typical STRC generated by Morris Lecar model.

5.23. To generate STRCs of this type of neuron, the synaptic input is modeled by a square-wave pulse. For consistency with the synaptic input from the presynaptic neuron in the model, the width of the square-wave pulse is set to the active duration of the presynaptic neuron which is short and fixed for the spiking pattern and the magnitude of the square-wave pulse is the synaptic strength of the presynaptic neuron. A typical shape of the STRC generated by this model looks like type I (Figure 5.22) and very similar to the STRCs generated by QIF model (Figure 5.9).

First we assume the synapses both from neuron A to B and that from B to A are non-depressing. The synaptic strength is constant with non-depressing synapses. Although the explicit or analytical functions for the STRCs of neurons A and B are unknown, we numerically generate the STRCs using the adjoint method [25] in XPPAUT. The values of $z_B(\theta_i)$ and $z_A(\phi_i)$ in 1D map (5.1), where $\phi_i = \frac{\tilde{T}}{\tilde{P}}(1 - \theta_{i-1} - z_B(\theta_{i-1}))$, $i = 1, 2, \cdots$, can be obtained from the numerically generated STRCs of the corresponding neurons. So, the map (5.1) and the equation (5.2) can still be used to find the fixed point and the phased-locked solution. The relation between

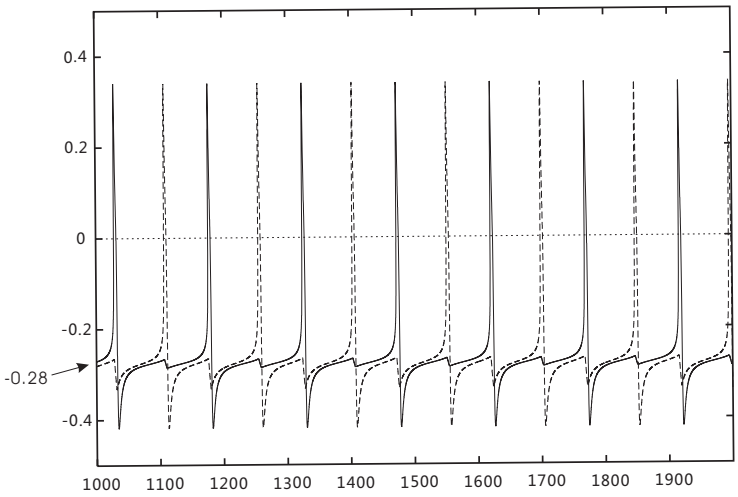

Figure 5.23 Voltage traces of two neurons generated by Morris-Lecar model.

the steady state phase θ^* and the synaptic strength from A to B $\bar{g}_{synA}$ is shown in Figure 5.24. Figure 5.24(b) is the zoom-in of Figure 5.24(a). In this figure, there are three curves. The blue curve is the solution obtained from 1D map (5.1). The red and green curves are simulation results of Morris-Lecar model in XPPAUT. The red curve is generated by a simplified formula for the synapse, $I_{syn} = -\bar{g}_{syn}s$ and the green one is obtained by setting $E_{inh} \approx V_{rest} - 1$. The reason for this choice is we need the synaptic input form in the model to be consistent with the synaptic input used to produce the STRCs. The solution from 1D map (5.1) is very close to the simulation results.

When the synapse from A to B is depressing, in the 2D map (5.4), the synaptic strength d_i varies cycle by cycle. Different d_i values correspond to different STRCs. $z_B(\theta_i, d_i)$ in (5.4) is determined by choosing the appropriate STRC corresponding to the d_i value. Figure 5.24 shows the dependance of θ^* on the synaptic strength $\bar{g}_{synA}$ in the depressing synapse case. The blue curve is from the 2D map and the numerically generated STRCs and the red and green curves are from XPP simulation with different setting as described in the above paragraph.

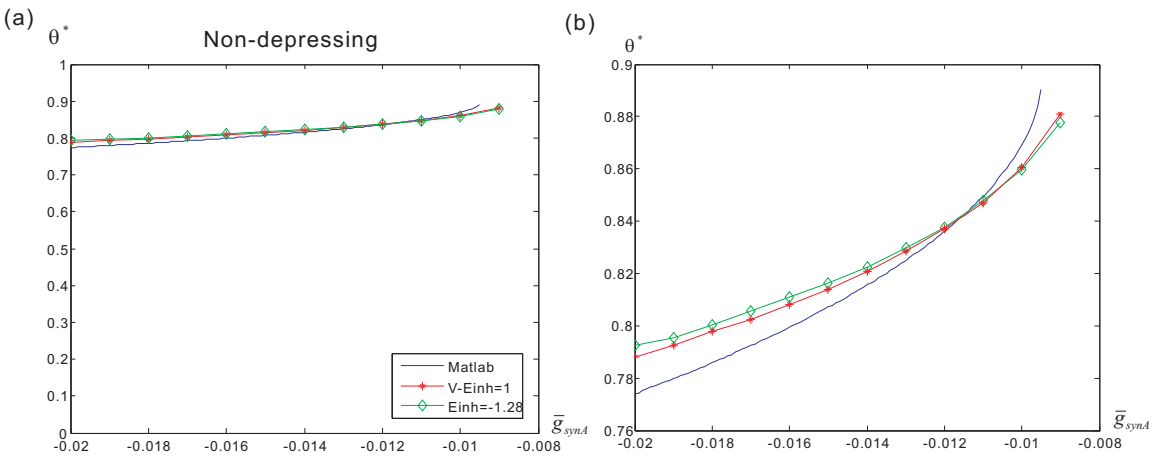

Figure 5.24 The relation between the phase of A θ^* and the synaptic strength of A $\bar{g}_{synA}$ when the synapses are non-depressing. (a) The blue curve is the solution of the 1D map (5.1). The red curve is obtained by setting $I_{syn} = -\bar{g}_{syn}s$ in the Morris-Lecar model. The green curve is obtained by setting $E_{inh} \approx V_{rest} - 1$ in the Morris-Lecar model. (b) The zoom-in of (a).

The phase-locked solution can also be obtained using geometric methods. Plotting the two equations in (5.5) in the $\theta - d$ plane as shown in Figure 5.26(a), the intersections of these two curves are the fixed points of the map (5.4). The red curve corresponds to the first equation in (5.5) and the blue curve corresponds to the second equation. There are two fixed points and the one with smaller θ value is stable. Different from the QIF model, the PRC functions $z_A(\phi)$ and $z_B(\theta, d)$ in (5.5) do not have analytical expressions, but numerically generated by the adjoint method in XPP. The green stars in the figure are the θ, d values in each cycle obtained from simulation. They quickly converges to the stable fixed point obtained from the analytical method with consistent parameter values. Figure 5.26(b) is the voltage traces of neurons A and B modeled by the Morris-Lecar model. The black trace represents the voltage of A and the red one is for neuron B. The stable fixed point in (a) $(\theta^*, d^*) \approx (0.86, 0.868)$ and the simulation result in (b) is $(\theta^*, d^*) \approx (0.8498, 0.8679)$ which are very close.

Comparing the results obtained from QIF model in Section 5.4 and the results from the Morris-Lecar model, we find they are very similar as shown in Figure

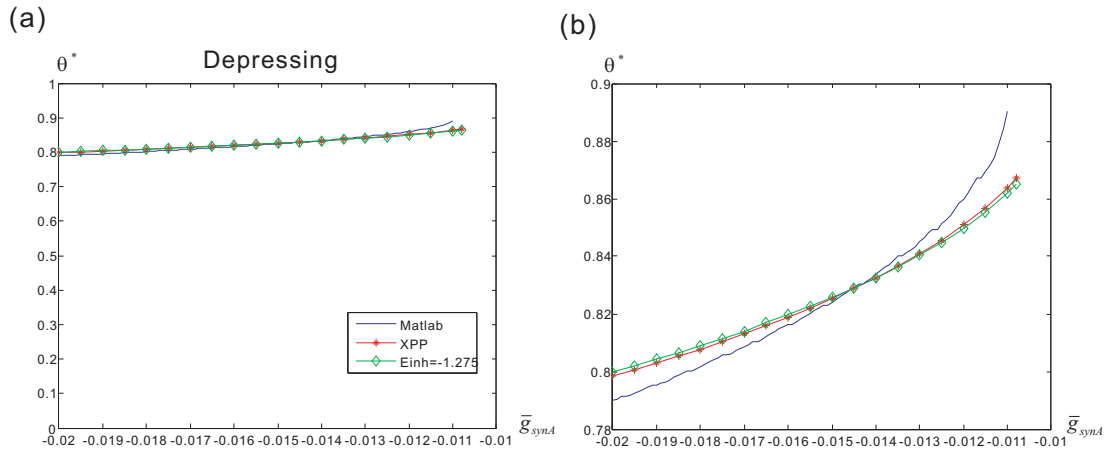

Figure 5.25 The relation between the phase of A θ^* and the synaptic strength of A $\bar{g}_{synA}$ when the synapse from neuron A to B is depressing. (a) The blue curve is the solution of the 2D map (5.4). The red curve is obtained by setting $I_{syn} = -\bar{g}_{syn}s$ in the Morris-Lecar model. The green curve is obtained by setting $E_{inh} \approx V_{rest} - 1$ in the Morris-Lecar model. (b) The zoom-in of (a).

5.27. Figure 5.27(a) shows the results of the Morris-Lecar model by using either $V - E_{inh} = 1$ or $E_{inh} = -1.275$ as described in Figure 5.24, showing the dependence of the phase on the synaptic strength and Figure 5.25(b) show results from the QIF model. In these two models, the steady state phase both decreases with increasing synaptic strength. Figure 5.26 shows a comparison of the depression variable d^* at the steady state from the two models. The curves in Figure 5.28(a) are the solution of Morris-Lecar model and Figure 5.28(b) is from QIF model. Both show d^* first increasing and then decreasing with increasing synaptic strength. The similarity between the results of two very different models is due to the fact that they have similar STRCs.

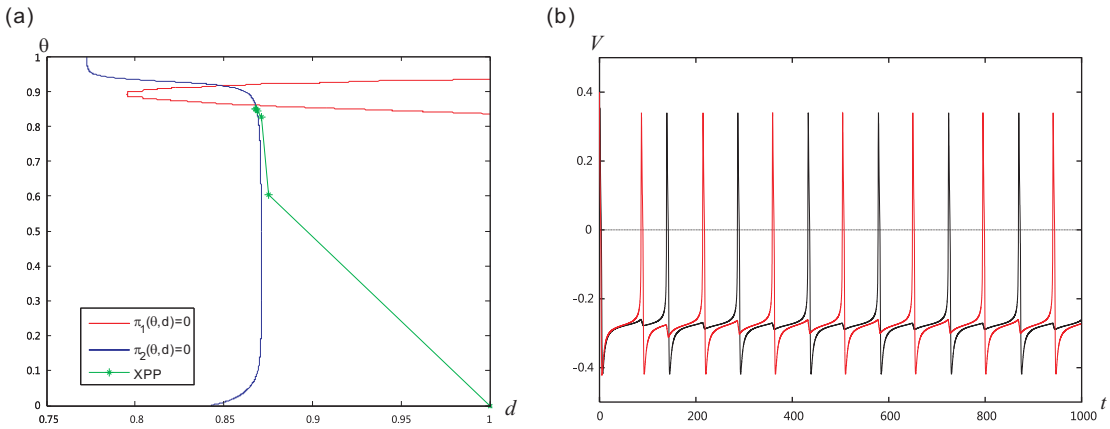

Figure 5.26 Phase-locked activity of the feedback network with synaptic depression modeled by the Morris-Lecar model. (a) Solution from 2D map. (b) Voltage traces of neurons A and B from simulation in XPPAUT.

5.6 Geometric Method of Predicting Phase-locked Activity of a Two Neuron Feedback Network

Given the STRC of the neuron or how it is affected by the spiking of the presynaptic neuron in the feed-forward network as well as the information of the feed-forward network in the opposite direction, we can predict the phase-locked activity of the feedback network through geometric methods.

First, we examine the non-depressing synapse case. Let $\phi^* = \frac{\tilde{T}}{\tilde{P}}(1-\theta^*-z_B(\theta^*))$. Equation (5.2) can be rewritten as two equations.

$$\begin{cases} \phi^* = \frac{\tilde{T}}{\tilde{P}}(1-\theta^*-z_B(\theta^*)) \\ \theta^* = \frac{\tilde{P}}{\tilde{T}}(1-\phi^*-z_A(\phi^*)) \end{cases}$$

Each equation provides feed-forward information. The first equation involves the information how neuron A affects neuron B or the STRC of B, $z_B(\theta)$ and the second one includes the information in the other direction $z_A(\phi)$. Plot the curves for each equation on the $\phi-\theta$ plane and the intersection of these two curves is the phase-locked solution of the feedback network. In Figure 5.29, the blue curve corresponds to

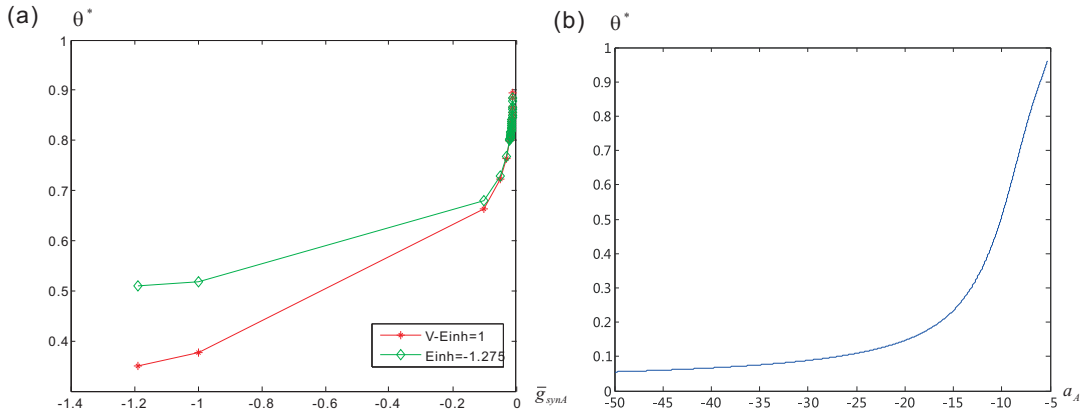

Figure 5.27 Comparison of results from two models. (a) The dependance of θ^* on $\bar{g}_{synA}$ from Morris-Lecar model. (b) The dependance of θ^* on a_A from QIF model.

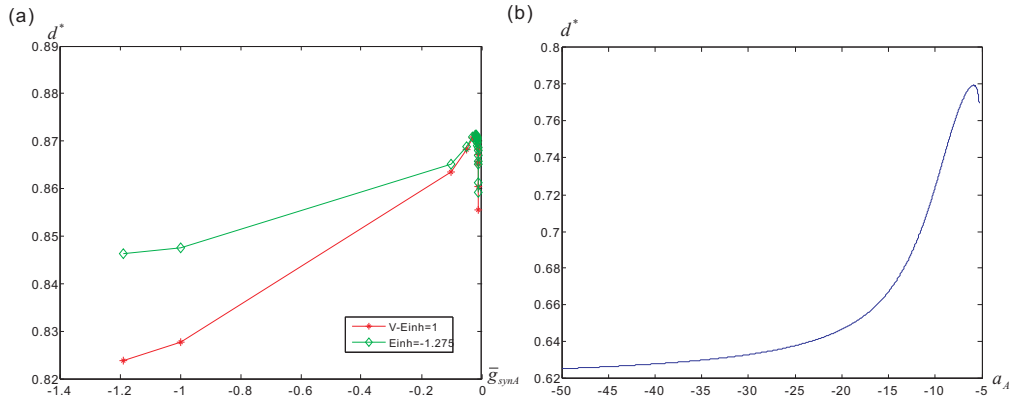

Figure 5.28 Comparison of results from two models. (a) The dependance of d^* on $\bar{g}_{synA}$ from Morris-Lecar model. (b) The dependance of d^* on a_A from QIF model.

the first equation $\phi = \frac{\tilde{T}}{\tilde{P}}(1-\theta-z_B(\theta))$ and the red one is for the equation $\theta = \frac{\tilde{P}}{\tilde{T}}(1-\phi-z_A(\phi))$. The intersection (θ^*, ϕ^*) is the phase-locked solution of the feedback network.

When the synapse from A to B is depressing, substitute $\phi^* = \frac{\tilde{T}}{\tilde{P}}(1-\theta^*-z_B(\theta^*))$ into the two equations (5.5), which is then rewritten as the three equations

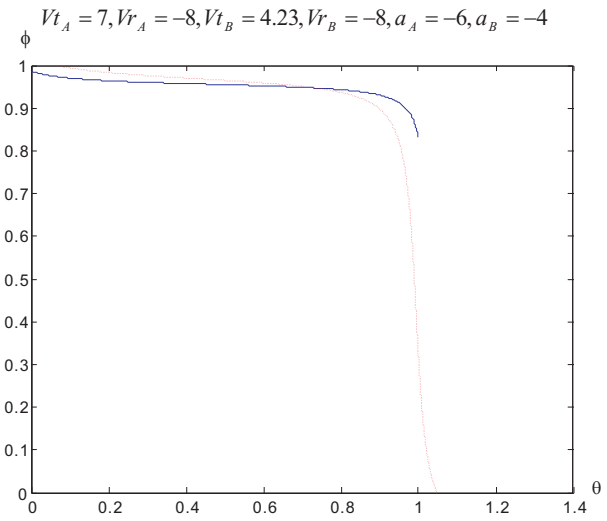

Figure 5.29 Geometric method of predicting the phase-locked activity of a feedback network without synaptic depression. The intersection of these two curves corresponds to a phase-locked solution of the feedback network.

$$\begin{cases} \phi^* = \frac{\tilde{T}}{\tilde{P}}(1 - \theta^* - z_B(\theta^*, d^*)) \\ \theta^* = \frac{\tilde{P}}{\tilde{T}}(1 - \phi^* - z_A(\phi^*)) \\ d^* = \frac{exp(\frac{\tilde{P}}{\tau_d}(1 - z_A(\phi^*))) - 1}{exp(\frac{\tilde{P}}{\tau_d}(1 - z_A(\phi^*))) - f} \end{cases} \tag{5.11}$$

The first equation involves the information how neuron A affects neuron B with synaptic depression. The second one is the same as the second equation for the non-depressing synapse case. The last equation describes the dependence of the depression on the phase of B through the PRC function of A. Figure 5.30 shows an example for the intersection of these three surfaces generated by the QIF model in Matlab. The surface parallel with the d-axis is generated by the second equation $\theta = \frac{\tilde{P}}{\tilde{T}}(1 - \phi - z_A(\phi))$, the surface parallel with the θ-axis corresponds to the third equation $d = \frac{exp(\frac{\tilde{P}}{\tau_d}(1 - z_A(\phi))) - 1}{exp(\frac{\tilde{P}}{\tau_d}(1 - z_A(\phi))) - f}$ and the other one is generated by the first equation $\phi = \frac{\tilde{T}}{\tilde{P}}(1 - \theta - z_B(\theta, d))$, which includes all three variables. The intersection of these three surfaces corresponds to a phase-locked solution of the feedback network with

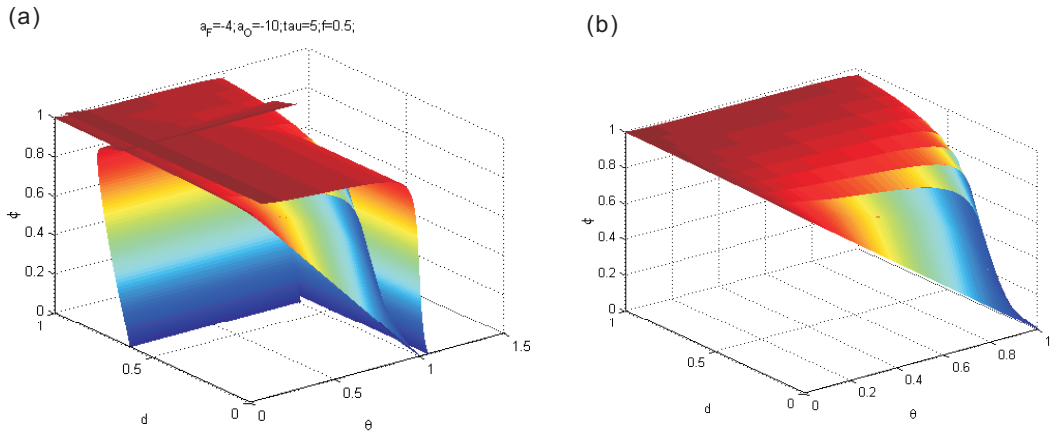

Figure 5.30 Geometric method of predicting the phase-locked activity of a feedback network with synaptic depression. (a) The intersection of these three surfaces corresponds to a phase-locked solution of the feedback network. The surface parallel with the d-axis is generated by the second equation in (5.11). The surface parallel with the θ-axis corresponds to the third equation in (5.11). The other one is generated by the first equation in (5.11), which is related all three variables and plotted separately in (b).

synaptic depression. Geometrically, we can analyze how the parameter values affect the phase-locked activity of the network by observing how the surfaces move with the alteration of the parameter values.

CHAPTER 6

DISCUSSION

6.1 Conclusion and Discussion

The rhythmic behaviors of animals or human beings are related to the coordinated activities of neurons in Central Pattern Generators(CPGs) [39, 54]. Exploring the dynamics of neuronal systems is important to understand the generation of rhythmic patterns. For a large complex network, it is often more tractable to examine the effects of component networks from the simplified system rather than from the system as a whole. In this study, we provided a method of combing information about feed-forward networks to infer the phase-locked activity of a feedback network. Based on the information on how the presynaptic neuron affects the activity of the postsynaptic neuron as well as the feed-forward information in the other direction, we predicted the phase-locked activity of neurons in a feedback network. Also, we examined the contributions of the feedback synapse and the short-term synaptic depression to the activity of the network. Moreover, we investigated the circumstances under which neurons are phase-locked in a specific pattern.

We considered a network of two reciprocally coupled heterogenous neurons A and B. Our analysis was done in two parts: In the first part, we assumed neuron A is oscillatory while neuron B is not. As an application, we extended this work to the analysis of a reduced three neuron model for the pyloric network of the STG, in which there are one oscillator and two follower neurons. In the second part, both neurons A and B are assumed to be oscillatory and they are pulse coupled with each other. For both cases, we examined the conditions for the phase-locked activity of these neurons with a focus on the 1:1 firing pattern. We derived specific maps for the phase-locked activity when they are reciprocally coupled. A stable fixed point of the

map corresponds to the phase-locked solution of the feedback network. We examined the conditions for the existence and stability of the fixed point for each case. The fixed point can be obtained by analytically solving certain equations or geometrically found from the intersection of two curves or three surfaces associated with difference pieces of feed-forward information. Further, the stability of the fixed point can be checked by observing the slope of the curves at the fixed point or through the eigenvalues of the Jacobian matrix for the map. Synaptic depression, a common form of short-term synaptic plasticity [6, 32, 37, 74], is incorporated in our work. Previously, it has been shown that the presence of synaptic depression promotes phase maintenance of neurons [6, 62] in an oscillatory feed-forward network as the period of the network is changed. Here, we found that synaptic depression may destabilize the stability of the fixed point due to the property of frequency dependence. Without synaptic depression, there exist stable fixed points close enough to the synchronous phase locked solution, but these fixed points lose their stability when synaptic depression is present in the network.

Specifically, in the first part of this study, neuron A is oscillatory while neuron B is of high-voltage resting potential. In the feed-forward network of A inhibiting B, we found that the relation between the period of A and the firing time of B relative to the last spike of A is piecewise linear. For the feed-forward information in the other direction, the dependency of the relative firing time of B on the period of A was examined in [51]. We combined these two pieces information to derive a map of the relative firing time of B when the synapses are non-depressing on feed-forward networks. Assuming the synapse from A to B is depressing, the map is constructed based on the synaptic strength of neuron A at the moment it fires in one cycle. We found that without synaptic depression, the fixed point of the map is always stable, while with synaptic depression, the slopes of the intersection curves at the fixed point need to bounded in an appropriate region for the solution to be stable. This implied

that the effect of the relative spiking time of B on the period of A can not be too large, and vice versa.

In this part, we used separate time scales for different parameters. For example, for the synapse of neuron B, we set the time constants for the gating variable s_B, τ_{η_B} and τ_{κ_B} in different time scales, thus, the trace of s_B is modeled by a square wave, which leads to the constant change in the period of A on Part I and Part III as shown in Figure 3.2(b). Without this extreme assumption, we expect the period curve in Figure 3.2(b) to be piece-wise linear with different slopes in distinct parts as shown in Figure 2.5 in Chapter 2. But this does not affect the application of our method, the period curve can still be transformed to predict the phase-locked solution by the map.

There is much work on the pyloric rhythm of the crustacean stomatogastric ganglion (STG). Hooper [38] found from experiments that the neurons in this network show strong phase maintenance as the cycle frequency is altered. Manor et al. [51] investigated a two neuron model consisting of an oscillator and a follower. They examined how the phase of the follower changes as the period of the oscillator is altered and found that the depressing synapse helps the phase maintenance between neurons. Mouser et al. [62] examined the relation between the phases of LP and PY with the period of AB. Mathematical equations were derived for the steady state of this tri-phasic network. In the network they studied, AB sends feed-forward inhibitory synapses to LP and PY which reciprocally inhibit one another. In our work, we looked for the phase-locked activity of this network by constructing a map cycle by cycle and found that in some parameter regimes, the steady state of the feed-forward network is unstable. These three neurons ar not period-1 phase-locked, but display a period-2 1:1 locking pattern, in which the cycle period of LP is first lengthened and then shortened in the next cycle, while PY does in the opposite way. It is an 1:1 phase locking pattern, but the repetitive period is twice the period of AB/PD. We found

that the occurrence of this period-2 solution is due to the dependency of recovery of LP neuron from depression on the cycle period, which is a sigmoidal function of the period.

We incorporated the synapse from LP to the pacemaker pair AB/PD into this network and examined the role of this feedback synapse to the activity of the network. Without this inhibitory feedback synapse, the network is driven by AB and the network frequency is completely determined by the frequency of AB. In the presence of this feedback synapse, the spiking of AB is delayed by the inhibition from LP and the rhythm of the network is slowed down. We constructed a 6D map based on the four variables in the 4D map and two additional variables, the period of AB and the depression variable when AB fires in one cycle, which both appear as parameters in the 4D map. The fixed point of this map corresponds to the phase-locked activity of the tri-phasic feedback network. Interestingly, we found that the period-2 region shrinks as the strength of the LP to AB feedback synapse increases, and this region eventually vanishes when the synapse is strong enough. A small perturbation in the period of the network induces the rapid variation of the depression variable of LP under certain parameter regimes and subsequent variation of the depression variable of PY, leading to instability of the phase-locked solution. The presence of the feedback synapse from LP to AB/PD slows down the rhythm of the network, which alleviates the variation in the depression of PY and helps to obtain a stable, 1:1 phase-locked activity of the feedback network.

From the view of experiments, under the circumstance that the recovery of LP from depression is nonlinearly dependent on the period of the network, the intact pyloric network is regularly 1:1 phase-locked, blocking the feedback synapse from LP to the pacemaker pair AB/PD may lead to a period-2 phase-locked pattern. Also, gradually weakening the synapse from LP to AB/PD is expected to break down the period-1 phase-locked pattern and the neurons would exhibit a period-2 phase locking.

In this part, the maps for the phase-locked activity of the network were derived under the two time scale assumption. We neglected the time neurons spend on the trajectories with double arrows which represents a fast time scale. See Figure 4.3. Two time scale assumption also guarantees the neurons to travel along their nullclines and jump from the local minimum of one nullcline which constitute the jump curve. Although the map is based on this simplified circumstance, our findings are not related to the two time scale assumption or restricted to this specific model. The roles of synaptic depression and feedback inhibitory synapses can be generalized to more realistic models.

In the second part, we considered two neurons A and B which are both oscillators with tonic spiking patterns but having slightly different periods. PRCs and STRCs of neurons are often used to analyze the phase-locked activity of the network [3, 20, 31, 53]. Since the neurons we consider are not necessarily weakly coupled, we used STRCs as our feed-forward information, and the perturbation used to generate the STRCs of neurons are similar to the effect of the action potential of the presynaptic neuron. We constructed a 1D map for the phase-locked activity of the feedback network of A and B connected by non-depressing synapses using the STRCs of these two neurons. We found that the conditions for 1:1 firing pattern of A and B are looser in the feedback network than in a feed-forward network (compare Figure 5.3 and Figure 5.6). In the feedback network, the STRC should be above a line, while in the feed-forward network, the STRC should be bounded by two lines. This result is consistent with the results in Chapter 4, i.e., the feedback synapse from LP to AB/PD helps to regulate 1:1 phase-locked activity of the pyloric network. When the synapse from A to B is depressing, we derived a 2D map for the phase-locked activity of the feedback network with an additional variable, the depression variable of AB. The presence of this short-term synaptic depression destabilize the fixed points θ^* near 1. Thus, the stable phase-locked solution for two heterogeneous neurons is

bounded away from synchrony. When B fires right after A fires, it does not change the period of A too much according to the STRC of A, which is close to 0 near $\phi = 0$ or 1. So the depression resources do not have much time to recover, which leads to smaller depression strength, thus the synapse is too weak to keep the neurons phase-locked. We used the QIF model and the Morris-Lecar model to generate Type I STRCs for the neurons and found that these two very different models yield similar results. Therefore, the information about the STRCs of the component neurons can be used to predict the phase-locked activity of the network, independent of the specific models. Here, we also found that the neurons with slightly different periods are not exactly synchronized, which is consistent with the previous findings [20, 78].

In many studies, phase response curves and spike time response curves were used to predict the phase-locked activity of feedback networks. Dror et al. [20] derived mathematical criterion for the stability of phase-locked activity in a ring of pulse coupled neurons. The conditions are based on the slope of the PRCs at the steady state. Maran and Canavier [53] investigated the activity of two mutually coupled heterogenous neurons. Under the interaction of intrinsic frequencies of neurons and the synaptic strength between them, these two neurons exhibit preserved firing order or alternating firing order, each of which includes two patterns, near synchrony and near anti-phase. For a busting neuron, a stimulus may change not only the period of the postsynaptic neuron, but also the burst duration. The dependency of the burst duration change on the stimulus phase was examined in [64] using Type II Morris-Lecar model, which is named as burst resetting curve (BRC). A stability condition based on PRCs and BRCs for the phase-locked activity of two mutually coupled neurons was derived. All these works assumed the strength of the stimulus is fixed, thus the frequency of the postsynaptic neuron is only affected by the timing of the stimulus. But in most networks, the synaptic strength between coupled neurons is not constant, but depends on the frequency of the presynaptic neuron which is

in turn affected by the synaptic strength. In our work, we incorporated synaptic depression into our work. We constructed the map for the depression variable cycle by cycle and examined the influence of this short-term synaptic plasticity on the activity of the network. We found that in the presence of synaptic depression, the stable phase-locked solution for two heterogeneous neurons is bounded away from synchrony.

Our method of combining known information from simplified or smaller systems provides an approachable way to predict the activity of the large complex system. Moreover, through this method, we can analyze the contributions and roles of the variables or parameters involved in the network. Although we used some specific models in our analysis and in the simulation, e.g., the QIF and Morris-Lecar models, this method is not restricted to any specific model. As long as we know the feed-forward information, we can combine these pieces of information to predict the activity of a large feedback network. The feed-forward information can be generated by mathematical or biological models or obtained from experiments. If it cannot be analytically formulated, the phase-locked activity can still be predicted using geometric methods.

6.2 Future Work

In this study, we have not taken into account the effect of the active duration of a neuron. In the first part, we assume the relative firing time of B does not affect the active duration of neuron A. In the second part, we assume the two neurons are pulse coupled. As an extension of the first part, I am going to take the duration as an additional variable in our method. Manor et al. [51] investigated the relationship between the phase of the follower and the period of the oscillator by changing the period in three different ways. Beside the situation we already utilized in this work that the period is changed by varying the inactive time and fixing the active duration,

there are two more ways to change the period. One is fixing the inactive time and varying the active duration and the other is varying both and keeping the duty cycle constant. We are going to utilize these information in our method as a piece of feed-forward information. For the second part, we will explore the activity phase of two mutually coupled bursting neurons from the STRCs as well as the bursting resetting curves (BRCs) [64]. The concept of BRC was proposed by Oprisan and Canavier in [64], describing how the burst duration changes with the stimulus phase. We are going to use the STRCs as well as BRCs of neurons to predict the phase-locked activity of the network. Presumably, the map for the phase-locked activity should be two dimensional without the short-term synaptic plasticity and be three dimensional with the synaptic depression from A to B.

Another natural extension of our current work is to consider depressing synapses in both directions in a mutually coupled network. For this network, another depression variable is needed to represent depression of the synapse from neuron B to neuron A. This variable also changes with the period of neuron B. Thus, the map would be three dimensional, including the phase and two depression variables. The phase-locked activity of the feedback network can be predicted by the fixed point of this 3D map.

We are also interested in the resonance phenomenon in neurons. It was proposed that synapses with short-term dynamics can preferentially respond to input currents at a given frequency [42]. This property is called synaptic resonance, which is caused by the competing effects of short-term depression and facilitation. We are going to investigate how the synaptic resonance affects the feed-forward and feedback networks in the context of central pattern generating networks.

Finally, we would like to generalize our method applicable to any form of firing patterns. In my current research, the map is constructed based on $1:1$ firing patterns. Ermentrout [24] found the conditions based on the natural frequencies of the oscillators for the $n:m$ phase locking pattern of two weakly coupled neurons.

Without the weak coupling assumption, Maran and Canavier [53] found the conditions for $2:2$ phase locking of two heterogenous oscillators with preserved firing order or alternating firing order. We aim to find a general method applicable to $n:m$ firing patterns of two mutually coupled neurons and find the circumstances under which some specific firing pattern occurs.

REFERENCES

[1] L Abbott and W Regehr. Synaptic computation. *Nature*, 431:796-803, 2004.

[2] S Achuthan and C Canavier. Phase-resetting curves determine synchronization, phase locking, and clustering in networks of neural oscillators. *J. Neurosci.*, 29:5218-5233, 2009.

[3] C Acker, N Kopell, and J White. Synchronization of strongly coupled excitatory neurons: relating network behavior to biophysics. *J. Comput. Neurosci.*, 15:71-90, 2003.

[4] R Bertram and A Sherman. Dynamical complexity and temporal plasticity in pancreatic beta-cells. *J. Biosci.*, 25:197-209, 2000.

[5] D Blitz, K Foster, and W Regehr. Short-term synaptic plasticity: a comparison of two synapses. *Nat. Rev. Neurosci.*, 5:630-640, 2004.

[6] A Bose, Y Manor, and F Nadim. Bistable oscillations arising from synaptic depression. *SIAM J. Appl. Math.*, 62:706-727, 2001.

[7] A Bose, Y Manor, and F Nadim. The activity phase of postsynaptic neurons in a simplified rhythmic network. *J. Comput. Neurosci.*, 17:245-261, 2004.

[8] P Buono and A Palacios. A mathematical model of motorneuron dynamics in the heartbeat of the leech. *Physica D*, 188:292-313, 2004.

[9] G Buzsaki. Hippocampal sharp waves: Their origin and significance. *Brain Res.*, 398:242-252, 1986.

[10] G Buzsaki. Theta oscillations in the hippocampus. *Neuron*, 33:1-20, 2002.

[11] C Canavier. Phase response curves. *Scholarpedia*, 1(12):1332, 2006.

[12] C Canavier and S Achuthan. Pulse coupled oscillators and the phase resetting curve. *Math. Biosci.*, 226:77-96, 2010.

[13] F Chance, S Nelson, and L Abbott. Synaptic depression and the temporal response characteristics of v1 cells. *J. Neurosci.*, 18:4785-4799, 1998.

[14] L Chandrasekaran, S Achuthan, and C Canavier. Stability of two cluster solutions in pulse coupled networks of neural oscillators. *J. Comput. Neurosci.*, 30:427-445, 2011.

[15] L Chandrasekaran, V Matveev, and A Bose. Multistability of clustered states in a globally inhibitory network. *Physica D*, 238:253-263, 2009.

[16] G Davis and R Murphey. A role for postsynaptic neurons in determining presynaptic release properties in the cricket cns: evidence for retrograde control of facilitation. *J. Neurosci.*, 13:3827-3838, 1993.

[17] A DeFranceschi. A phases sensitivity based method for prediction of modes of behavior in quadrupedal locomotion. Master's thesis, Rice Univerisity, 1995.

[18] R DiCaprio, G Jordan, and T Hampton. Maintenance of motor pattern phase relationships in the ventilatory system of the crab. *J. Exp. Biol.*, 200:963-974, 1997.

[19] J Dittman, A Kreitzer, and W Regehr. Interplay between facilitation, depression, and residual calcium at three presynaptic terminals. *J. Neurosci.*, 20:1374-1385, 2000.

[20] R Dror, C Canavier, R Butera, J Clark, and J Byrne. A mathematical criterion based on phase response curves for stability in a ring of coupled oscillators. *Biol. Cybern.*, 80:11-23, 1999.

[21] J Drover, V Tohidi, A Bose, and F Nadim. Combining synaptic and celluar resonance in a feed-forward neuronal network. *Neurocompting.*, 70:2041-2045, 2007.

[22] Fortune E and Rose G. Short-term synaptic plasticity contributes to the temporal filtering of electrosensory information. *J. Neurosci.*, 20:7122-7130, 2000.

[23] J Eisen and E Marder. Mechanisim underlying pattern generation in lobster. *J. Exp. Biol.*, 200:963-974, 1982.

[24] B Ermentrout. $n : m$ phase-locking of weakly coupled oscillators. *J. Math. Biology*, 12:327-342, 1981.

[25] B Ermentrout. *Simulating, Analyzing and Animating Dynamical Systems: A Guide to XPPAUT for Researchers and Students.* SIAM, Philadelphia, 2002.

[26] B Ermentrout. Type i membranes, phase resetting curves, and synchrony. *Neural Comput.*, 8:979-1001, 2007.

[27] B Ermentrout and Kopell N. Oscillator death in systems of coupled neuroal oscillators. *SIAM J. Appl. Math.*, 50:125-146, 1990.

[28] H Fischer, J Schmidt, R Haas, and A Buschges. Pattern generation for walking and searching movements of a stick insect leg. i. coordination of motor activity. *J. Neurophys.*, 85:341-353, 2001.

[29] E Fortune and G Rose. Short-term synaptic plasticity as a temporal filter. *Trends Neurosci.*, 24:381-385, 2001.

[30] G Fuhrmann, A Cowan, I Segev, M Tsodyks, and C Stricker. Multiple mechanism govern the dynamics of depression at neocortical synapses of young rats. *J. Physiol.*, 557:415-438, 2004.

[31] P Goel and B Ermentrout. Synchrony, stability, and firing patterns in pulse-coupled oscillators. *Physica D*, 163:191-216, 2002.

[32] L Grande and W Spain. Synaptic depression as a timing device. *Physiol.*, 20:201-210, 2005.

[33] CM Gray. Synchronous oscillations in neuronal systems: Mechanisms and functions. *J. Comput. Neurosci.*, 1:11-38, 2007.

[34] J Hale and H Kocak. *Dynamics and Bifurcations*. Springer-Verlag Press, New York, 1991.

[35] D Hansel, G Mato, and C Meunier. Synchrony in excitatory neural networks. *Neural Comput.*, 7:307-337, 1995.

[36] A Hodgkin. The local electric changes associated with repetitive action in a non-modulated axon. *J. Physiol.*, 107:165-181, 1948.

[37] S Hooper. Phase maintenance in the pyloric pattern of the lobster (*panulirus interruptus*) stomatogastric ganglion. *J. Comput. Neurosci.*, 4:191-205, 1997.

[38] S Hooper. The pyloric pattern of the lobster (*panulirus interruptus*) stomatogastric ganglion comprises two phase-maintaining subsets. *J. Comput. Neurosci.*, 4:207-219, 1997.

[39] S Hooper. Central pattern generators. *Current Biology*, 10:R176-R179, 1999.

[40] S Hooper and M Moulins. Switching of a neuron from one network to another by sensory-induced changes in membrane properties. *Science*, 244:1587-1589, 1989.

[41] E Izhikevich. *Dynamical systems in neuroscience: the geometry of excitability and bursting*. The MIT Press, Massachusetts, 2007.

[42] E Izhikevich, N Desai, E Walcott, and F Hoppensteadt. Bursts as a unit of neural information: selective communication via resonance. *Trends Neurosci.*, 26:161-167, 2003.

[43] C Koch and I Segev. *Methods in neuronal modeling: from ions to networks*. The MIT Press, Massachusetts, 1998.

[44] J Lewis and L Maler. Dynamics of electrosensory feedback: short-term plasticity and inhibition in a parallel fiber pathway. *J. Neurophysiol.*, 88:1695-1706, 2002.

[45] J Lewis and L Maler. Synaptic dynamics on different time scales in a parallel fiber feedback pathway of the weakly electric fish. *J. Neurophysiol.*, 91:1064-1070, 2004.

[46] R Llinas and U Ribary. Intrinsic and network rhythmogenesis in a reduced traub model for ca3 neurons. *J. Comput. Neurosci.*, 1:39-60, 1996.

[47] R Llinas and M Steriade. Bursting of thalamic neurons and states of vigilance. *J. Neurophys.*, 95:3297-3308, 2006.

[48] K MacLeod, T Horiuchi, and C Carr. A role for short-term synaptic facilitation and depression in the procssing of intensity information in the auditory brain stem. *J. Neurophys.*, 95:3297-3308, 2007.

[49] J Magee, D Hoffman, C Colbert, and D Johnson. Electrical and calcium signaling in dentrites of hippocampal pyramidal neurons. *Annu. Rev. Physiol.*, 60:327-346, 1998.

[50] A Malyshev and P Norekian. Phase-locked coordination between two rhythmically active feeding structures in the mollusk *Clione limacina*. i. motor neurons. *J. Neurophysiol.*, 87:2996-3005, 2001.

[51] Y Manor, A Bose, V Booth, and F Nadim. Contribution of synaptic depression to phase maintenance in a model rhythmic network. *J. Neurophysiol.*, 90:3513-5621, 2003.

[52] Y Manor, F Nadim, L Abbott, and E Marder. Temporal dynamics of graded synaptic tansmission in the lobster stomatogastric ganglion. *J. Neurosci.*, 17:5610-5621, 1997.

[53] S Maran and C Canavier. Using phase resetting to predict 1:1 and 2:2 locking in two neuron networks in which firing order is not always preserved. *J. Comput. Neurosci.*, 24:37-55, 2008.

[54] E Marder and RL Calabrese. Principles of rhythmic motor pattern generation. *Physiol. Rev.*, 76:687-717, 1996.

[55] H Markram, A Gupta, A Uziel, Y Wang, and M Tsodyks. Information processing with frequency-dependent synaptic connections. *Neurobio. Learning and Memory*, 70:101-112, 1998.

[56] H Markram, D Pikus, A Gupta, and M Tsodyks. Potential for multiple mechanisms, phenomena and algorithms for synaptic plasticity at single synapses. *Neuropharmacol.*, 37:489-500, 1998.

[57] V Matveev, A Bose, and F Nadim. Capturing the bursting dynamics of a two-cell inhibitory network using a one-dimensional map. *J. Comp. Neurosci.*, 23:169-187, 2001.

[58] D Maynard and K Walton. Effects of maintained depolarization of presynaptic neurons on inhibitory transmission in lobster neuropil. *J. Comp. Physiol.*, 97:215-243, 1975.

[59] D McCormick and T Bal. Sleep and arousal: thalamocortical mechanisms. *Annu. Rev. Neurosci.*, 20:185-215, 1997.

[60] E Mishchenko and N Rosov. *Differential Equations with Small Parameters and Relaxation Oscillation*. Plenum Press, New York, 1980.

[61] C Morris and H Lecar. Voltage oscillations in the barnacle giant muscle fiber. *Biophys. J.*, 35:193-213, 1981.

[62] C Mouser, F Nadim, and A Bose. Maintaining phase of the crustacean tri-phasic pyloric rhythm. *J. Math. Biol.*, 57:161-181, 2008.

[63] M Oh and V Matveev. Loss of phase-locking in non-weakly coupled inhibitory networks of type-i model neurons. *J. Comput. Neurosci.*, 26:303-320, 2009.

[64] S Oprisan and C Canavier. Stability criterion for a two-neuron reciprocally coupled network based on the phase and burst resetting curves. *Neurocomp.*, 6566:733-739, 2005.

[65] L Perko. *Differential Equations and Dynamical Systems*. Springer Press, New York, third edition, 1980.

[66] P Rabbah and F Nadim. Synaptic dynamics does not determine proper phase of activity in a central pattern generator. *J. Neurosci.*, 25:11269-11278, 2005.

[67] M Richardson, O Melamed, G Silberberg, W Gerstner, and H Markram. Short-term synaptic plasticity orchestrates the response of pyramidal cells and interneurons to population bursts. *J. Comput. Neurosci.*, 18:323-331, 2005.

[68] F Skinner, J Chung, I Ncube, P Murray, and S Campbell. Using heterogeneity to predict inhibitory network model characteristics. *J. Neurophysiol.*, 93:1898-1907, 2005.

[69] F Skinner, N Kopell, and E Marder. Mechanisms for oscillation and frequency control in reciprocally inhibitory model neural networks. *J. Comput. Neurosci.*, 1:69-87, 1994.

[70] D Somers and N Kopell. Rapid synchronization through fast threshold modulation. *Biol. Cyber.*, 68:393-407, 1993.

[71] J Tabak, W Senn, M O'Donovan, and J Rinzel. Modeling of spontaneous activity in developing spinal cord using activity-dependent depression in an excitatory network. *J. Neurosci.*, 20:3041-3056, 2000.

[72] D Terman, N Kopell, and A Bose. Dynamics of two mutually coupled slow inhibitory neurons. *Physica D*, 117:241-275, 1998.

[73] A Thomson. Molecular frequency filters at central synapses. *Prog. Neurobiol.*, 62:159-196, 2000.

[74] A Thomson and A Bannister. Release-independent depression at pyramidal input onto specific cell targets: dual recordings in slices of rat cortex. *J. Physiol.*, 508:351–363, 1999.

[75] M Tsodyks and H Markram. The neural code between neocortical pyramidal neurons depends on neurotransmitter release probability. *Proc. Natl. Acad. Sci. USA*, 94:719-723, 1997.

[76] C Van Vreeswijk, L Abbott, and B Ermentrout. When inhibition not excitation synchronizes neural firing. *J. Comput. Neurosci.*, 1:313-321, 1994.

[77] J Varela, K Sen, J Gibson, J Fost, L Abbott, and S Nelson. A quantitative description of short-term plasticity at excitatory synapses in layer 2/3 of rat primary visual cortex. *J. Neurosci.*, 17:7926-7940, 1997.

[78] J White, C Chow, J Ritt, C Soto-Trevino, and N Kopell. Synchronization and oscillatory dynamics in heterogeneous, mutually inhibited neurons. *J. Comput. Neurosci.*, 5:5-16, 1998.

[79] S Wiggins. *Introduction to Applied Nonlinear Dynamical Systems and Chaos*. Springer Press, New York, second edition, 2003.

[80] Y Zhang, A Bose, and F Nadim. Predicting the activity phase of a follower neuron with a-current in an inhibitory network. *Biol. Cybern*, 99:171-184, 2008.

[81] R Zucker. Short-term synaptic plasticity. *Annu. Rev. Neurosci.*, 12:13-31, 1989.

[82] R Zucker. Calcium- and activity-dependent synaptic plasticity. *Curr. Opin. Neurobiol.*, 9:305-313, 1999.